

1998

Resuspension of plutonium contamination at the Taranaki Nuclear Test Site

Nicholas Anthony Bertoldo
San Jose State University

Follow this and additional works at: https://scholarworks.sjsu.edu/etd_theses

Recommended Citation

Bertoldo, Nicholas Anthony, "Resuspension of plutonium contamination at the Taranaki Nuclear Test Site" (1998). *Master's Theses*. 1618.

DOI: <https://doi.org/10.31979/etd.3ag8-6qdm>

https://scholarworks.sjsu.edu/etd_theses/1618

This Thesis is brought to you for free and open access by the Master's Theses and Graduate Research at SJSU ScholarWorks. It has been accepted for inclusion in Master's Theses by an authorized administrator of SJSU ScholarWorks. For more information, please contact scholarworks@sjsu.edu.

INFORMATION TO USERS

This manuscript has been reproduced from the microfilm master. UMI films the text directly from the original or copy submitted. Thus, some thesis and dissertation copies are in typewriter face, while others may be from any type of computer printer.

The quality of this reproduction is dependent upon the quality of the copy submitted. Broken or indistinct print, colored or poor quality illustrations and photographs, print bleedthrough, substandard margins, and improper alignment can adversely affect reproduction.

In the unlikely event that the author did not send UMI a complete manuscript and there are missing pages, these will be noted. Also, if unauthorized copyright material had to be removed, a note will indicate the deletion.

Oversize materials (e.g., maps, drawings, charts) are reproduced by sectioning the original, beginning at the upper left-hand corner and continuing from left to right in equal sections with small overlaps. Each original is also photographed in one exposure and is included in reduced form at the back of the book.

Photographs included in the original manuscript have been reproduced xerographically in this copy. Higher quality 6" x 9" black and white photographic prints are available for any photographs or illustrations appearing in this copy for an additional charge. Contact UMI directly to order.

UMI

A Bell & Howell Information Company
300 North Zeeb Road, Ann Arbor MI 48106-1346 USA
313/761-4700 800/521-0600

**RESUSPENSION OF PLUTONIUM CONTAMINATION
AT THE TARANAKI NUCLEAR TEST SITE**

A Thesis

Presented to

The Faculty of the Department of Nuclear Science

Radiological Health Physics Program

San Jose State University

In Partial Fulfillment

of the Requirements for the Degree

Master of Science

Radiological Health Physics

by

Nicholas Anthony Bertoldo

May 1998

UMI Number: 1389629

Copyright 1998 by
Bertoldo, Nicholas Anthony

All rights reserved.

UMI Microform 1389629
Copyright 1998, by UMI Company. All rights reserved.

This microform edition is protected against unauthorized
copying under Title 17, United States Code.

UMI
300 North Zeeb Road
Ann Arbor, MI 48103

© 1998

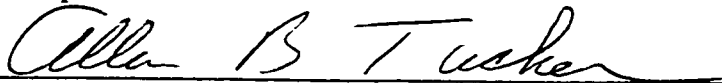
Nicholas A. Bertoldo

ALL RIGHTS RESERVED

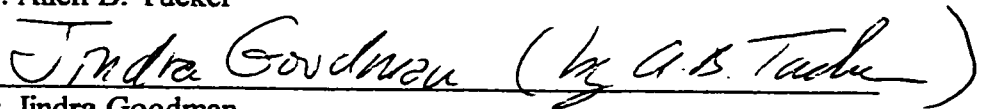
APPROVED FOR THE DEPARTMENT OF NUCLEAR SCIENCE
RADIOLOGICAL HEALTH PHYSICS PROGRAM



Dr. Joseph H. Shinn



Dr. Allen B. Tucker



Dr. Jindra Goodman

APPROVED FOR THE UNIVERSITY



ABSTRACT

RESUSPENSION OF PLUTONIUM CONTAMINATION AT THE TARANAKI NUCLEAR TEST SITE

by Nicholas A. Bertoldo

Plutonium resuspension studies were conducted at the Taranaki Nuclear Test Site located at Maralinga, South Australia, to assess the soil cleanup effort. Ultra high volume air samplers capable of sampling greater than 25 times the standard volumetric flow rates were used to increase the effectiveness of mass collection for radiological analysis. Air concentrations were significantly larger under elevated wind and dust storm conditions ranging from 80 to 1830 $\mu\text{Bq}/\text{m}^3$ in November, 1996 and 91 to 178 $\mu\text{Bq}/\text{m}^3$ in March, 1997.

Total particulate size experiments were also conducted yielding detailed multi-modal distribution data. Mass median aerodynamic diameters (MMAD) were found to range overall from 3.78 to 10.32 μm for the parent distributions unfolded from the mixed distributions. Average MMAD parent component values ranged from $5.23 \pm 1.20 \mu\text{m}$ to $8.71 \pm 1.63 \mu\text{m}$ for corresponding wind speeds ranging from 1.73 to 7.36 m/s.

This Work is Dedicated to
My Parents
Nicholas and Rosemary
My Daughter Lyndsay Nicole
and
Especially
Mary McHale
For Her Love and Support
Throughout this Project

INTRODUCTION

Plutonium resuspension research was conducted at Taranaki, a former British Nuclear Test Site located in Maralinga, South Australia, in November 1996 and March 1997. Taranaki was the site of the last of seven major trials in 1957, (i.e., nuclear device detonations) consisting of an approximate 27 kiloton yield tethered balloon shot code named "Taranaki" in Operation Antler (Williams 1994). In addition to being a site for the "Taranaki" atomic blast, it was also used in a series of minor trials (i.e., non-nuclear detonations of plutonium referred to as "safety shots") known as the Vixen B trials from 1960 to 1963. Approximately 22 kg of plutonium (Pu) was dispersed in the 12 Vixen B trials resulting in 1350 Curies (Ci) of $^{239+240}\text{Pu}$ soil contamination (Lokan 1985). This contamination was detectable at a 100 km distance downwind (Johnston et al. 1989).

In 1967, Operation Brumby was conducted by the British as a first cleanup effort. The soil was plowed to a depth of approximately 30 cm to reduce exposure, which was a typical practice of the past even at the Nevada Test Site. In 1996, a second campaign was begun to remove the worst of the plutonium contamination. As a result of the regrowth of desert scrub over the years, the cleanup process has required the removal of trees and scrub prior to uncovering the originally plowed activity by scraping.

This study was conducted to assess the plutonium concentrations in the air due to resuspension by natural and mechanical processes occurring over bare soil conditions at the cleanup site. The experimental control site selected was sparsely covered with scrub and dead trees ranging in height from 1.0 to 1.5 meters (m) as a result of the atomic blast 40 years earlier. The present soil activity at this location was below the cleanup criteria

level and was representative of the regrowth conditions. The soil conditions are sandy but form a very thin crust at the uppermost surface that is easily broken up by mechanical traffic revealing the soil's powdery consistency. Dust clouds mechanically generated by the movement of heavy equipment during operations were easily visible at a distance of 3 to 4 kilometers.

The scientific investigative team was composed of staff from the Lawrence Livermore National Laboratory (LLNL) Health and Ecological Assessment Division of the Environmental Programs Directorate in conjunction with the staff of the Australian Radiation Laboratory (ARL). Power installation and general assistance with equipment was provided by the Department of Primary Industries and Energy of Australia.

This paper describes the field data collection techniques employed to characterize the distribution of total suspended particulates (TSP) and the airborne activity associated with plutonium resuspension. Contaminant aerosols are composed of agglomerates of plutonium oxide due to aging and the natural soil from the sandy desert area. The aerosol particle measurements made in November 1996 and March 1997 by cascade impactor collection methods are presented and compared to those of the aerosol particulate size distribution (APSD) experiment conducted in March. These cascade impactor data are compared to the particle size distribution derived from an optical particle counter response coupled with a pulse height analyzer (PHA). The APSD results are useful as the optical particle counter measurements yield detailed size information in addition to number density of the TSP.

The discussion that follows is presented in two sections. Part I is devoted to the Ultrahigh-Volume Air Sampler (UHVAS) developed at LLNL by Dr. Joseph H. Shinn. The UHVAS reduces the sampling time required to achieve the same results as contemporary high-volume (HV) air samplers requiring extended sampling time. The UHVAS chapter describes the system design, calibration, performance characteristics, and field role in resuspension studies that the author assisted in carrying out. Part II is devoted to characterization of the Taranaki TSP by use of an optical particle counter of an older design, which had been fitted by the author with instrumentation modifications and connected to a personal computer programmed for ease of downloading data files in the field. Field implementation allowed automated data acquisition with minimal instrument supervision. Part II details the system design, calibration, data handling, data reduction and analysis.

The results of each part are components of the complete assessment of the Taranaki resuspension experiment consisting of the cooperative efforts of the scientific team using numerous instruments. The work done is by no means conclusive. Many questions regarding the physical and chemical components at work in the dynamic environment are left unanswered. Further investigation of these processes will undoubtedly reveal more information which will be of significant value to the scientific community in the future.

BACKGROUND

Plutonium was identified by Dr. Glenn Seaborg in the late 1940s by neutron activation of uranium-238 (^{238}U) in a graphite moderated reactor. The process of formation yields percentages of ^{238}Pu , $^{239+240}\text{Pu}$, ^{241}Pu , ^{242}Pu , and ^{241}Am isotopes. "Some

classified percentage of ^{241}Am is present at $t = 0$ which is also formed in the plutonium manufacturing process” (Shinn 1998). Americium-241 (^{241}Am) with gamma decay energy of 59.5 kilo-electron Volts (keV) is formed by negative beta emission (β^-) in the decay of ^{241}Pu with a 14.4 year half-life. The general equation of the growth of ^{241}Am from the ^{241}Pu decay is expressed by the linear differential equation Eq.1a solved by conventional means and expressed in Eq.1 below as:

$$dN_2/dt = \lambda_1 N_1^0 (e^{-\lambda_1 t}) - \lambda_2 N_2 \quad (\text{Eq. 1a})$$

$$N_2 = \lambda_1 (\lambda_2 - \lambda_1)^{-1} N_1^0 (e^{-\lambda_1 t} - e^{-\lambda_2 t}) + N_2^0 e^{-\lambda_2 t} \quad (\text{Eq. 1})$$

where N_2^0 = the “classified percentage of ^{241}Am present at $t = 0$ ” (Shinn, 1998).

The resulting percentage of ^{241}Am ingrowth serves as a tracer for the primary decay mode alpha emitters of $^{239+240}\text{Pu}$ in isotopic ratios determined by their manufactured grade. Isotopic ratios for $^{239+240}\text{Pu}/^{241}\text{Am}$ were found to range from 6 to 11 as determined from soil analysis from samples collected in November 1996. Plutonium soil activity may be derived from the *in situ* gamma spectroscopy data once the $^{239+240}\text{Pu} / ^{241}\text{Am}$ ratio and the depth distribution have been determined from soil sample analysis and profiling, respectively.

ARL used *in situ* gamma spectroscopy with a high purity germanium (HPGe) detector mounted on a boom in front of a “Class I” High Efficiency Particulate Air (HEPA) filtered vehicle and an array of NaI detectors mounted on the front of a small pick-up truck to quantitatively map the americium-241 (^{241}Am) surface activity of Taranaki when background corrected and calibrated by ARL.

Although (Lokan 1985) states that the *in situ* gamma spectroscopy field measurements performed by ARL are not considered to be a quantitative measure of the plutonium concentration due to the absorption of the 59.5 keV energy gamma emission of ^{241}Am by surface soil it should be noted that this technique has been successfully employed at the Nevada Test Site (NTS) and the Marshall Islands in addition to Taranaki. Proper site characterization is required with the *in situ* gamma spectroscopy technique with knowledge of the Pu/Am ratios, depth distribution, soil moisture content and density. Calibration protocols derived by the author in previous work assisting in the characterization the residual cesium-137 (^{137}Cs) (i.e., barium-137 metastable ($^{137\text{m}}\text{Ba}$)) soil activity on several islands for LLNL's Marshall Islands Program enable this measurement technique to yield confident quantitative results.

The measurement uncertainty referred to by Lokan may be reduced by utilizing calibration protocols which are enhanced by characterization of soil data derived from profiles and analysis. Soil absorption is only one of the difficulties precluding proper data interpretation with the *in situ* measurement technique. Taranaki soil also contains the gamma emitting fission product europium-152 at sufficiently high levels near the ground zero (GZ) site of the blast as determined by ARL's gamma spectroscopy. Although isotopic determination is easily attained with the well defined spectral resolution of the HPGe detector, the author concurs with Lokan to the extent that the practical application of *in situ* gamma spectroscopy best serves to qualitatively determine elevated soil activity levels at the Taranaki within a factor of two site for mapping purposes.

Taranaki has concentric ring roads approximately 1km apart encompassing a semicircular area. The west plume (W) has the lowest surface activity by comparison to the northwest (NW), north (N), and northeast (NE) plumes (Williams, 1994). The surface activity in the west plume at ring road F, (FW), is below the cleanup criteria of 12 kBq/m² (0.3 μCi/m²) of ²⁴¹Am. This area had not been plowed during operation Brumby in 1967. At that time the cleanup level sought was to reduce the soil activity to 1 μCi/kg of soil (40 kBq/kg). Adding perspective to this the 1967 level by comparison was 50 times greater. This comparison is made on the basis of converting the 40 kBq/kg concentration to a deposition activity per unit area (kBq/m²) and taking the ratio of the 1967 level to that of the 1996 level. The concentration is assumed to be in the top 1 cm of soil with an average soil density of 1.5 g/cm³.

RESUSPENSION STUDY METHODS

The control sites setup at FW in November, and on Lot 19 at FN in March consisted of the following instrumentation and apparatus:

1. *Air Samplers*

- **Ultrahigh-Volume air sampler:** A newly designed vertical collection cylinder covered by fiber media and powered by a centrifugal motor-blower operating at 1000 m³/hr. Quantity (1)
- **High-Volume (HV) air samplers:** Conventional Graseby-Anderson units with 8x10 inch fiber filters operating at 85 m³/hr (50 cfm). Quantity (2)

- Cascade Impactors (CI): Graseby-Anderson Model 65-000, 5-stage jet impactors collecting on fiber media to enhance collection efficiency, operating at 34 m³/hr (20 cfm). Quantity (2)
- AQ-10 Particle Counters: Bulk scatter nephelometers with analog DC output linearly proportional to TSP. Quantity (2)
- Optical Particle Counter with vane mounted isokinetic sampler: Climet Model 208, Manually recorded counts on FW; APSD on Lots 18C and 19 at FN. Quantity (1)
- Logarithmic particle sizing amplifier: Nuclear Data Inc. Model 82-0176 connected to the optical particle. Quantity (1)
- Davidson PHA: Model 1056C connected to the logarithmic particle sizing amplifier. Quantity (1)

Meteorological Tower

The following sensors were used to determine the energy balance:

- Net Radiometer: Quantity (1)
- Ground Heat Flux sensor: Quantity (2)
- Temperature Sensors: Quantity (4)

The energy balance was supplementary to this project to determine the changes in turbulent diffusivity and will not be discussed here.

In addition to the instruments listed above for the energy balance, the following were also used:

- Sonic Anemometer: Used to measure vertical component of the wind velocity. Quantity (1)
 - Tri-Cup Anemometers: Used to measure horizontal wind speed. Quantity (2)
 - Vane-type Wind Direction Sensor: Quantity (1)
 - Thornthwaite Lightweight Tri-Cup Anemometer System: Used to profile the horizontal wind speed and determine the surface roughness length and estimate the friction velocity u_* .
2. The experimental setup for Lot 37 in November and Lot 18C in March was as follows: Lot 37 was a newly cleaned area at FNE, and subject to an observed dust storm. Lot 18C was an uncleaned area north of FN that had been additionally contaminated by redistribution as a result of successive dust storms from November 1996 to March 1997.

Air Samplers

- Ultrahigh-Volume air sampler: As described above. Quantity (1)
- High-Volume air sampler: As described above. Quantity (2)
- Cascade Impactors: As described above. Quantity (2)
- AQ-10 Particle Counters: Bulk scatter nephelometers with analog DC output linearly proportional to TSP. Quantity (2)
- Optical Particle Counter: APSD on Lot 18C as described above. Quantity (1)

Meteorological Tower

- Wind Speed Sensor: Used for horizontal wind speed measures. Quantity (1)

- Vane-type Wind Direction Sensor: Quantity (1)

Campbell Data Logger

Meteorological data for both sites described above was recorded via a Campbell Scientific data logger. The data logger stores the data in eight channels subdivided by series numbers corresponding to the categories of data within each channel. For example, the data map is shown in Table I-3 Appendix I-A. The data for wind speed sensor $WS_{z=0.585\text{ m}}$ (at height z) is located in channel 4 and similarly $WS_{z=2.18\text{ m}}$ (at height z) is located in channel 5. Both data sets are in series No. 10. The remaining data collected follows in the same manner.

RESULTS AND DISCUSSION

November wind conditions were elevated compared to those of March. Observations showed that the $^{239+240}\text{Pu}_{\text{Air}}$ activity was 3.0 Bq/g (81 pCi/g) at the F-ring road control site in the west plume (FW) and 1.9 Bq/g (51.4 pCi/g) at our experimental site located in Lot 37 at the F-ring road of the northeast plume (FNE) which was cleared one week prior to our arrival. The $^{239+240}\text{Pu}_{\text{Air}}$ of Lot 37 under windy conditions was the same as FW under normal conditions.

The derived air concentration (DAC) as defined by International Commission on Radiological Protection (ICRP) Publication 23 is the radionuclide concentration in air breathed continuously by a radiological worker in one work year (2000 hrs) that would irradiate Reference Man to the limits for occupational exposure which is defined as the annual limit of intake (ALI) in units of activity (i.e., μCi or Bq). The DAC is expressed in Eq. 2 in S.I. units Bq/m^3 as:

$$\text{DAC} = \text{ALI} / \text{m}^3 \quad \text{Eq. (2)}$$

Although the lung model has become more sophisticated in recent years, the Environmental Protection Agency (EPA) of the United States has tabulated ALI and DAC values based on ICRP Publication 30 with revisions for plutonium values in ICRP Publication 48. Under the elevated wind conditions the highest plutonium concentration was found to be $1830 \mu\text{Bq}/\text{m}^3$. Comparing this result to the regulatory DAC limit for Y-Class (i.e, lung retention class years for insoluble compounds of which plutonium-oxide is characteristic of aged plutonium) plutonium of $3 \times 10^{-7} \text{MBq}/\text{m}^3$ (Eckerman, Wolbarst, and Richardson 1989), it is shown that even under continuous exposure at sustained extreme conditions the FNE resuspended concentration in air listed in Table I-5 of Thesis Part I is calculated as:

$$\chi_{\text{air FNE}} = 1830 \times 10^{-6} \text{Bq}/\text{m}^3 \bullet 1 \times 10^{-6} \text{MBq}/\text{Bq} = 1.83 \times 10^{-9} \text{MBq}/\text{m}^3$$

which is 164 times less than the regulatory limit quantifying the effectiveness of the soil scraping activities.

The ratio of ($\text{TSP}_{\text{Elevated}}/\text{TSP}_{\text{Normal}}$) was found to be 69:1 for FNE Lot 37 compared to 3:1 for FW. Similarly, the ratio was 3:1 for FN Lot 19 compared to 5:1 for FN Lot 18C. Although high and gusty winds are characteristic of November weather, the values of ($\text{TSP}_{\text{Elevated}}/\text{TSP}_{\text{Normal}}$) for Lots 19 and 18C are within a factor of 2 of the control site ratio. This is primarily due to TSP resuspension over cleared terrain as opposed to reduced air concentrations of TSP limited by ground cover at the FW site.

The locations chosen for the March expedition were selected on the assumption that there would be a significant redistribution of surface material from continued wind erosion

when the severe dust storm was observed in November. Lot 19 is located in the north plume at the F-ring road (FN) and the end of Lot 18 just north of FN recontaminated by erosion. This area was designated Lot 18C "contaminated by redistribution." The $^{239+240}\text{Pu}_{\text{Air}}$ for Lot 18C was 2.2 times greater in the windy condition and the $^{239+240}\text{Pu}_{\text{Air}}$ over cleared Lot 19 was 5 times greater than that observed for the normal wind conditions.

Thesis Part I

ULTRAHIGH-VOLUME AIR SAMPLER

(UHVAS)

INTRODUCTION

The Ultrahigh-Volume Air Sampler (UHVAS), was designed by environmental researchers to optimize aerosol particulate sampling. The UHVAS maximizes the airflow volume sampled over the sampling interval, which allows field research to be conducted in remote areas with minimal support requirements and operational monitoring by the researcher. In addition, the UHVAS is a low-maintenance electrically powered machine. With the exception of the large filter surface area being exposed to the environment, the UHVAS is fairly durable in extreme weather conditions. It is well suited for any climate in which sampling conditions for aerosol particulates would be proper. Under extremely wet conditions (which are not conducive to air sampling), cellulose fiber filters would tear quite easily. The electric motor and fan assembly are shrouded for both protection of the apparatus and field safety. Thus the UHVAS is a self-contained sampling system that operates on 220 Volts alternating current (VAC) at 60 Hz in the US or 440 VAC at 50 Hz as operated in Australia.

BACKGROUND

Two UHVAS prototypes were deployed in their first operational field use during a plutonium resuspension study conducted in 1993 by Shinn at a former U.S. B-52 Bomber crash site in Palomares, Spain. The UHVAS was designed with minimal fabrication.

The system employs a standard industrial blower-motor assembly which is mounted at the face of the fan-housing inlet to a filter assembly. The UHVAS was designed with two interchangeable sample filter assemblies. Each houses filters of different surface areas.

One assembly option allows the use of a horizontally mounted circular filter of diameter $D_f \approx 24.5$ in (") inside diameter (ID), subtracting the edges of the housing assembly yields a net $D_{f-net} \approx 22.5$ " ID and thus a $SA_{F-plate} = 2.3 \text{ ft}^2 (0.21 \text{ m}^2)$. The other assembly was a vertical cylinder mount of the same ID for ease of exchange. The resulting net surface area of the cylinder mount after subtracting the restraining band widths and the filter overlap was $SA_{F-cylinder} = 13 \text{ ft}^2 (1.2 \text{ m}^2)$.

A special flow diverter was designed by Shimm to maximize "flow straightening" in order to reduce the backpressure on the system under increased fan speeds. The airflow follows a 90° downturn from impaction on the cylindrical filter surface which is perpendicular to the ground, and upon entering the flow chamber turns 90° horizontally to enter the fan housing. The high flow rates required were attained by using higher fan speeds and minimizing load-induced cavitation with the flow diverter.

Anticipating the power loss running 440 VAC with a line frequency of 50 Hz from that of 220 VAC - 60 Hz at LLNL, a variable pitch sheave (i.e., Congress Model VP350 x $\frac{1}{2}$) was added to increase the fan speed up to 30% to compensate for the calculated power loss. Once this was done the plate-type filter assembly was rejected due to significant increased loading (i.e., 3 Hp motor failure) and the cylindrical design was selected as the

preferred design for the conditions anticipated. In order to maintain the high flow rates achieved at LLNL during calibration when moved to Australian field conditions, the motor power was increased from 3 to 5 horsepower to compensate for the increased loading at higher fan speeds due to the variable pitch sheave.

METHODS

Calibration

Instruments

The following instruments were used in the final calibration of the UHVAS:

- Meriam Laminar Flow Element (LFE): Model 50MC2-8F Serial No. F-32112.
Quantity (1)
- Meriam Incline Wall Manometer (WM): Model 442HE35 WM. Quantity (1)
- Standard U-tube manometer to measure the differential pressure (d_p) in $^{\circ}\text{H}_2\text{O}$.
Quantity (1)
- Kurz Velocity Probe (Hot-Wire Anemometer type): Model 442 used to measure the velocity of the discharge flow. Quantity (1)
- Pitot Tube: Used to compare velocities measured by the Kurz Probe, determine a field calibration equation, and to derive the flow rates from the field measurements. Quantity (1)
- Magnahelic dial manometers used to measure d_p in two scales depending on the reading obtained ($^{\circ}\text{H}_2\text{O}$ or $^{\text{cm}}\text{H}_2\text{O}$). Quantity (1 each)

- Whatman-41 cellulose fiber filter paper: Used to simulate loading conditions (i.e., two filters stacked for the plate-type filter configuration or double wrapped for cylindrical filter configuration).
- Monarch Non-Contact Tachometer: Model Pocket-Tach. 100 used to measure the motor RPM. Operational range: 5 - 100,000 RPM \pm 1 RPM; powered by 9V battery.

Method of Calibration

The Meriam LFE was mounted with a sheetmetal flow divergent adapter of 24" diameter atop the UHVAS intake plenum. The unit was sealed with vinyl tape to minimize air flow leaks at the inlet. Differential pressure readings were taken at the LFE primary and secondary taps corresponding to the upstream and downstream flow at the LFE venturi.

Meriam calibrates their LFEs using a master flowmeter that is traceable to the National Institute of Standards and Technology (NIST). The calibration data are standardized to an equivalent dry gas flow rate at 70 °F (21.1 °C) and 29.92" Hg (101.3 kPa abs.). The calibration procedure began by obtaining the calibration equation used by Meriam Instruments for the LFE.

Due to the unavailability of the dated factory calibration, the coefficients needed to be determined for the 2nd order polynomial expression used by Meriam given in Eq. (1.2a) below as:

$$\text{Eq. (1.2a)} \quad Q_{\text{LFE}} = A(d_p)^2 + B(d_p) + C$$

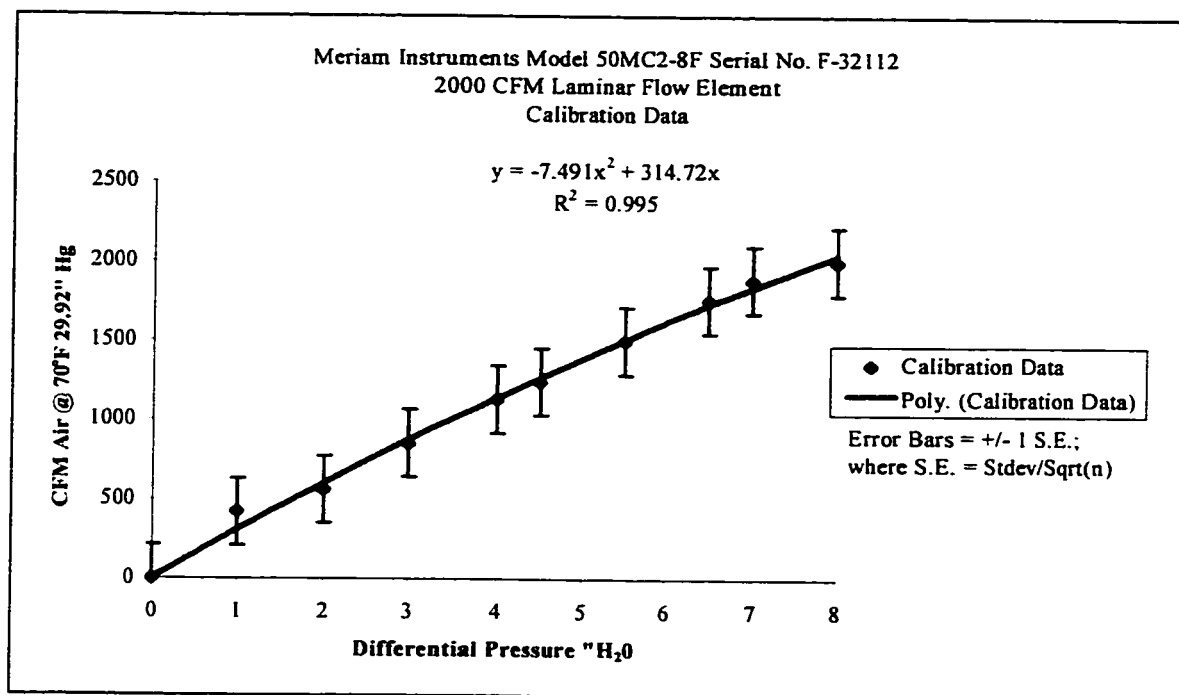
where $C = 0$.

Equation (1.2) below is the polynomial expression used to compare the WM reading to the LFE flow rate (Q_{LFE}), in units of cubic feet per minute (CFM.)

$$\text{Eq. (1.2)} \quad Q_{LFE} = -7.49(d_p)^2 + 314.72(d_p) \quad R^2 = 0.995$$

The LFE “best fit” curve is depicted in Figure I-1 below which shows the correlation of the Meriam LFE calibration with the coefficients of the equation representing the coefficients of the polynomial expression described in Eq. (1.2).

Figure I-1: Meriam Laminar Flow Element Calibration



The actual volumetric flow rate Q_A is then obtained by multiplication of Eq. (1.2) by the ratio of the viscosity of air under standard conditions (μ_{sd}) to the viscosity of wet air (μ_f) (i.e., μ_{sd}/μ_f), where μ_f is determined from the following relation:

$$\mu_f = \mu_{\text{air}} \cdot (\mu_{\text{wet}}/\mu_{\text{dry}})$$

where $\mu_{\text{wet}}/\mu_{\text{dry}}$ is the air viscosity correction factor for humidity which was obtained from a Meriam chart not reproduced here. For our calibration the value of $\mu_{\text{wet}}/\mu_{\text{dry}} \approx .998$ which we have taken to be essentially equal to 1 considering the uncertainty in our d_p readings of two significant figures which affect the calculation more than normalizing the viscosity ratio to one. Thus, the relation is reduced to $\mu_f = \mu_{\text{air}}$, where we calculate μ_{air} from Equation (1.3) as:

$$\text{Eq. (1.3)} \quad \mu_{\text{air}} (T = ^\circ\text{F}) = \frac{14.58[(459.67 + ^\circ\text{F})/1.8]^{3/2}}{110.4 + [(459.67 + ^\circ\text{F})/1.8]}$$

and Q_A then becomes:

$$Q_A = Q_{\text{LFE}} \cdot \mu_{\text{std}}/\mu_{\text{air}}$$

where $\mu_{\text{std}} = \mu_{\text{air}} (T = 70^\circ)$.

The standard volumetric flow rate is then obtained by correcting for the volumetric changes associated with the operational temperature and pressure. This yields Equation (1.4) for the standard volumetric flow rate (Q_S) as given by Meriam:

$$\text{Eq. (1.4)} \quad Q_S = Q_A \cdot (T_{\text{std}})/(T_f) \cdot (P_f/P_{\text{std}}) \cdot (\rho_{\text{wet}}/\rho_{\text{dry}})$$

where T_{std} = standard temperature; T_f = flowing temperature; P_{std} = standard pressure; P_f = flowing pressure; $\rho_{\text{wet}}/\rho_{\text{dry}}$ is the humidity correction factor.

The WM and U-tube manometers were connected to the LFE such that independent measurements could be made and compared. The U-tube manometer readings provided the d_p used in Eq. (1.2) corrected by the relations above to obtain a calculated Q_S as

shown below in Example (1) derived by substituting the values for the variables listed in Eq. (1.2), Eq. (1.3), and Eq. (1.4) as shown in Table I-1 (Meriam Instruments) below.

Table I-1: Variables used in Meriam Eq. 1.4

| | | | |
|--|---|--|--|
| $d_p = 4.1 \text{ } \mu\text{H}_2\text{O}$ | $\mu_{std} = 181.87 \text{ } \mu\text{Poise}$ | $T_{std} = 70 \text{ } ^\circ\text{F}$ | $\rho_{wet}/\rho_{dry} = 0.9921$ |
| $P_f = 30.00 \text{ } \text{"}\text{Hg}$ | $\mu_{air} = 183.2 \text{ } \mu\text{Poise}$ | $T_f = 75 \text{ } ^\circ\text{F}$ | $P_{std} = 29.92 \text{ } \text{"}\text{Hg}$ |

where ρ_{wet}/ρ_{dry} is obtained from interpolation for the values listed in Table I-2 (Meriam Instruments) for $T = 75 \text{ } ^\circ\text{F}$ at 80% relative humidity.

Table I-2: Humidity Correction Factor for Air = ρ_{wet}/ρ_{dry}

| °F | % Relative Humidity | | | | |
|-----|---------------------|--------|--------|--------|--------|
| | 20% | 40% | 60% | 80% | 100% |
| 40 | 0.9993 | 0.9987 | 0.9981 | 0.9975 | 0.9969 |
| 50 | 0.9990 | 0.9981 | 0.9973 | 0.9964 | 0.9955 |
| 60 | 0.9986 | 0.9973 | 0.9960 | 0.9955 | 0.9934 |
| 70 | 0.9981 | 0.9962 | 0.9944 | 0.9934 | 0.9907 |
| 80 | 0.9974 | 0.9948 | 0.9922 | 0.9907 | 0.9870 |
| 90 | 0.9964 | 0.9928 | 0.9892 | 0.9857 | 0.9821 |
| 100 | 0.9951 | 0.9902 | 0.9854 | 0.9805 | 0.9756 |

Example (1) is then written from Eq. (1.4):

$$Q_s = Q_A \cdot (T_{std}/T_f) \cdot (P_f/P_{std}) \cdot (\rho_{wet}/\rho_{dry})$$

$$\text{Example 1: } Q_s = (1156) \cdot (70/75) \cdot (30.00/29.92) \cdot (0.9921) = 1073.3 \text{ CFM}$$

WM solves the equation:

$$\text{SCFM} = \text{CFM} (P_a/P_o)(\mu_o/\mu_a)(t_o/t_a)$$

where the variables are defined below.

Meriam variable definitions for Model 442HE35 WM (Meriam Instruments)

| | | |
|---------|---|---|
| SCFM | = | Standard cubic feet per minute (at 70°F, 29.92" Hg) |
| CFM | = | Indicated reading of the instrument |
| P_a | = | P_f = Actual operating pressure in "Hg |
| P_o | = | P_{std} = Original pressure at calibration in "Hg |
| μ_a | = | μ_f = Actual operating viscosity in micropoises |
| μ_o | = | μ_{std} = Original calibration viscosity in micropoises |
| t_a | = | T_f = Actual operating temperature in °F |
| t_o | = | T_{std} = Original temperature at calibration °F |

Meriam Incline Wall Manometer Adjustments for Calibration Readings

The instrument is first aligned such that the indicating fluid of specific gravity = 1.0, reads appropriately (i.e., zero) when the adjusting knobs are set for standard operating conditions of 70° at 29.92 "Hg. The outer dial of the compensator is set to actual pressure at the upstream tap of the LFE primary. The temperature adjustment knob is then aligned with the reference pointer. The flow meter reading is now expressed in SCFM for the operating temperature and pressure.

Standard Volumetric Flow Agreement for WM and LFE Calculation

Q_s was then compared to the values read on the WM as standard cubic feet per minute (SCFM) which compared well. This value agreed with the calculation made above where the WM reading corrected by its calibration adjustments yielded a value of $Q_s = 1073$ SCFM.

Field Calibration

Now that a check on the LFE calibration had been made, a calibration must be made under field conditions (i.e., by removal of the LFE and installation of the cylindrical filter assembly). In comparing the flow rate measurements at the LFE inlet to the flow rate at discharge measured by the Pitot tube, it was determined that a “leak factor” had to be accounted for. The leak was likely to be located between the fan shroud and the Pitot tube near the end of the exhaust pipe. The UHVAS flow calibration equation was derived from the plot of Figure I-2 below.

The calibration equation is:

$$Q_{UHVAS} \text{ (ft}^3\text{/min)} = 0.8997(Q_{Pitot}) - 50$$

Thus, $0.8997 \cdot Q_{Pitot}$ is converted to the relation:

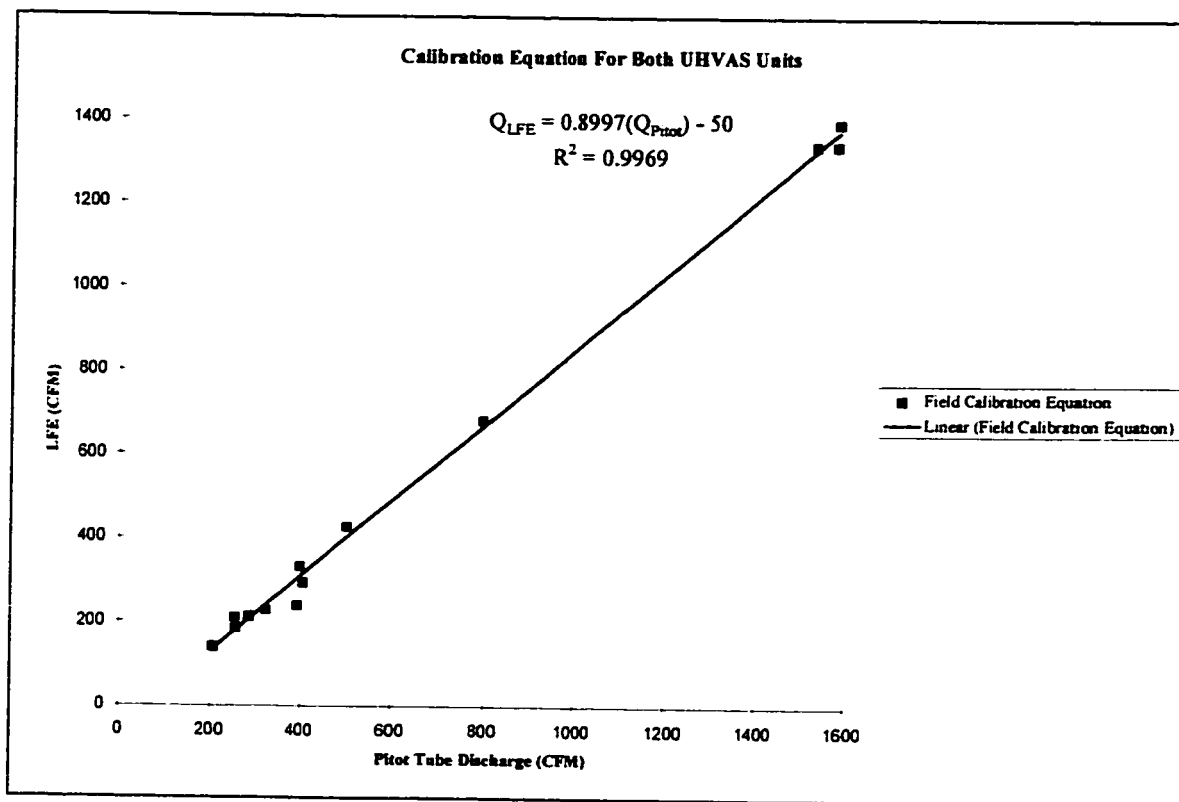
$$729 \cdot (P_{Pitot-field})^{1/2}$$

and the final form of the field calibration equation (E_{qField}) in a convenient form of m^3/hr as shown below:

$$E_{qField} = Q_{UHVAS} \text{ (m}^3\text{/Hr)} = 1.7 \cdot [-50 + 729 \cdot (P_{Pitot-field})^{1/2}]$$

where the constant of (-50) may represent a “leak factor” (i.e., our change in mass flow rate from inlet to discharge).

Figure I-2: UHVAS Field Calibration Equation



Field Operations Overview

Discharge flow leakage was significantly reduced in the system by sealing the connection between the cylindrical filter base and the assembly housing with vinyl tape. Anticipating this requirement, the same taping procedure was followed during calibration.

Power was provided by portable diesel generators towed to the site. These rugged generators provided continuous power 24 hours per day for the seven-day experiment. Due to the elevated wind conditions and dust generated by soil removal equipment, access to Lot 37 was restricted by the project's health physicist charged with the safety of the Taranaki work force. The concentration of $^{239+240}\text{Pu}_{\text{Air}}$ during these conditions was

calculated to be 13% above the DAC according to the Health Physicist on duty and restricted travel was ordered for movement in and out of the Lot 37 area. This restriction required the use of a Class I vehicle protecting the occupants by a full HEPA filtered cabin in order to service the experimental instruments on Lot 37.

The UHVASs ran for extended hourly periods with only occasional monitoring and d_p measurement readings for the data analysis. Although typical filter changes were infrequent, significant dust loading did occur with windy conditions at experimental sites due to bare soil conditions and were consequently changed based upon dust loading. The effectiveness of the UHVAS enhanced the collection of low-level aerosol air activity.

LLNL UHVAS Protocol (Shinn 1997)

1. Use Whatman 41 cellulose fiber filters for ease of dissolution in chemical analysis. Cut filters from roll in a laboratory environment with clean paper on the laboratory bench. Minimize handling of the filters and wear rubber gloves if possible. Allow approximately 10 cm overlap of the circumference of the cylindrical filter holder. This gives an effective filter surface area of 1.0 m².
2. Load the cylindrical filter holders in a laboratory environment after wiping the filter holders with laboratory alcohol. Do not use water as corrosion may occur before the water dries. Use two people to load the filters and use closure bands with tape on the under side to eliminate filter tears. There should be two bands, one on top and bottom; add a third band around the middle when in the field, and wash the third band in field with laboratory alcohol. Locate the stored components of the UHVAS system stored in footlockers or crates (i.e., exhaust, Pitot tube, and spare filter assemblies).
3. The UHVAS motors can be powered on 3-phase 208V to 3-phase 480V, check motor for wiring instructions. If rewiring, check motor direction of rotation

before starting an experiment. Never test run the blowers without a filter or artificial load; the motors will quickly burn out. An artificial load may be just a cardboard disk with a 15 cm hole in the center (usually shipped with each motor). Use the steel ring as a hold down of the cardboard disk. The motors and belts should be inspected before starting an experiment. A little belt wear is normal, and the pulleys can be adjusted as necessary. The fan axle bearings should be lubricated with automotive grease periodically, but wipe off excess grease to reduce unwanted collection of particles. Spare motors are kept on hand but will usually change the fan speed.

4. Locate the UHVAS at the desired sampling site in a position that will be away from the exhaust drift from the generator. This may require relocation of the UHVAS or the generator if the prevalent winds are not known initially. The range of trajectories effecting a sample is taken to be about 100 m (75% within 65 m and 90% within 175 m). Install the solid pipe exhaust section onto the blower exhaust by means of a short rubber pipe link and steel clamps. Add the long flexible exhaust pipe downstream of the solid pipe. Install the Pitot tube in the exhaust end of the solid pipe through the hole provided. The number of the Pitot tube should match the number written on the motor power switch. The Pitot tube points upstream in the exhaust flow.
5. The pressure is read with a manometer in the range from $p = 0 - 4$ cm of water pressure. The dial manometer provided is calibrated in inches of water, and has a range from 0 - 1 inch. Occasionally a new filter flow will start off-scale of this manometer but never greater than $p = 1.2$ inches (look for a filter leak if this happens). The "Magnehelic" dial manometers and Pitot tubes are stored in footlockers prior to installation. The calibration of the Pitot tube and UHVAS combination is: $Q \text{ (m}^3\text{/h)} = 1240 (p^{0.5}) - 84$, and the manometer p is in inches (at 200 m altitude).

- Note: It is possible but not recommended that a disk filter (approximately 48.5 cm diameter) can be mounted directly on the plenum screen in place of the cylindrical filter holder, by using the steel ring as a filter hold down. In this case, tape must be placed around the inner band of the plenum screen; the disadvantage is that there will be lower flow discharges.

Data Analysis

Table I-4A and I-4B of Appendix I-A lists the UHVAS data collected in the field. Following significant data reduction yields summary Table I-5 for both the November and March expeditions shown below.

Table I-5: Plutonium Resuspension at Taranaki

COMPARISON OF CONTROL AND CLEANED SITES

ULTRAHIGH-VOLUME AIR SAMPLERS, NOVEMBER 1996 & MARCH 1997

| | Control Site | Cleaned Lot 37 | Cleaned Lot 19 | Re-deposition Lot 18C |
|---|-------------------------|---------------------------|--------------------------|--------------------------|
| | FW | FNE | FN | North of FN |
| ²³⁹⁺²⁴⁰ Pu Soil Activity | 4.5 Bq/g | 2.8 Bq/g | 1.3 Bq/g | 2.6 Bq/g |
| Soil Depth ¹ | 2.0 cm | 1.0 cm | 1.0 cm | 1.0 cm |
| ²⁴¹ Am Deposition ² | 12.0 kBq/m ² | 5.5 kBq/m ² | 1.18 kBq/m ² | 5.9 kBq/m ² |
| Pu/Am Ratio in Air Samples | 9.9 | 6.9 | 16.5 | 13.2 |
| Pu _{Air} (Elevated Wind) | 80.0 µBq/m ³ | 1830.0 µBq/m ³ | 91.0 µBq/m ³ | 178.0 µBq/m ³ |
| Pu _{Air} (Normal Wind) | 17.0 µBq/m ³ | 11.0 µBq/m ³ | 6.0 µBq/m ³ | 14.0 µBq/m ³ |
| TSP (Elevated Wind) | 27.0 µg/m ³ | 963.0 µg/m ³ | 22.0 µg/m ³ | 54.0 µg/m ³ |
| TSP (Normal Wind) | 9.0 µg/m ³ | 14.0 µg/m ³ | 7.0 µg/m ³ | 10.0 µg/m ³ |
| ²³⁹⁺²⁴⁰ Pu _{Air} Activity (Elevated Wind) | 3.0 Bq/g | 1.9 Bq/g | 4.1 Bq/g | 3.3 Bq/g |
| ²³⁹⁺²⁴⁰ Pu _{Air} Activity (Normal Wind) | 1.9 Bq/g | 0.79 Bq/g | 0.90 Bq/g | 1.5 Bq/g |
| Resuspension Factor (Elevated Wind) | 6.6 E-9 m ⁻¹ | 333.0 E-9 m ⁻¹ | 4.7 E-9 m ⁻¹ | 2.3 E-9 m ⁻¹ |
| Resuspension Factor (Normal Wind) | 1.4 E-9 m ⁻¹ | 2.0 E-9 m ⁻¹ | 0.32 E-9 m ⁻¹ | 0.19 E-9 m ⁻¹ |

¹ Depth which includes 95% of plutonium.

² Americium measured from vehicle by *in situ* gamma spectroscopy by ARL.

AEROSOL PARTICLE SIZE DISTRIBUTION (APSD)

INTRODUCTION

The purpose of this study was to characterize the distribution of Total Suspended Particulate (TSP) aerosols resuspended at Taranaki by natural and mechanical processes. Two methods were utilized with the Climet 208C optical particle counter. In this study, a comparison of the “manual” counting method is made to a refined “automated” technique utilizing the same instrument modified by the addition of a Particle Sizing Amplifier (PSA), Pulse Height Analyzer (PHA), and computer-controlled data storage.

In the manual method, the Climet’s internal comparator circuitry bins the data according to a predetermined size threshold for five ranges. The ranges are 0.5 μm to <1 μm ; 1 μm to < 3 μm ; 3 μm to < 5 μm ; 5 μm to < 10 μm ; and 10 μm to < 25 μm . The number displayed is determined by a range of interest from an operator panel selector switch for the sampling period of one or four minutes. Although each range may be viewed independently following a sampling run, all ranges are represented for a single sampling period by setting the selector switch to the desired range of interest. This method limits the number of particles displayed to those that lie between the threshold limits (i.e., Threshold Limit $\leq \Sigma N <$ Next Threshold). The resultant is not a clear representation of the aerosol distribution present as this hardware severely limits the ability to determine distribution parameters (i.e., the geometric mean equivalent physical particle diameter μ_g , and geometric standard deviation σ_g).

In the automated method, continuous sampling over the instrument's limits is accomplished without size threshold discrimination. The only limitation of this method is the resolution of the distribution based on the number of channels subdividing the range. This is primarily due to signal voltage amplification exceeding the limits of the PHA. The limitation is therefore only relative to the desired size range of interest predetermined by PHA calibration. Therefore, the limitation does not restrict the performance for particles measured in the respirable range of resuspended aerosols, i.e., $\leq 10 \mu\text{m}$.

1. The manual method may be used to compare with the automated method for the detection of particles in the range of $10 \mu\text{m}$ to $25 \mu\text{m}$ by logging any relative observations. This larger aerosol range does not have any particular health physics consequences, therefore the option to use these additional data was not chosen. One present technique for acquiring size distribution data is accomplished via cascade impactors. Data from the November expedition are presented in Table II-A below. The large geometric standard deviations are primarily due to the collection efficiency of the impactor stages as the particle size approaches the stage cut-off limit. It is also not uncommon to have larger GSDs as the data is fit by a single log-normal distribution function for the wide range of $0.5 \mu\text{m}$ to $10 \mu\text{m}$.

Table II-A. Percent Mass TSP of less than indicated size from Cascade Impactor Filters

| Site | FW Nov. 14-19 | FNE Nov.16-18 | FNE Nov.16-18 | FNE Average | |
|-----------------|--|---------------|---------------|-------------|-------------|
| TSP (mg) | 73.2 | 2946.0 | 2422.0 | 2684.0 | |
| Stage | Percent Mass of TSP less than indicated size | | | | Median Size |
| Backup | 0.4 | 23.0 | 19.8 | 21.4 | 1.1 |
| 5 - 8 | 24.6 | 6.4 | 5.4 | 5.9 | 2.0 |
| 4 - 5 | 19.3 | 10.1 | 11.9 | 11.0 | 3.3 |
| 3 - 4 | 26.6 | 22.0 | 26.6 | 24.3 | 7.0 |
| 2 - 3 | 29.1 | 38.5 | 36.3 | 37.4 | |
| | Cumulative Percent less than indicated size | | | | |
| Backup | 0.4 | 23.0 | 19.8 | 21.4 | 1.1 |
| 5 - 8 | 25.0 | 29.4 | 25.2 | 27.3 | 2.0 |
| 4 - 5 | 44.3 | 39.5 | 37.1 | 38.3 | 3.3 |
| 3 - 4 | 70.9 | 61.5 | 63.7 | 62.6 | 7.0 |
| 2 - 3 | 100.0 | 100.0 | 100.0 | 100.0 | |
| Median Diameter | 3.98 ± 0.06 | 4.65 ± 0.13 | 4.68 ± 0.11 | 4.67 ± 0.12 | |
| GSD | 2.45 ± 0.06 | 5.56 ± 0.36 | 4.15 ± 0.20 | 4.77 ± 0.26 | |

In summary of the Cascade Impactor data, the geometric mean or (median diameter) of the TSP collected ranged from 3.98 to 4.68 with geometric standard deviations (GSDs) ranging from 2.45 to 4.77. The “high” GSDs are due to the “smearing” of data on the mass basis. The mean diameters however compared favorably to the manual count data for the same period.

METHODS

Sampling System

The components of the APSD experiment are:

- Climet 208C Optical Particle Counter (CI-208). Aerosol detector-counter, see Figure II-4, Appendix II-A. Quantity (1)
- Nuclear Data Inc. Model 82-0176 Logarithmic Particle Sizing Amplifier (PSA); used in conjunction with the Climet-PHA. Quantity (1)
- Davidson Model 1056 Multi-Channel Scaler/Pulse Height Analyzer; used in pulse height analyzer mode, to keep tally of the counts associated within a specific voltage range determined by the instruments. Quantity (1)
- Serial I/O Cable for standard RS-232 Port connection with 15-pin to 9-pin adapter; used for mating the PHA output port to the PC serial port. See Appendix E; Table II-5. Quantity (1)
- Vertical Stabilizer; used in conjunction with the sampler to allow sampling response to changes in wind direction. Quantity (1)
- Isokinetic Sampling Tips; each used for differing wind speed conditions. See Figure II-1, Appendix II-B. Quantity (3)
- 440 - 120 VAC Transformer; used to convert Australian power for the CI-208. Quantity (1)
- 486 Portable Personal Computer; used for data storage. See Appendix II-D, Download Code. Quantity (1)

The Climet sampling inlet protrudes vertically upward through the instrument case. A tripod sample collector stand is mounted to the case over the inlet which rises approximately 10 inches. One of three isokinetic sampling tips is mounted to the end of a ¼ inch ID copper tube with a gradual radius (r) bend ($r \approx 6$ inch) of 90° normal to the sampling plane such that sampling occurs parallel to ground level. A vertical stabilizer is mounted to the collection tube and the assembly is positioned through the tripod and connected to the Climet sampling inlet. With the sample collection assembly fixed atop the Climet case, the sampler remains free to swivel 360° maintaining its position facing the prevailing wind by response of the vertical stabilizer to changes in wind direction. The complete isokinetic sample collection assembly configuration is shown in Figure II-1 of Appendix II-A.

APSD Integrated Electronic Component Configuration and Operational Characteristics

The Climet signal voltage output ranges from 0 V to 10 V. The PHA accepts signals from 0 V to 4 V input, therefore a logarithmic amplifier (PSA) is used in serial from the Climet output to scale the signal voltage appropriate for PHA input. The PHA contains a built-in printed circuit board dedicated for serial input/output (I/O). The PHA is connected to the PC serial port via a 15-pin to 9-pin mating cable. A basic computer program was written to accept the data via serial input downloaded from the memory as the PHA internal timing circuit stops on present live time which is the user preset count time.

The PHA allows two modes of memory download operation: (1) Manual, by Push Button; or (2) Automatic, by computer control. There are advantages to both modes.

The PHA has eight memory channels. Each may be selected for sequential sampling by selection of the next channel, clearing the memory buffer by pushing the reset button, and beginning a new counting sequence by pushing the accumulate button. The download operation then requires the selection of the memory channel of interest followed by pushing the read-out (R/O) button. The advantage of this mode allows the user to examine the count displayed by the Climet digital display and record this data in addition to the data stored in the PHA.

In contrast, the advantage to using mode (2) is that it reduces experimental error caused by accidental clearing of the memory buffer as the data are automatically downloaded to the PC's memory buffer awaiting final storage by naming the data file. This may be done while the counting sequence is continued by simply pushing the PHA's reset button and beginning a new counting sequence by pushing the accumulate button. In this mode, the sample sequencing requires one less step and consequently a reduced sampling dead-time of approximately 1 second, (s). The experimenter may then return to the bookkeeping operation of naming the previous data file.

Calibration Overview

Several sizes of poly-styrene latex (PSL) spheres were used as the calibration aerosols. These microsphere standards are packaged in aqueous suspensions in 15 ml dropper-tip bottles which are measured by the manufacturers NIST traceable optical microscopy methods and certified. In calibrating the APSD sampling system, each standard is prepared by mixing three drops per 250 ml of deionized water and generated by a nebulizer pressurized by compressed air. The aerosol is passed over the Climet inlet

in room air at a approximate distance of 5 inches from the Climet inlet to allow some aerosol “drying” enroute and to avoid the water vapor domination of the low end channels. This was an additional reason to eliminate the data below 0.6 μm . Each run of the calibration was done with the following nominal PSL sizes: $0.607 \pm 0.02 \mu\text{m}$, $1.07 \pm 0.02 \mu\text{m}$, $3.12 \pm 0.03 \mu\text{m}$, and $7.3 \pm 0.05 \mu\text{m}$.

The PHA gain is adjusted to place the signal within the range of the analog to digital converter (ADC) full-scale analog input range of (0 V to 4 V). The Lower Level Discriminator (LLD) is adjusted to zero and the Upper Level Discriminator (ULD) is set at 100% of the ADC full-scale analog input range. As the LLD setting would normally be set above the level of input noise, this factor was accounted for in the data reduction and therefore all event signals from the Climet were accepted with the zero setting.

The PSA is used in logarithmic (log) mode with coarse gain settings of (1, 2, 4, 8) which precedes the log conversion stage and ten-turn fine gain range of (1 to 6) is then adjusted such that a well-defined Gaussian peak is seen in a specific channel of PHA. The log-bias of the PSA 0 V to 100 mV establishes the lower-level threshold of the log converter with a range of 0 V to 1 V. This shifts the log converter operating point and suppresses the input pulse level the same amount. The log conversion ratio is 0.5 V per decade. The adjustment of the PSA gain is continued until all PSL peaks are clearly defined corresponding to their respective channels such that the PHA channel range from 1 to 127 accommodates all calibration sizes allowing for sizes above and below the calibration sizes to be detectable.

Climet CI-208 Particle Detection

The flow rate of the CI-208 is 0.25 cfm @ 1" H₂O differential pressure. A schematic diagram of the airflow through the system is depicted in Figure II-2, Appendix II-A. As the sample flow enters the sensor chamber, purge air that has been drawn through a filter is admitted free of particles greater than 0.1 μm. This filtered flow acts as a sheath surrounding the sample flow preventing particles from scattering and recirculating as they pass through the view volume of the optical chamber (see Figure II-3, Appendix II-A) inhibiting multiple counting. Light emitted from a halogen bulb is scattered by the passing particle which is reflected by the elliptical mirror at the primary focal point over 5.1 Steradians (15° to 105°). The reflected light is transmitted to a photomultiplier tube (PMT) located at the secondary focal point. The PMT produces a low-level current output signal of amplitude equal to the area of the particle. The system's electronics convert this signal to the output displayed on the digital counter as the number of particles per cubic foot sampled. A three-position multiplier switch (1, 10, 100) prevents the rollover of the five-digit display with a capability of 1×10^7 particles per cubic foot display capacity.

Pulse Generator Calibration Tests

An EG&G ORTEC[®] Model 448 Research Pulser was used as a surrogate Climet output as a calibration check on the PSA and PHA subsystem. The 448 is a highly stable precision pulse generator that enables a discrete signal to be passed into the PSA such that the output signal is placed in a single channel of the PHA. This provided a complete

calibration data set under laboratory conditions verifying the voltage range represented by field data using the same gain and log-bias settings as depicted by the calibration curve in Figure II-5 Appendix II-A. The equation in Figure II-5 represents the PHA channel as a function of PSA output voltage. The PSA performs the necessary voltage scaling for PHA input meeting the analog full-scale range of (0 V - 4 V).

CI-208 Internal Comparator Calibration Tests

An additional calibration check was performed to determine the voltage range associated with the CI-208's internal comparator circuit. This required partial disassembly of the unit and connecting an oscilloscope to the D6519 logic card and reading the signal voltage produced by the CI-208 optics for the respective PSLs that were known to be within the five comparator range settings (i.e. 0.5 μm to 1.0 μm ; 1.0 μm to 3.0 μm ; 3.0 μm to 5.0 μm ; 5.0 μm to 10 μm ; and $\geq 10 \mu\text{m}$).

The output voltages produced by the corresponding PSL are shown in Table II-6 which is graphically represented in Appendix II-B; Figure II-6.

Table II-6. CI-208 Internal Comparator Calibration Voltages

| Comparator Range (μm) | Vout (mV) | Line Equations $F(x) = V_{\text{out}}; x = \text{PSL}$ | PSL (μm) | Output Voltage corresponding to PSL Vin PSA (mV) |
|---------------------------------------|--------------|---|--------------------------|--|
| 0.30 | 24.30 | | | |
| 0.50 | 62.00 | $y_1 = 188.5x - 32.25$ | 0.398 | 42.8 |
| 0.50 | 62.00 | | | |
| 1.00 | 151.80 | $y_2 = 179.6x - 27.8$ | 0.607 | 81.2 |
| 1.00 | 151.80 | $y_3 = 387.85x - 236.1$ | 1.07 | 178.9 |
| 3.00 | 927.50 | $y_3 = 387.85x - 236.1$ | 2.01 | 543.5 |
| 3.00 | 927.50 | | | |
| 5.00 | 2456.00 | $y_4 = 764.25x - 1365.3$ | 3.12 | 1019.2 |
| 5.00 | 2456.00 | | | |
| 10.00 | 9780.00 | $y_5 = 1464.8x - 4868.0$ | 10.0 | 9780.0 |

Field Calibration

The APSD sampling system was calibrated using the PSL aerosols generated with the compressed air nebulizer in room air within ARL's gamma counting laboratory located in Maralinga Village. The nonlinearity of the calibration curve in the low-voltage region of the optics for sizes 0.5 μm to 3.12 μm is characteristic of the CI-208. The full-scale range is best represented by segmented curves between the calibration points. Three calibration equations are used to represent the full-scale range of the APSD sampling system as shown in Figure II-7.

Substitution of channels 1 and 127 of the PHA yields the full-scale range limits of observation as 0.4 μm to 11 μm . The results of the PSA and CI-208 Internal Comparator Calibration voltage tests have verified that the field data collected are within the full-scale range of the calibration. Although the lower limit of the calibration at 0.4 μm is near the limit of detection for the instrumentation, the data below 0.6 μm is considered unreliable. These values would have been discriminated by the LLD setting of the PHA had this been elected. As mentioned above, the data below the first calibration PSL size of 0.6 μm are treated as being within the noise of the system and were therefore discarded in the data reduction process.

Field Protocol for Sample Collection

The field setup location for the November 1996 expedition was control site (FW) for the resuspension study. FW was selected as the control site due to a low surface activity level of 12 kBq/m² which is the cleanup criteria for Taranaki. In March 1997, the experiment sites were Lot 18C and Lot 19. As previously mentioned, the November experiment was conducted using the manual counting method and the March experiment utilized the automated technique.

Manual Counting Protocol

1. A Diesel generator was used to provide all electrical power for site instruments.
2. 440 VAC 50 Hz was converted by a transformer to 120 VAC 60 Hz required for the CI-208. This requirement was needed solely for the CI-208 as the PHA, PSA, and laptop computer will function at either voltage.

3. One Isokinetic Sampler was selected based on approximate wind speed. For light and variable conditions < 2 m/s, the larger sampler was used; for medium wind speeds 2 to 4 m/s, the midsize tip was used; and the small tip was used for windy conditions > 4 m/s. These tips were previously developed by LLNL personnel and details regarding the tip dimensions and flow dynamics will not be presented in this discussion.
4. The CI-208 power is turned on and allowed to warm-up for approximately 30 minutes prior to adjusting the internal calibration adjustment knob. An internal calibration chopper indicates proper optic calibration with an indicator light on the panel. This is accomplished by the PMT receiving light impulses of amplitude and frequency from the fiber-optic calibrator. (See Figure II-3 Appendix II-A). Note: During calibration mode, the air pump is not functioning.
5. Once calibration is achieved, the mode selector (i.e., size selector or calibrate mode) is set to the size region of interest and the carbon-vane air pump begins drawing airflow into the sampler. The differential pressure scale is then read and adjusted to a reading of maximum flow rate or 0.25 cfm.
6. The CI-208 time base selector (1 or 4 minute) was set to a 4-minute (min) count interval for the manual counting method.
7. During collection time, the ambient conditions were noted and logged along with the time, date, and data (i.e., number of particles counted per ft³).

Automated Counting Protocol

For the automated counting sequence, steps 1-5 are followed with the following protocol changes for 6 and 7, designated as 6* and 7* respectively, with the addition of 8*.

- 6*. The Alarm Level selector switch is set to Audible which overrides the Time Base selector allowing continuous sampling. Counting time is then controlled by the PHA which was set for the desired time interval. The PHA allows time intervals from 10 s to 40,000 s (11.11 Hr), which provides added flexibility for the count time limitations of the manual method. The mode of time selection for these experimental runs was varied between 400 s (6.67 min) and 1000 s (16.67 min).
- 7*. The rear panel of the PHA has three settings (Auto, Semi-auto, or Manual) which control the data download to the PC. When set to Auto, the data are downloaded to the computer via a Basic software program when the PHA preset live time has been reached and the unit returns to accumulate mode. In Semi-auto or Manual mode, the data are downloaded by pushing the R/O button. If the switch is set to Semi-auto, the unit goes to stop after R/O. The memory channel will be reset if the switch is set to Auto or Semi-auto and the Reset switch on the rear panel is selected. Otherwise (i.e., when the switch is set to manual) the memory must be cleared prior to accumulation or data will be added to the memory.
- 8*. The Download Code of Appendix II-D produces a data file of two columns of data (channel and count). The program then requests the input of a file name. The file name is then written in the first field of the data file with the time of download taken from the PC's internal clock. The clock time corresponds to Pacific Standard Time

(PST) when the program was written therefore all recorded sampling indicates PST date and time.

Data Reduction

Manual Sample Collection: November 1996.

Tables II-7A, II-7B, and II-7C below represent the data collected from the CI-208 display panel. For purposes of comparing the one-minute and four-minute sampling runs, the four-minute run data are reported per minute.

Taranaki Field Notes: 21 November, 1996

Site: FW; Sampling Height above ground level (AGL) = 1.46 m

Table II-7A: Averages of Four 1-Minute Runs and Three 4-Minute Runs at FW Site

| Sample | Average of Four 1-Minute Runs Reported: $\bar{N} \text{ min}^{-1}$ See Table II-7B | 1-Minute Average of Three 4-Minute Runs Reported: $\bar{N} \text{ min}^{-1}$ See Table II-7C |
|--------------------|--|--|
| Wind Speed | Strong | Strong |
| Isokinetic Sampler | Medium | Medium |
| Comparator | $T_{\text{local}} = 08:30-08:45$ | $T_{\text{local}} = 08:45-09:45$ |
| Threshold | $[\Sigma \bar{N} (R1-R4)/4]^a$ | $[\Sigma \bar{N} (R5-R7)/3]^a$ |
| 0.5 | 23091.0 | 17068.0 |
| 1.0 | 9392.0 | 6473.0 |
| 3.0 | 402.0 | 1522.0 |
| 5.0 | 70.0 | 257.0 |
| 10.0 | 16.0 | 39.0 |

^a N = Number of particles sampled in the threshold range for the given sample period.
R = Run number (e.g., R-1, "Run 1," etc.).

Table II-7B: Four 1-Minute Sampling Runs at FW Site

| Sample | 1-Minute Run | 1-Minute Run | 1-Minute Run | 1-Minute Run |
|--------------------|----------------------------|----------------------------|----------------------------|----------------------------|
| Wind Speed | Strong | Strong | Strong | Strong |
| Isokinetic Sampler | Medium | Medium | Medium | Medium |
| Comparator | T _{local} = 08:30 | T _{local} = 08:35 | T _{local} = 08:40 | T _{local} = 08:45 |
| Threshold | [N R-1] ^b | [N R-2] ^b | [N R-3] ^b | [N R-4] ^b |
| 0.5 | 25454.0 | 23873.0 | 22623.0 | 20415.0 |
| 1.0 | 10564.0 | 9262.0 | 9334.0 | 8408.0 |
| 3.0 | 266.0 | 250.0 | 731.0 | 361.0 |
| 5.0 | 159.0 | 23.0 | 73.0 | 25.0 |
| 10.0 | 36.0 | 5.0 | 20.0 | 1.0 |

^b N = Number of particles sampled in the threshold range for the given sample period.
R = Run number (e.g., R-1, "Run 1," etc.).

Table II-7C: Three 4-Minute Sampling Runs at FW Site
Data Reported per Minute for Comparison

| Sample | 4 Minute Run | 4 Minute Run | 4 Minute Run |
|--------------------|----------------------------------|---------------------------------|----------------------------------|
| Wind Speed | Strong | Strong | Strong |
| Isokinetic Sampler | Medium | Medium | Medium |
| Comparator | T _{local} = 08:45-09:05 | T _{local} = 09:05-9:25 | T _{local} = 09:25-09:45 |
| Threshold | [\bar{N} R-5] ^c | [\bar{N} R-6] ^c | [\bar{N} R-7] ^c |
| 0.5 | 20864.0 | 16047.0 | 14293.0 |
| 1.0 | 8518.0 | 5745.0 | 5157.0 |
| 3.0 | 548.0 | 232.0 | 3785.0 |
| 5.0 | 52.0 | 248.0 | 472.0 |
| 10.0 | 15.0 | 49.0 | 54.0 |

^c \bar{N} = Average Number of particles min⁻¹ sampled in the threshold range for the given sample period converted for comparison purposes to 1 min runs (i.e., actual data collected is 4 \bar{N} in each threshold range).

R = Run number (e.g., R-1, "Run 1," etc.).

The manual sampling data collected in March 1997 are presented in Tables II-8A, and II-8B below in the *Taranaki Field Notes* section. These data sets may be compared to the automated data collected simultaneously, although manual data sets were not collected for all runs as this was not the primary focus of the experiment. Therefore, only the data sets corresponding to the manual data presented in Table II-8A and Table II-8B may be compared.

Taranaki Field Notes

Taranaki Field Notes: 21 March 1997
 Site: Lot18C; Sampling Height AGL = 1.46 m

Table II-8A: Four 1-Minute Sampling Runs at Lot 18C

| Sample | 1-Minute Run | 1-Minute Run | 1-Minute Run | 1-Minute Run |
|--------------------|---|---|---|---|
| Wind Speed | Calm | Calm | Moderate | Moderate |
| Isokinetic Sampler | Large | Large | Large | Large |
| Comparator | T _{local} = 14:33 ^a | T _{local} = 14:33 ^a | T _{local} = 16:24 ^a | T _{local} = 16:24 ^a |
| Threshold | [N R-5] ^{b,c} | [N R-5] ^{b,c} | [N R-6] ^{b,c} | [N R-6] ^{b,c} |
| 0.5 | 6107.0 | 6340.0 | 6328.0 | 7008.0 |
| 1.0 | 1870.0 | 2099.0 | 2539.0 | 8361.0 |
| 3.0 | 82.0 | 129.0 | 787.0 | 780.0 |
| 5.0 | 8.0 | 49.0 | 60.0 | 65.0 |
| 10.0 | 2.0 | 3.0 | 30.0 | 14.0 |

^a T_{local} is reported at the end of the APSD sample collection period as logged in the PC Data file corresponding to PSA Live Time.

^b N = Number of particles sampled over the threshold range for the given sample period.
 R = Run number (e.g., R-1, "Run 1," etc.).

^c Run number used to compare CI-208 Display data to APSD Lot18C Data collected simultaneously (i.e., Lot 18C R-5; Lot18C R-6, respectively).

Taranaki Field Notes: 22 March, 1997
 Site: Lot19; Sampling Height AGL = 1.46 m

Table II-8B: Four 1-Minute Sampling Runs at Lot 19

| Sample | 1-Minute Run | 1-Minute Run | 1-Minute Run | 1-Minute Run |
|--------------------|---|---|---|---|
| Wind Speed | Moderate | Moderate | Moderate | Moderate |
| Isokinetic Sampler | Large | Large | Large | Large |
| Comparator | T _{local} = 13:51 ^a | T _{local} = 14:00 ^a | T _{local} = 15:13 ^a | T _{local} = 15:21 ^a |
| Threshold | [N R-1] ^{b,c} | [N R-2] ^{b,c} | [N R-3] ^{b,c} | [N R-4] ^{b,c} |
| 0.5 | 1707.0 | 2108.0 | 2722.0 | 2516.0 |
| 1.0 | 597.0 | 1900.0 | 1554.0 | 1228.0 |
| 3.0 | 20.0 | 100.0 | 171.0 | 52.0 |
| 5.0 | 2.0 | 28.0 | 2.0 | 4.0 |
| 10.0 | 1.0 | 0.0 | 1.0 | 0.0 |

^a T_{local} is reported as the end of the APSD sample collection period as logged in the PC Data file corresponding to PSA Live Time.

^b N = Number of particles sampled over the threshold range for the given sample period. R = Run number (e.g., R-1, "Run 1," etc.).

^c Run number used to compare CI-208 Display data to APSD Lot18C Data collected simultaneously (i.e., Lot 19 R-1; Lot19 R-2; Lot 19 R-3; Lot 19 R-4 respectively).

Automated Sample Collection: 21-23 March 1997

The sample runs collected in Lot 18C and Lot19 show a significant improvement in the particle size distribution detail as compared with the manual methodology which is hardware limited. Although the technology used in this experiment is somewhat dated (20-25 years old), the system components proved to be quite field ready and reliable. The only required adaptation was instrument connection and communication for automated data collection.

The data analysis though somewhat complex, was adapted from (Shinn 1997), and earlier work by (Koval 1974) who employed the use of a PHA without a PSA in series from the particle counter. The methodology employed in these works calculates physical

Equivalent Spherical Diameter (ESD) of particulates known to be shaped irregularly. It was previously stated that the optics of the CI-208 produce a low voltage signal from the light absorbed by the PMT which was scattered by the “surface area” of the particle in the view volume of the optics chamber. The particle size distribution is derived from a volume density function for particles of spherical geometry from the number density sampled as determined by the particle counter.

In the work of (Shinn 1997) and (Koval 1974) the number density function is calculated as:

$$\Delta N / \Delta L \ln D \quad (1)$$

where $D = \text{ESD}$. The volume density function develops a bell curve. The volume density function Shinn used is defined as:

$$\Delta V / \Delta L \ln D \quad (2)$$

where the volume of particles sampled (V_p) with equivalent spherical diameter for the number of particles counted with the i^{th} ESD is given by the relation:

$$V_p = N_i \pi / 6 D_i^3 \quad (3)$$

Although Koval employed the use of a PHA his method yields little detail, in contrast to Shinn who relied on the CI-208 display data alone to develop similar distributions from (1) and (2).

The PSL sizes used in Koval’s calibration were 0.48 μm to 7.3 μm and depict the same nonlinearity for similar PSLs used in this study as seen in Figure II-7 Appendix II-A. Koval determined a linear calibration equation which yield several outliers over both the

low and mid-range of the data set. Koval's method assumes that the given channel corresponds to the center of a distribution of each nominal PSL size. Koval ignores the nonlinear response of the optics in the low-end range from the lower limit of the detector response up to approximately 3 μm (see Koval, 1974).

Due to this variance in the instrument response, the calibration method of determining the ESD that was used in this study proved to reflect the instrument's voltage response when the comparator voltage tests were made. These linear segmented calibration equation curves depicted in Figure II-7 Appendix II-A.

APSD methodology enhances the density function significantly as depicted in Figures II-8 through II-22 of Appendix II-B corresponding to the APSD runs of Lot 18C and Lot 19, respectively. In the author's attempt to explain the unusual density function depicted by the Taranaki data, it was found that conventional methods of parameter estimation were insufficient in defining the APSD. By conventional methodology, it is meant that distribution parameters are readily determined from the cumulative frequency distribution of the log-normally distributed aerosols as determined in numerous earlier environmental studies.

The conventional methodology determines the geometric mean $\mu_g = \exp(\mu_y)$ and the geometric standard deviation $\sigma_g = \exp(\sigma_y)$ of the distribution as calculated from (Aitchison and Brown 1969); in (Gilbert 1987):

$$\mu_y = \ln x_{0.50} \quad (3)$$

where the x subscript denotes the 0.50 percentile. The variance is then calculated as:

$$\sigma_y^2 = \{\ln[1/2(x_{0.50}/x_{0.16} + x_{0.84}/x_{0.50})]\}^2 \quad (4)$$

According to (Gilbert 1987), the mean and standard deviation of the log-normal distribution may be estimated by computing the values of (3) and (4) above as:

$$\mu_g = \exp(\mu_y + \sigma_y^2/2) \quad (5)$$

$$\sigma_g = \mu_g[\exp(\sigma_y^2) - 1]^{1/2} \quad (6)$$

where (5) and (6) are given by $x_{0.50}$ and $1/2(x_{0.50}/x_{0.16} + x_{0.84}/x_{0.50})$, respectively, as stated by Gilbert.

Gilbert adds that probability plotting is a “quick way” of evaluating whether the data are from a two-parameter log-normal distribution by linear regression fit through the data points. This is somewhat subjective since the straight-line fit to the data is done visually.

APSD Data Reduction

The volume density function was calculated such that the volume density equation became used is a percentage of particles in the given size interval:

$$N_i/\Sigma N_i \Delta V_i/\Delta \ln D_i \quad (7)$$

as it was found from the graphical representation that the distribution appeared to have multi-modal qualities. In an attempt to find the parameters of the distribution, the conventional plotting method described by Gilbert was tried with unsatisfactory results. If the distribution was solely defined by two parameters then the log probability straight line fit to the data would have proved successful. The APSD had a distinguishable “first” mode which is seen to occur on the rise toward the central tendency or “second” mode,

and a small “third” mode, which appeared near the upper third of the diameter range of the distribution.

Upon first examination of the distribution’s characteristics it was thought that the segmented linear calibration equations discussed earlier may have affected the shape. The non-linearity characteristic of the CI-208 voltage response suggest that some uncertainty in the calibration lies below the 2 μm range while the remainder of the range from 3 μm to + 10 μm remains linear and a power fit to the data yields similar calibration values for D_i .

RESULTS

Modeling

A graphical solution was employed to find that each of the APSDs could be approximated quite closely by fitting individual log-normal distribution functions with modeled parameters of μ_g and σ_g for each part of the distribution. It was found that in fact the entire distribution could be modeled by the summation of three log-normal distribution functions with their respective model parameters.

This model seems to describe the shape of the volume density function (VDF) quite well. In an attempt to understand why this model represents the data, further ad hoc procedures were explored. From a qualitative perspective, it appeared that a correlation may exist between wind speed and the peak amplitude of the density function. Exploring this hypothesis proved futile. It seems reasonable to assume that a greater density of large particles would be present under elevated wind speed conditions.

Attempting to explain the multi-modal qualities of the VDF it was hypothesized that the three underlying log-normal distributions of the VDF may be due to wind speed variations or gust driven response functions for the given sample period. Sustained gusting extending over a period less than that of the sample collection period may increase the TSP size enough to see a distribution “shape change” and drop off within the 10 min wind speed sampling interval giving rise to the vertical wind speed component and thereby increasing the number density of larger particles over the sampling period.

This hypothesis cannot be explored from this study due to the unavailability of short term wind speed averages and gust values corresponding to the APSD sampling times. An alternative to shorter wind speed averaging times would be to augment the APSD sampling system with its own wind speed sensors matched to the sample collection period by means of an additional PHA logging wind speed averaged over a fraction of the APSD collection period.

Tables II-9A and II-9B of Appendix II-F summarize the data for Lot 18C and Lot 19 respectively. Figures II-8 to II-22 are graphical representations of each distribution and are presented in Appendix II B.

The APSD model is given by the equation:

$$f_n(d_p, \mu_{gn}, \sigma_{gn}) = \kappa_n \cdot 2\pi^{-1/2} \cdot \ln^{-1}(\sigma_{gn}) \cdot \exp\{-1/2(\ln(d_p) - \ln(\mu_{gn}))^2 \cdot \ln^{-2}(\sigma_{gn})\} \quad (8)$$

where κ_n is scaling parameter for the model VDF and subscript (n) denotes the mode number (i.e., "First mode", etc.).

$$N_i / \sum N_i \cdot [\Delta V_i / \Delta \ln D_i] \approx \sum [f_1(D_i, \mu_{g1}, \sigma_{g1}) + f_2(D_i, \mu_{g2}, \sigma_{g2}) + f_3(D_i, \mu_{g3}, \sigma_{g3})] \quad (9)$$

where $N_i/\sum N_i$ is the fraction of particles of the corresponding i^{th} size denoted by spherical particle of diameter D_i .

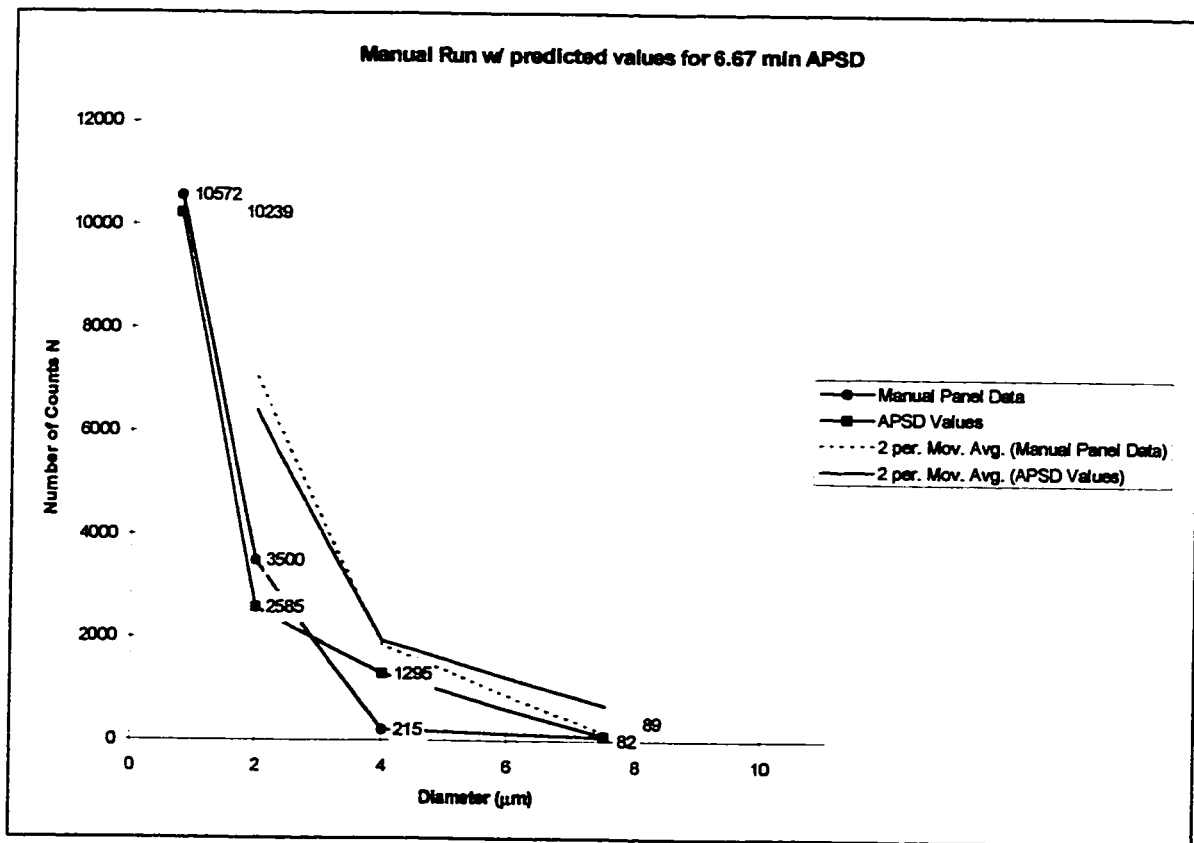
Each log-normal segment of the tri-modal distributions can be described by the following distribution characteristics as found in (Dennis 1976) and (Allen, 1975): A Count mode (d^*); Count median (d_g); Count mean (\bar{d}); Diameter of average area (d_a); Diameter of average mass (d_m); Area median (d'_a); Area mean (\bar{d}_a); Mass median (d'_m); Mass mean (\bar{d}_m). Each of these characteristics correspond consecutively for increasing particle diameters of the distribution.

The first mode of each distribution clearly dominates the distribution realized by its area percentage relative to the mixed distribution with the VDF. The VDF peak is formed by the second mode with the minor peak formed by the contribution of the third mode in most cases. The reason for the tri-modality of these Taranaki distributions is unclear. It may be due to the soil constituents particular to the desert area of Taranaki. Calibration of the instrument as well as sampling was conducted under conditions of less than 50% relative humidity therefore increased particle size due to air moisture is ruled out. Additionally the area has a small contribution of humus material per se. Further investigation of this and other data gathered may provide useful information as to the nature of these observations. A small fraction of the distribution may contain aggregates of soil material and fused plutonium but there is insufficient data to determine this.

Comparison of the Manual Count Method with APSD

Data were obtained by the manual counting method as previously described for the March expedition. As a general comparison for similar wind conditions, APSD Lot 18C R-5 was selected and the data compared is a 6.67 min predicted value from a 1 min run from the same run with panel data. Figure II-33 below illustrates the comparison of manual counts to APSD by converting the detailed APSD data to the threshold diameters (i.e., ranging) of the panel as determined by the size selector switch. Density comparisons will not made.

Figure II-33: Comparison of Manual Counts obtained with APSD Lot18C R-5



DISCUSSION

The likelihood of radioactive aerosols being a major contributor to the APSD data is qualitatively stated as a "low probability" when compared to the percent of the Pu concentration in air relative to the TSP. This is supported by the data collected in Part I of this study. As a background to the site, Lot 18C was an area of redeposition from wind erosion that was observed to have occurred over the four-month period from November 1996 to March 1997.

A side experiment was conducted in an attempt to collect a dust sample for analysis by other means (i.e., Scanning Electron Microscopy) of determining a size distribution for radioactive and nonradioactive constituents of the resuspended aerosols. Although this study will not be presented in the body of this paper, it is mentioned to add perspective to this work. A $^{239+240}\text{Pu}$ particle aggregate was collected and determined to be on the order of 10-15 μm based on a spherical geometry calculated from its activity which was determined from the ratio of $^{239+240}\text{Pu}$ to ^{241}Am found in a Taranaki soil sample obtained in November 1996.

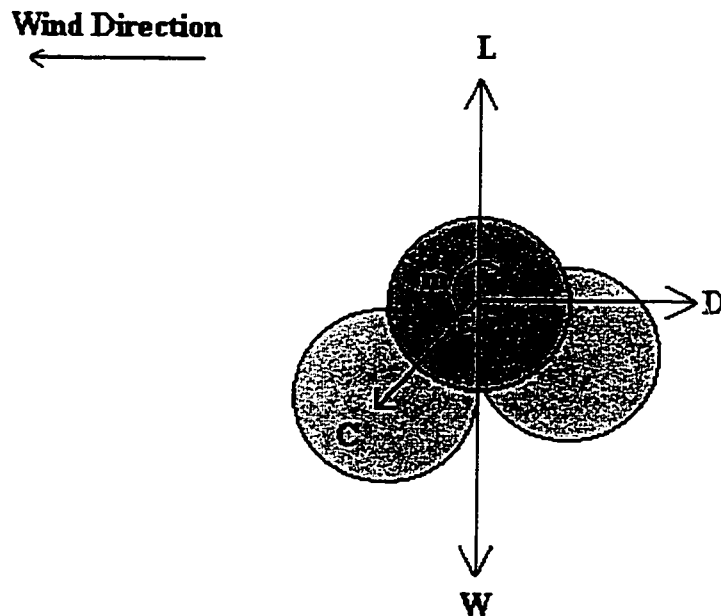
Due to the nature of the Taranaki being a site of safety shots, it is likely that an array of particle sizes may exist as aggregate forms. As in the case of the "hot particle" mentioned above, these aggregate forms may be either several smaller particles fused to metal or desert soil material as a result of these Vixen B safety shots. The work of (Pye 1987) shows that the traveling distance for small particles is quite large in contrast to much larger particles which will be discussed in the particle transport subsection.

Particle Transport

The factors affecting particle movement and consequently resuspension are dynamic in nature. "Aeolian dust transport involves three stages: (1) entrainment; (2) dispersion; and (3) deposition. The nature of wind sediment transport is controlled both by the nature of the airflow near the ground and by the properties of the ground surface over which the flow occurs" (Pye, 1987).

The forces acting on particles at rest are lift (L), drag (D), weight (W), moment (M), and interparticle cohesion (C) as discussed in (Pye, 1987) which is represented below.

Figure II-34: Forces acting on a particle at rest
Modified after Figure 3.1 in (Pye, 1987)



Many studies have been done over the years and the complete characterization of particle ejection from rest is complex. Drag is caused by friction retarding motion in the opposing direction. In the case of wind passing over a surface layer, the base of the flow is retarded at the interface of the surface and a thin boundary layer exists just above the surface where the velocity is zero. The height of this layer is referred to as the roughness height, z_0 . Variation in z_0 is dependent on ground cover and roughness objects.

As discussed in (Pye, 1987), z_0 had been found to be approximately 1/30 of the diameter of the particles on the surface as referenced in (von Karman, 1934; Prandtl, 1935; Bagnold, 1941). The net effect of ground cover on this boundary layer is to displace the height of the zero velocity plane upwards determined by the height of the roughness elements, their flexibility (as in the case of grasses), and permeability. This height is referred to as the zero plane displacement, (d).

According to Pye,

Above the height of zero velocity the time-averaged forward velocity (U) of the wind in a neutral atmosphere turbulent boundary layer increases approximately logarithmically with height. The slope of the logarithmic wind profile is defined by the Prandtl-von Karman equation:

$$u_* = kU / \log_n(z/z_0)$$

where

k is the von Karman constant which varies with temperature gradient but is usually taken to be 0.4

U is the wind velocity at a height z above the ground

z_0 is the height at which the velocity is zero

u_* is the drag velocity

The drag velocity is related to the shear stress (τ) exerted by the wind on the bed and to the density of air (ρ_a) by the expression:

$$u_* = (\tau/\rho_a)^{1/2}$$

Both u_* and τ increase as the wind velocity (U) increases. At some critical point grains on the bed start to move. This point, referred to by Bagnold (1941) as the 'fluid threshold', can be expressed by

$$u_* = A[(\rho_p - \rho_a)gD\rho_a^{-1}]^{1/2}$$

where

u_* is the fluid threshold

ρ_p is the relative density of the grains (2.65 gm cm^{-3} for quartz)

ρ_a is the relative density of air ($1.22 \times 10^{-3} \text{ gm cm}^{-3}$)

g is the acceleration due to gravity (980 cm s^{-2})

D is the mean grain diameter (cm)

A is an empirical coefficient equal to 0.1 for particle friction Reynolds numbers (Re_p) greater than 3.5 ($Re_p = u_*D/\nu$), where ν is the kinematic viscosity of the air. Re_p provides a measure of how turbulent the flow is around a particle.

According to (Pye, 1987), "(Bagnold, 1941) concluded that sand grains at the threshold of movement on a bed exposed to turbulent flow first began to roll and then to bounce" (i.e., saltation), "presumably due to the combined effect of the velocity pressure exerted by the air on the upwind side of the grain and the negative viscosity pressure on the downwind side. Other workers have found no evidence of rolling and bouncing at the onset of motion," instead they begin a rocking motion until the inertial forces due to friction and cohesion have been overcome and the particle is lifted (or ejected) into the flow stream of the wind, "apparently due to instantaneous differences in pressure near the ground" (Bisal and Nielsen, 1962).

A steady sheared flow near the ground decreases the static pressure at the top of a grain relative to the bottom (the Bernoulli effect), thereby creating lift (Chepil, 1945). Discontinuous lift forces also result from fluctuations in pressure above the bed due to turbulent eddy motion, and are probably partly responsible for the initial rocking movements (Lyles and Krauss, 1971). Short-term fluctuations in drag and lift forces are related and both contribute to entrainment of sand and silt particles (Chepil, 1959).

There is great diversity and complexity regarding the physics at work in particle movement and resuspension. It becomes evident that the particle sizes lifted vary relative to the time dependent fluctuations of the wind speed. These fluctuations give rise to laminar streamline flow separation induced by turbulent eddies, by surface roughness elements, and instantaneous pressure changes induced by turbulent vortices. Proper treatment of this subject matter is beyond the scope of this work and will not be discussed further. It has been presented merely to add a qualitative depiction of the problem.

As (Pye, 1987) states,

Clements *et al.* (1963) reported that the minimum wind speed required to generate blowing dust on different desert surfaces ranged from 6 m s^{-1} on sand dunes to $> 16 \text{ m s}^{-1}$ on crusted alluvial fans and mature desert pavements. Hall (1981) found that average wind speeds $> 11 \text{ m s}^{-1}$, with gust speeds $> 16 \text{ m s}^{-1}$, were required for blowing dust events with visibilities of 10 km or less at Winslow and Tucson, Arizona, and at Denver, Colorado.

With respect to the observed dust storm at Taranaki in November 1996, the wind speed was observed for $U_{2.18 \text{ m}} = 8+ \text{ m/s}$ gusting to $> 17 \text{ m/s}$.

Residence Time and Distance Traveled

The residence time for fine particles is intuitively greater and consequently they travel a much greater distance. The residence time of resuspended particles is related by two elements. The first being that of the vertical component of the wind velocity and the second the gravitational settling velocity. The basis for modeling particle settling velocities is Stokes's Law having components of grain diameter, particle density, gravitational acceleration, the dynamic viscosity of air, an empirical constant, and the Cunningham slip

correction factor which is an aerodynamic correction term for small particles that can “slip” between air molecules.

Stokes’s Law is presented here according to (Green and Lane, 1964) in (Pye, 1987), without the Cunningham slip correction factor as a function of the square of grain diameter:

$$U_f = KD^2$$

where

U_f = settling velocity (cm s^{-1})

D = grain diameter

$K = \rho_p g / 18\mu$

where ρ_p = particle density (g cm^{-3})

g = gravitational constant (g cm^{-3})

μ = dynamic viscosity of air

$K = 8.1 \times 10^{-5} \text{ cm}^{-1} \text{ s}^{-1}$ for air at 15 °C sea-level for quartz spheres

The horizontal component of wind velocity (u), and the vertical component (w) averaged over a specified time interval are designated \bar{u} and \bar{w} , respectively. The fluctuations in the vertical component (w') is defined as:

$$w' = w - \bar{w}$$

where w' is dependent on atmospheric stability conditions.

In a neutral atmosphere the distribution of vertical fluctuating velocity components, w' , near the surface but above the saltating layer is approximately normal with a (\bar{w}') of 0 since the upward and downward motions must be equal. The standard deviation of the vertical fluctuating velocity ($\sigma = (\overline{w'^2})^{1/2}$) represents the force opposing the tendency for fine particles to settle (Pye, 1987).

Particle residence time is therefore dependent on the ratio of upward to downward movements and must be >1 . According to (Pye, 1987), Gillette (1974, 1977), using the ratio of U_f/u_* showed that the grains having $U_f = 0.4u_* = 0.5$ have a high probability of settling in a short period of time. When $U_f \ll (\overline{w'^2})^{1/2}$, long-term suspension can be expected. If $U_f / (\overline{w'^2})^{1/2} = 0.6$ there is a high probability that a particle will be carried to a level well above the ground.

In order to determine the distance traveled by a particle, one more relation must be defined. It is the coefficient of turbulent exchange and is expressed as:

$$\varepsilon = (\overline{w'^2})^{1/2} l$$

where

l = the mixing length defined by (Prandtl, 1935) as:

$$l = \alpha k z$$

where

$\alpha = 1$ for neutral atmospheres, $\alpha > 1$ for unstable atmospheres, and $\alpha < 1$ for stable atmospheres

k = von Karman constant, 0.4

z = the height above the surface within the lowermost boundary layer

Thus:

$$\varepsilon = \alpha (\overline{w'^2})^{1/2} k z$$

substitution of $(\overline{w'^2})^{1/2} = U_f/0.6$ from the relation defined above for long-term suspension yields:

$$\varepsilon = \alpha U_f k z / 0.6$$

Finally the substitution can be made for ε in the equation defining distance traveled expressed as:

$$L = \overline{u}^2 \varepsilon / K^2 D^4$$

such that

$$L = \bar{u} 2\alpha U_{tkz} / 0.6 / K^2 D^4$$

where

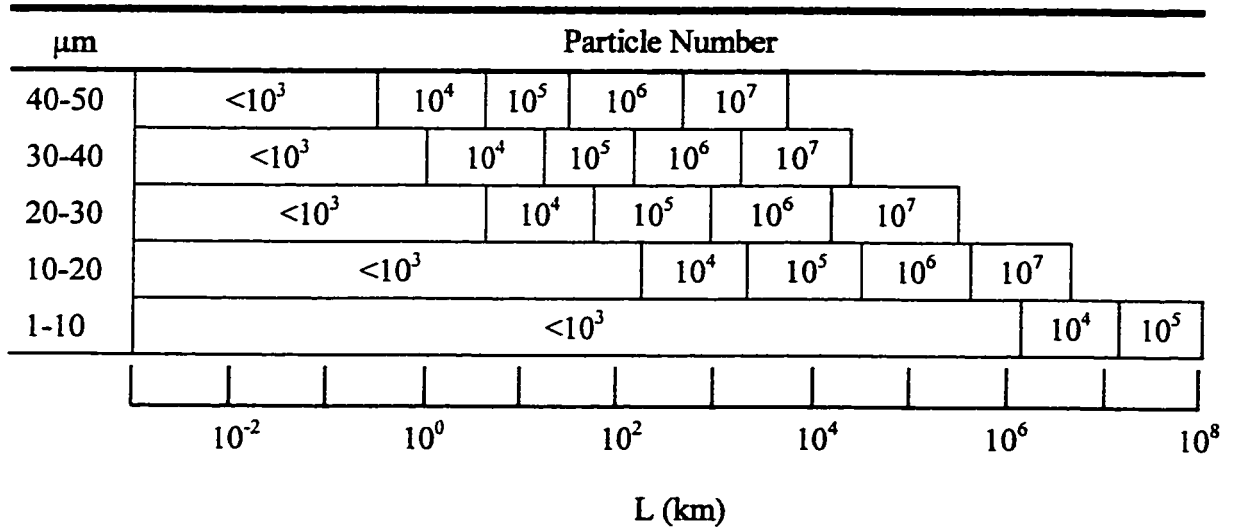
L = distance traveled

\bar{u} = mean wind velocity

$K = \rho_p g / 18\mu$

Figure II-35 below exemplifies the maximum likely distance traveled for a range of particle diameters for a mean wind speed $\bar{u} = 15$ m/s and ϵ ranging from 10^3 to 10^7 cm²/s, from (Pye, 1987).

Figure II-35: Probable distance traveled (L) by quartz particles for a mean wind speed of $\bar{u} = 15$ m/s and a range of turbulent coefficients $\epsilon = 10^3$ to 10^7 cm²/s; km = kilometers



REFERENCES

- Aitchison, J.; Brown, J.A.C. *The Lognormal Distribution*. First Printing. Cambridge: Cambridge University Press; 1969.
- Allen, T. *Particle Size Measurement*. Second Edition. London: Chapman and Hall Ltd.; 1975.
- Bagnold, R.A. *The Physics of Blown Sand and Desert Dunes*. London: Methuen; 1941.
- Bisal F.; Nielsen, K.F. Movement of soil particles in saltation. *Can. J. Soil Sci.* 42: 81-86; 1962.
- Chepil, W.S. Dynamics of wind erosion. IV. The Translocating and abrasive action of the wind. *Soil Sci.* 61: 167-177; 1945.
- Chepil, W.S. Equilibrium of soil grains at the threshold of movement by wind. *Proc. Soil Sci. Soc. Am.* 23: 422-428; 1959.
- Dennis, R., Editor. *Handbook on Aerosols*; GCA/Technology Division, GCA Corporation. TID-26608; 1976.
- Eckermann, K.F.; Wolbarst, A.B.; Richardson, A.C.B. *Limiting Values of Radionuclide Intake and Air Concentration and Dose Conversion Factors for Inhalation, Submersion, and Ingestion*. Federal Guidance Report No. 11. EPA 520/1-88-020. Oak Ridge, TN. Washington, D.C.: Oak Ridge National Laboratory and U.S. Environmental Protection Agency; 1989.
- Gilbert, R.O. *Statistical Methods for Environmental Pollution Monitoring*. First Printing. New York: Van Nostrand Reinhold; 1987.

- Gillette, D.A. On the production of soil wind erosion aerosols having the potential for long-range transport. *J. Rech. Atmos.* 8: 735-744; 1974.
- Gillette, D.A. Fine particulate emissions due to wind erosion. *Trans. Am. Soc. Agric. Eng.* 20: 890-897; 1977.
- Green, H.L.; Lane, W.R. *Particulate Clouds: Dusts, Smokes and Mists.* London: Spon; 1964.
- International Commission on Radiological Protection (ICRP) Report of the Task Group on Reference Man, ICRP Publication 23; Pergamon Press New York, 1975.
- Johnston, P.N.; Lokan, K.H.; Richardson, C.K.; Williams G.A. Plutonium Contamination in the Maralinga Tjarutja Lands. Australian Radiation Laboratory Report, ARL/TR085; 1989.
- Johnston, P.N.; Williams G.A.; Burns, P.A.; Cooper, M.B. Plutonium Resuspension and Airborne Dust Loadings in the Desert Environment of Maralinga, South Australia. *J. Environmental Radioactivity* 20: 117-131; 1993.
- Karman, T. von Turbulence and skin friction. *J. Aeron. Sci.* 1: 1-20; 1934.
- Koval, J.; Resuspension Element Status Report, Part E: *In-Situ* Optical Particle Size Analysis in Anspaugh, L. R. *The Dynamics of Plutonium in Desert Environments;* U.S. Energy and Research Development Administration (ERDA). Las Vegas, NV: U.S. Department of Energy, Nevada Operations Office; NVO-142; 1974.
- Lokan, K.H. Residual Radioactive Contamination at Maralinga and Emu, 1985. Australian Radiation Laboratory Report, ARL/TR070; 1985.

- Lyles, L.; Krauss, R.K. Threshold velocities and initial particle motion as influenced by air turbulence. *Trans. Am. Soc. Agric. Eng.* 14: 563-566; 1971.
- Prandtl, L. The mechanics of viscous fluids. In F. Durand (ed.) *Aerodynamic Theory*, Vol. III. Berlin: Julius Springer; 1935.
- Pye, K. *Aeolian Dust and Dust Deposits*. London: Academic Press Inc.; 1987.
- Shinn, J.H.; Homan, D.N.; Robison, W.L. Resuspension Studies in the Marshall Islands. *Health Phys.* 73: 248-257; 1997.
- Shinn, J.H. Background on Americium-241 production during the plutonium formation process. Personal communication, 1998.
- Shinn, J.H. LLNL Ultra High-Volume Air Sampler Protocol. Personal communication, 1997.
- Williams, G.A. Editor; *Inhalation Hazard Assessment at Maralinga and Emu*, Australian Radiation Laboratory Report, ARL/TR087; 1994.

INSTRUMENT COMPANY

REFERENCES

- Nuclear Data, Inc.: ND-PSA Particle Sizing Amplifier 82-0176; Schaumburg, Illinois 60172.
- D. S. Davidson Company: Pulse Height Analyzer Model 1056C; North Haven, Connecticut.
- EG&G ORTEC® : Research Pulser Model 441; Oak Ridge, TN 37831-0895.
- Kurz Instruments Inc.: Model 441 M-A Velocity Transducer; Monterey, CA 93940.

APPENDIX

Contents

List of Tables

List of Figures

Thesis Part I

Appendix I-A: Table I-3 Campbell Scientific Data Logger Map

Appendix I-A: UHVAS Field Data, Tables I-4A and I-4B

Thesis Part II

Appendix II-A: APSD Figures II-1 through II-7

Appendix II-B: APSD Figures II-8 through II-22

Appendix II-C: TARANAKI Winds Figures II-23 through II-32

Appendix II-D: APSD Software Download Program

Appendix II-E: Taranaki Site Map

Appendix II-F: APSD Volume Density Function Parameter Summary for Lots 18C and 19 Tables II-9A and II-9B

LIST OF TABLES

Thesis Part I Appendix

Table I-3: Campbell Scientific Data Logger Map

Table I-4: UHVAS Field Data

Thesis Part II Appendix

Table II-5: Serial I/O Cable Pin-Out for PHA 15 Pin to PC Nine Pin Connection

Table II-9A: APSD Volume Density Function Parameter Summary for Lot 18C

Table II-9B: APSD Volume Density Function Parameter Summary for Lot 19

LIST OF FIGURES

Thesis Part II

- Figure II-1: Isokinetic Sampling Assembly
- Figure II-2: Climet Air-Flow Schematic
- Figure II-3: Climet Optics Schematic
- Figure II-4: Climet Model CI-208 Instrument
- Figure II-5: PSA-PHA Laboratory Calibration Check
- Figure II-6: Graphical Representation of Table 2.6
(CI-208 Internal Comparator Calibration Voltages)
- Figure II-7: CI-208 Calibration Curves
- Figure II-8: APSD Lot 18C R-4
- Figure II-9: APSD Lot 18C R-5
- Figure II-10: APSD Lot 18C R-6
- Figure II-11: APSD Lot 18C R-7
- Figure II-12: APSD Lot 18C R-8
- Figure II-13: APSD Lot 18C R-9
- Figure II-14: APSD Lot19 R-1
- Figure II-15: APSD Lot19 R-2
- Figure II-16: APSD Lot19 R-3
- Figure II-17: APSD Lot19 R-4
- Figure II-18: APSD Lot19 R-5
- Figure II-19: APSD Lot19 R-6

- Figure II-20: APSD Lot19 R-7
- Figure II-21: APSD Lot19 R-8
- Figure II-22: APSD Lot19 R-9
- Figure II-23: TARANAKI WINDS, Lot 18C, 3-19-97 at 2.18 m
- Figure II-24: TARANAKI WINDS, Lot 18C, 3-20-97 at 2.18 m
- Figure II-25: TARANAKI WINDS, Lot 18C, 3-21-97 at 2.18 m
- Figure II-26: TARANAKI WINDS, Lot 18C, 3-22-97 at 2.18 m
- Figure II-27: TARANAKI WINDS, Lot 18C, 3-23-97 at 2.18 m
- Figure II-28: TARANAKI WINDS, Lot 19, 3-19-97 at 0.585 m and 2.18 m
- Figure II-29: TARANAKI WINDS, Lot 19, 3-20-97 at 0.585 m and 2.18 m
- Figure II-30: TARANAKI WINDS, Lot 19, 3-21-97 at 0.585 m and 2.18 m
- Figure II-31: TARANAKI WINDS, Lot 19, 3-22-97 at 0.585 m and 2.18 m
- Figure II-32: TARANAKI WINDS, Lot 19, 3-23-97 at 0.585 m and 2.18 m
- Figure II-34: Forces acting on a particle at rest
Modified after Figure 3.1 in (Pye, 1987)
- Figure II-35: Probable distance traveled by Quartz particles for a mean wind speed of $\bar{u} = 15$ m/s and a range of turbulent coefficients $\epsilon = 10^3$ to 10^7 cm²/s
- Figure II-36: Lot Map of Taranaki Cleanup Site

APPENDIX I-A

Table I-3: Campbell Scientific Data Logger Map

| DATA MAP | | Channel 1 | Channel 2 | Channel 3 | Channel 4 | Channel 5 | Channel 6 | Channel 7 | Channel 8 |
|----------|----|------------|-----------|------------|-----------|------------|-----------|-----------|-----------|
| Series | 1 | Julian Day | Time | yr | Bat | Temp Int | | | |
| Series | 5 | Julian Day | Time | WT' | WT'coef | Std W | | | |
| Series | 6 | Julian Day | Time | Net Rad | GFLUX1 | GFLUX2 | Aq10 Hi | Aq Lo | |
| Series | 10 | Julian Day | Time | WS1=0.585m | WS2=2.18m | WS3 Analog | Std WS2 | | |
| Series | 30 | Julian Day | Time | Sonic= m/s | Wdir | Std Wdir | | | |
| Series | 60 | Julian Day | Time | T0 = Grd | T1=0.32m | T2 = 0.75m | T3=1.04m | T4=2.12m | |

Table I-4A: UHVAS Field Data

| | H_2O | m^3/Hr | m^3/Hr | Hr | $\bar{Q}\Delta T$ |
|----------------|----------------------|------------------------|---------------------------------|------------|-------------------|
| Run-1-Lot 18 | p | Q | \bar{Q} | ΔT | ΔV |
| 3-14-97: 16:20 | 0.82 | 1037 | 1096 | 16.67 | 18270 |
| 3-15-97: 07:00 | 1.00 | 1154 | 1116 | 17.0 | 18972 |
| 3-16-97: 06:54 | 0.88 | 1077 | 1050 | 23.9 | 25095 |
| 3-17-97: 06:15 | 0.80 | 1023 | 1070 | 23.25 | 24878 |
| | 0.94 | 1117 | $\Sigma =$ | 80.82 | 87215 |
| | | Q Ave = | $\Sigma\Delta V/\Sigma\Delta T$ | 1079 | |
| Run-2-Lot 18 | p | Q | \bar{Q} | ΔT | ΔV |
| 3-18-97: 16:15 | 1.00 | 1154 | 1023 | 24.33 | 24890 |
| 3-19-97: 13:45 | 0.62 | 891 | 875 | 21.5 | 18813 |
| 3-19-97: 15:05 | 0.58 | 859 | 859 | 1.33 | 1142 |
| 3-20-97: 10:14 | 0.58 | 859 | 834 | 19.09 | 15921 |
| | 0.52 | 809 | $\Sigma =$ | 66.25 | 60766 |
| | | Q Ave = | $\Sigma\Delta V/\Sigma\Delta T$ | 917 | |
| Run-3-Lot 18 | p | Q | \bar{Q} | ΔT | ΔV |
| 3-21-97: 10:50 | 1.20 | 1273 | 1113 | 22.58 | 25132 |
| 3-22-97: 15:27 | 0.70 | 952 | 929 | 6.03 | 5602 |
| 3-23-97: 09:37 | 0.64 | 906 | 849 | 18.17 | 15426 |
| 3-23-97: 13:37 | 0.50 | 791 | 783 | 4.47 | 3500 |
| 3-24-97: 09:20 | 0.48 | 774 | 765 | 19.25 | 14726 |
| | 0.46 | 756 | $\Sigma =$ | 70.5 | 64386 |
| | | Q Ave = | $\Sigma\Delta V/\Sigma\Delta T$ | 913 | |

Table I-4B: UHVAS Field Data

| | "H ₂ O | m ³ /Hr | m ³ /Hr | Hr | $\bar{Q}\Delta T$ |
|----------------|-------------------|---|--------------------|------------|-------------------|
| Run-1-Lot 19 | p | Q | \bar{Q} | ΔT | ΔV |
| 3-14-97: 12:10 | 0.72 | 966 | 981 | 5.00 | 4905 |
| 3-15-97: 17:10 | 0.76 | 996 | 974 | 16.66 | 16227 |
| 3-16-97: 09:39 | 0.70 | 952 | 925 | 22.95 | 21229 |
| 3-17-97: 10:07 | 0.63 | 898 | 850 | 24.47 | 21387 |
| 3-18-97: 10:17 | 0.51 | 802 | 850 | 24.17 | 20545 |
| 3-18-97: 13:02 | 0.63 | 898 | 898 | 2.75 | 2338 |
| | | | $\Sigma =$ | 96.0 | 86631 |
| | | Q Ave = $\Sigma\Delta V/\Sigma\Delta T$ | | 902 | |
| Run-2-Lot 19 | p | Q | \bar{Q} | ΔT | ΔV |
| 3-18-97: 16:55 | 0.66 | 922 | 914 | 15.6 | 14258 |
| 3-19-97: 08:31 | 0.64 | 906 | 874 | 6.5 | 5681 |
| 3-20-98: 15:01 | 0.56 | 842 | 851 | 19.5 | 16595 |
| 3-21-97: 10:30 | 0.58 | 860 | 867 | 22.8 | 19768 |
| | | | $\Sigma =$ | 64.4 | 56302 |
| | | Q Ave = $\Sigma\Delta V/\Sigma\Delta T$ | | 874 | |
| Run-3-Lot 19 | p | Q | \bar{Q} | ΔT | ΔV |
| 3-21-97: 10:10 | 0.74 | 980 | 984 | 22.7 | 22337 |
| 3-22-97: 08:52 | 0.75 | 988 | 963 | 7.17 | 6905 |
| 3-22-97: 16:02 | 0.68 | 938 | 937 | 17.17 | 16088 |
| 3-23-97: 09:12 | 0.68 | 936 | 906 | 5.42 | 4911 |
| 3-23-97: 14:37 | 0.60 | 876 | 891 | 18.53 | 16510 |
| | | | $\Sigma =$ | 71.0 | 66751 |
| | | Q Ave = $\Sigma\Delta V/\Sigma\Delta T$ | | 940 | |

APPENDIX II-A

Figure II-1: Isokinetic Sampling Assembly

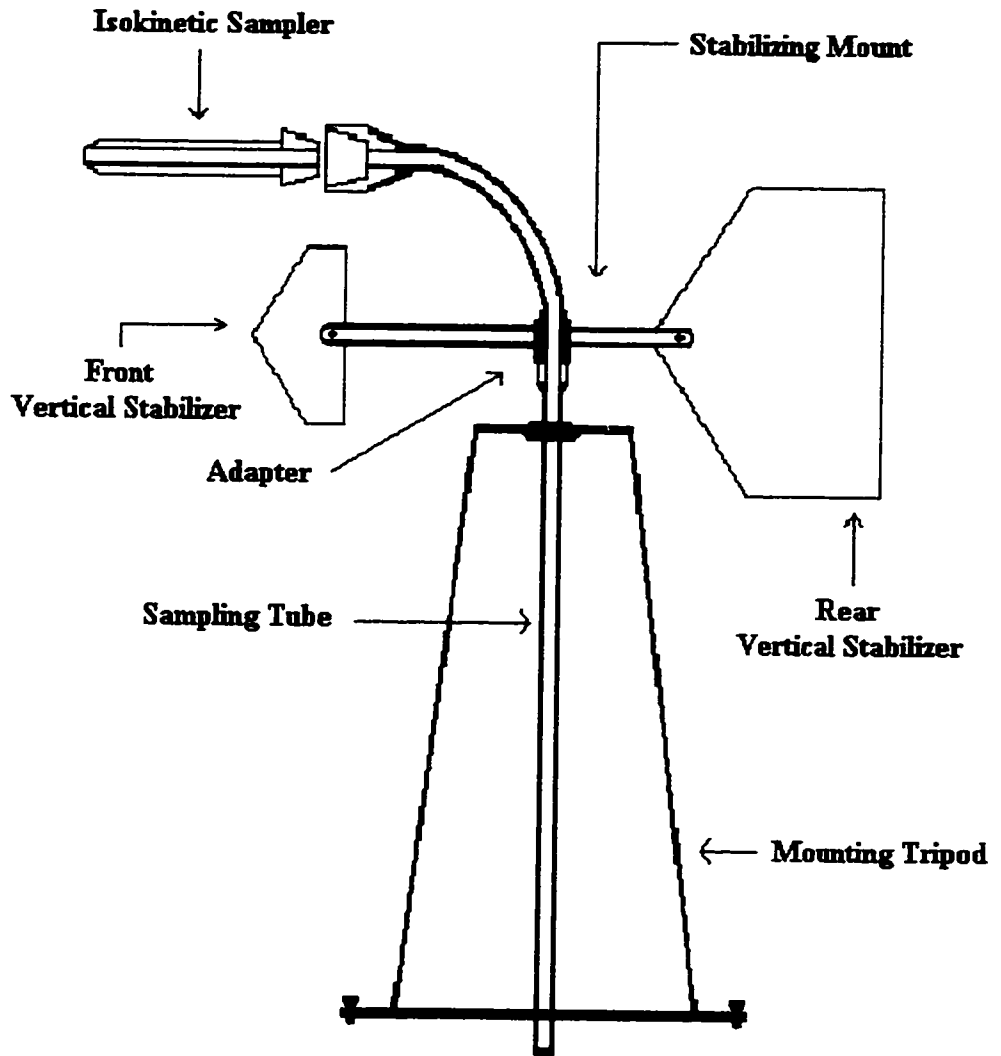


Figure II-2: Climet Air-Flow Schematic

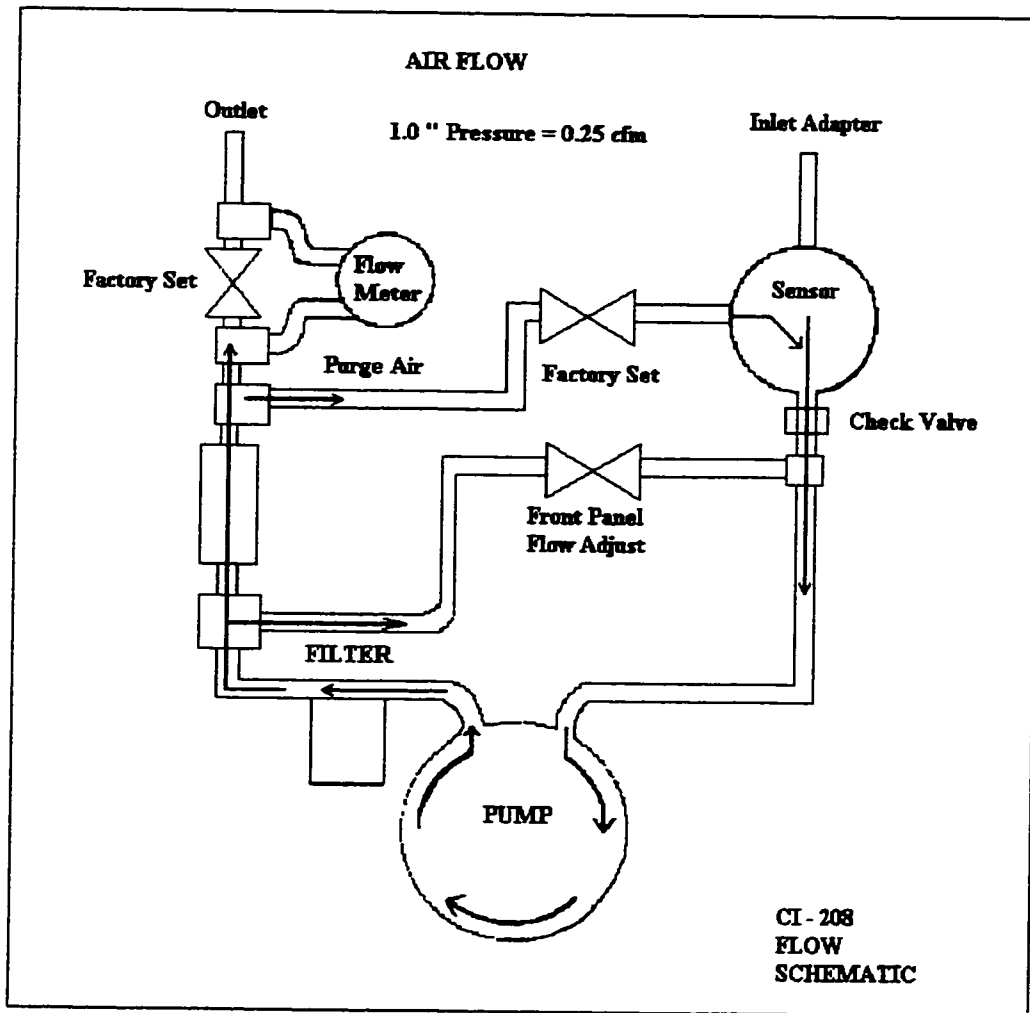


Figure II-3: Climet Optics Schematic

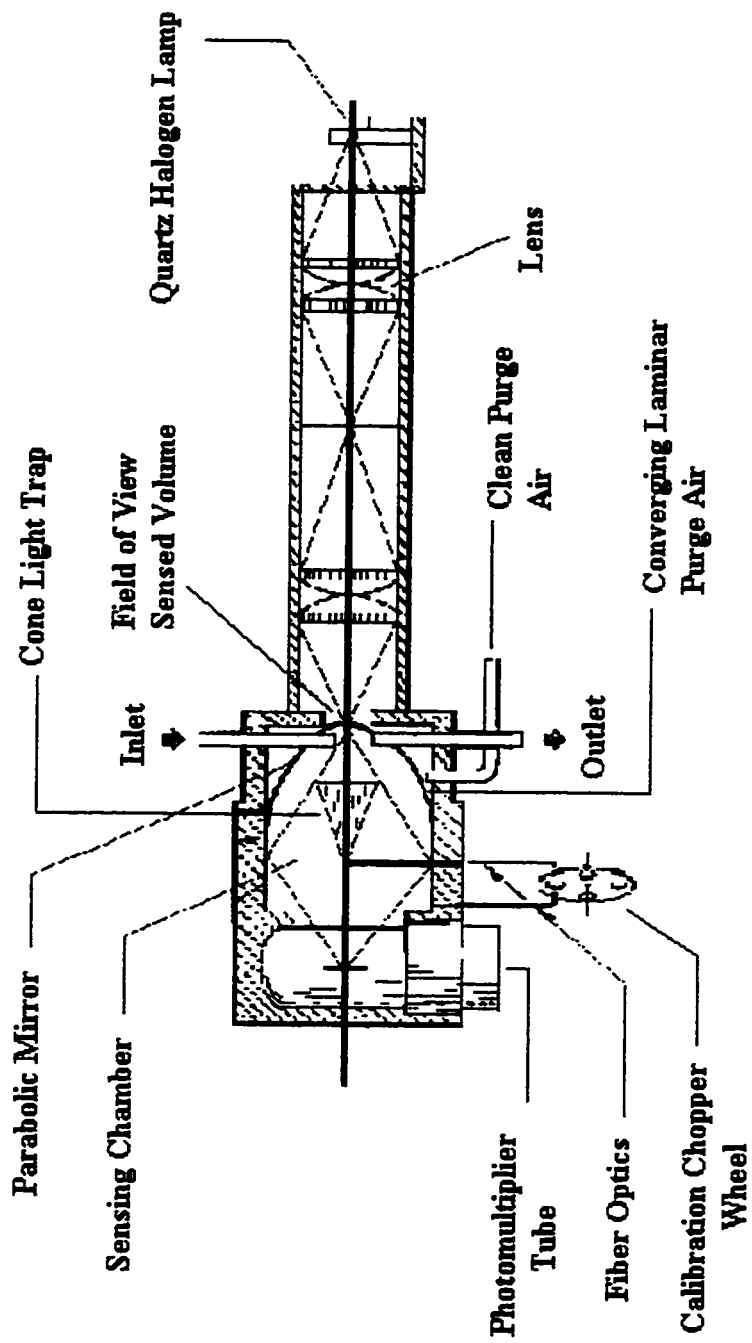


Figure II-4: Climet Model CI-208 Instrument

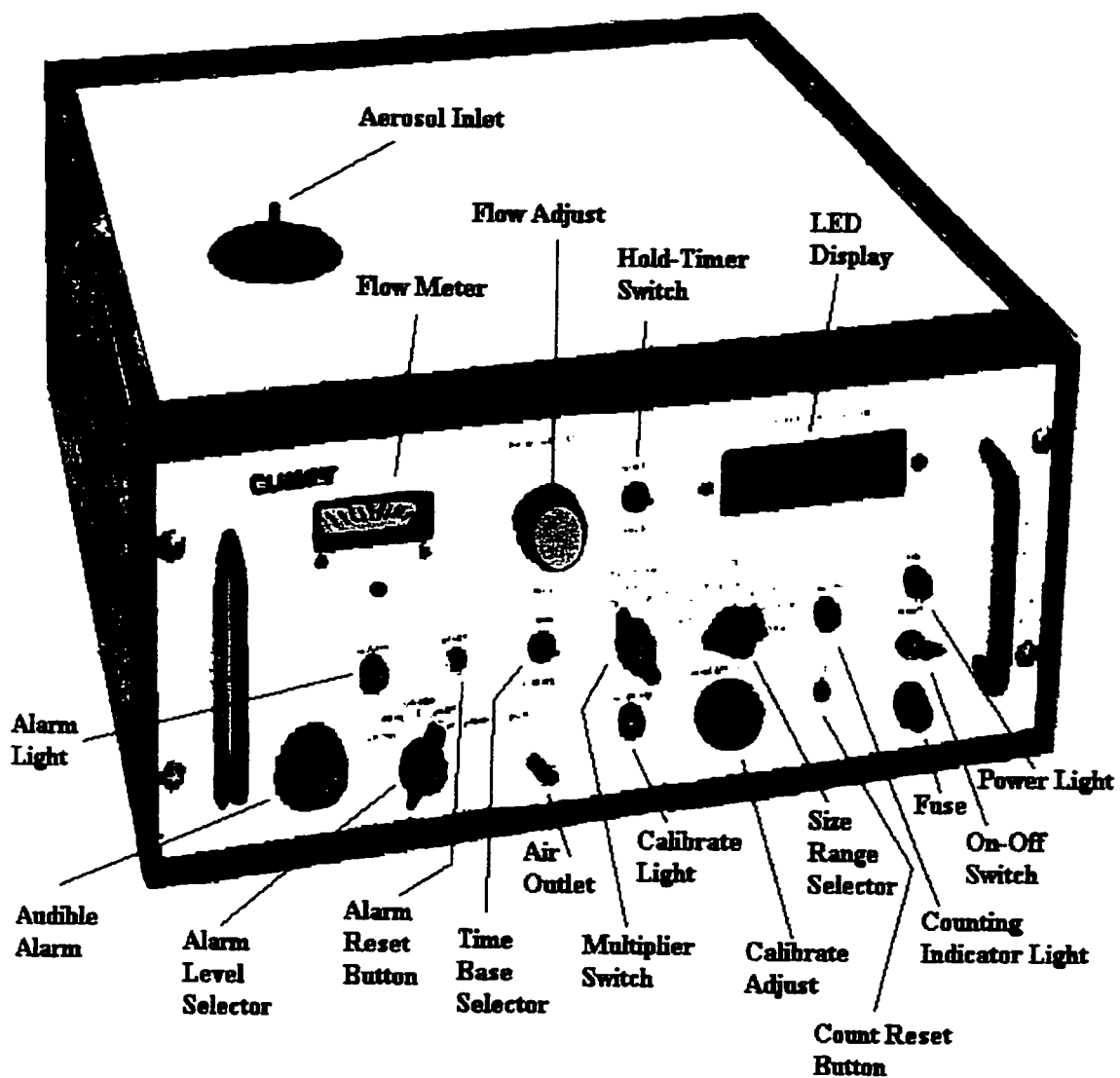


Figure II-5: PSA-PHA Laboratory Calibration Check

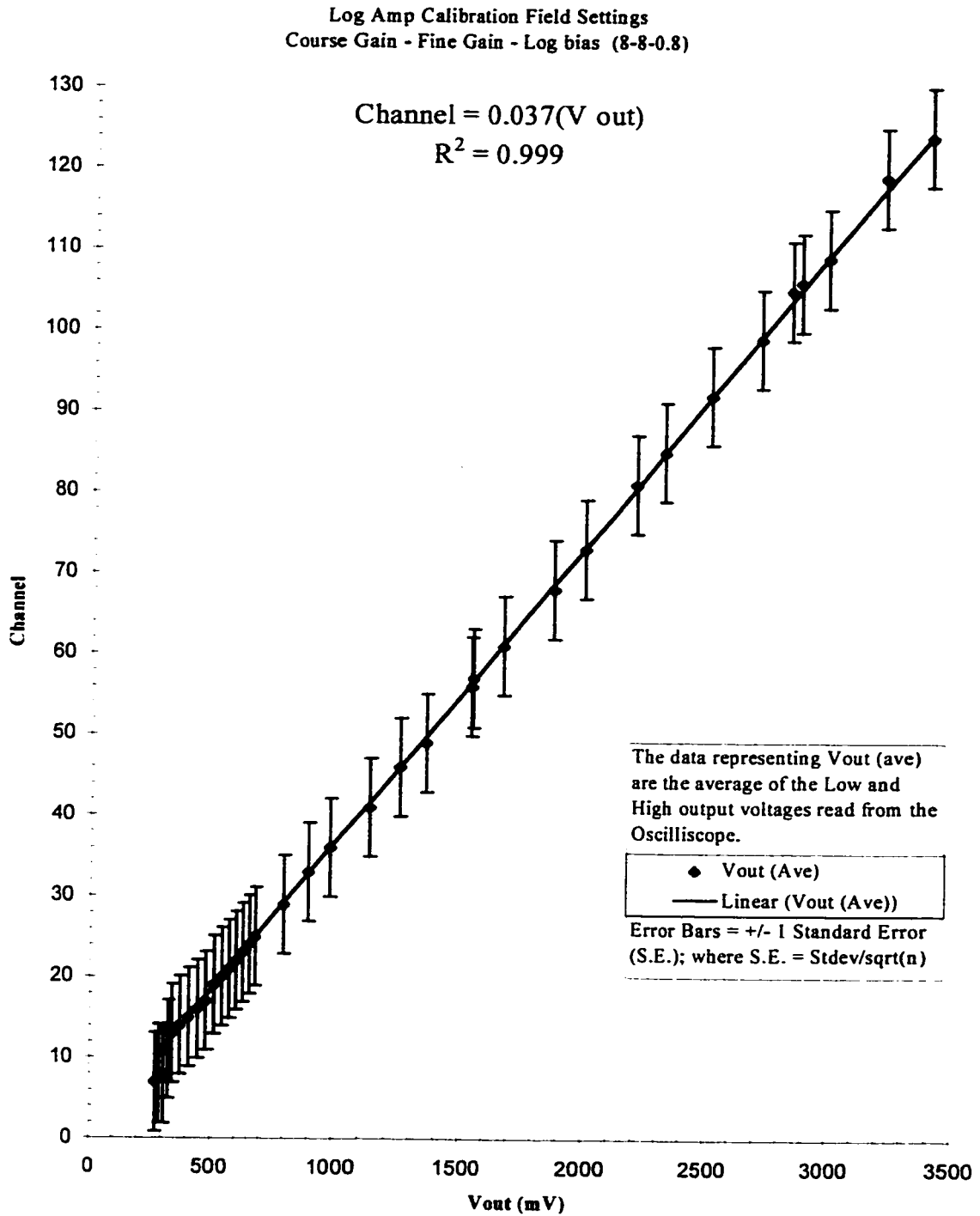


Figure II-6: Graphical Representation of Table II-6
(CI-208 Internal Comparator Calibration Voltages)

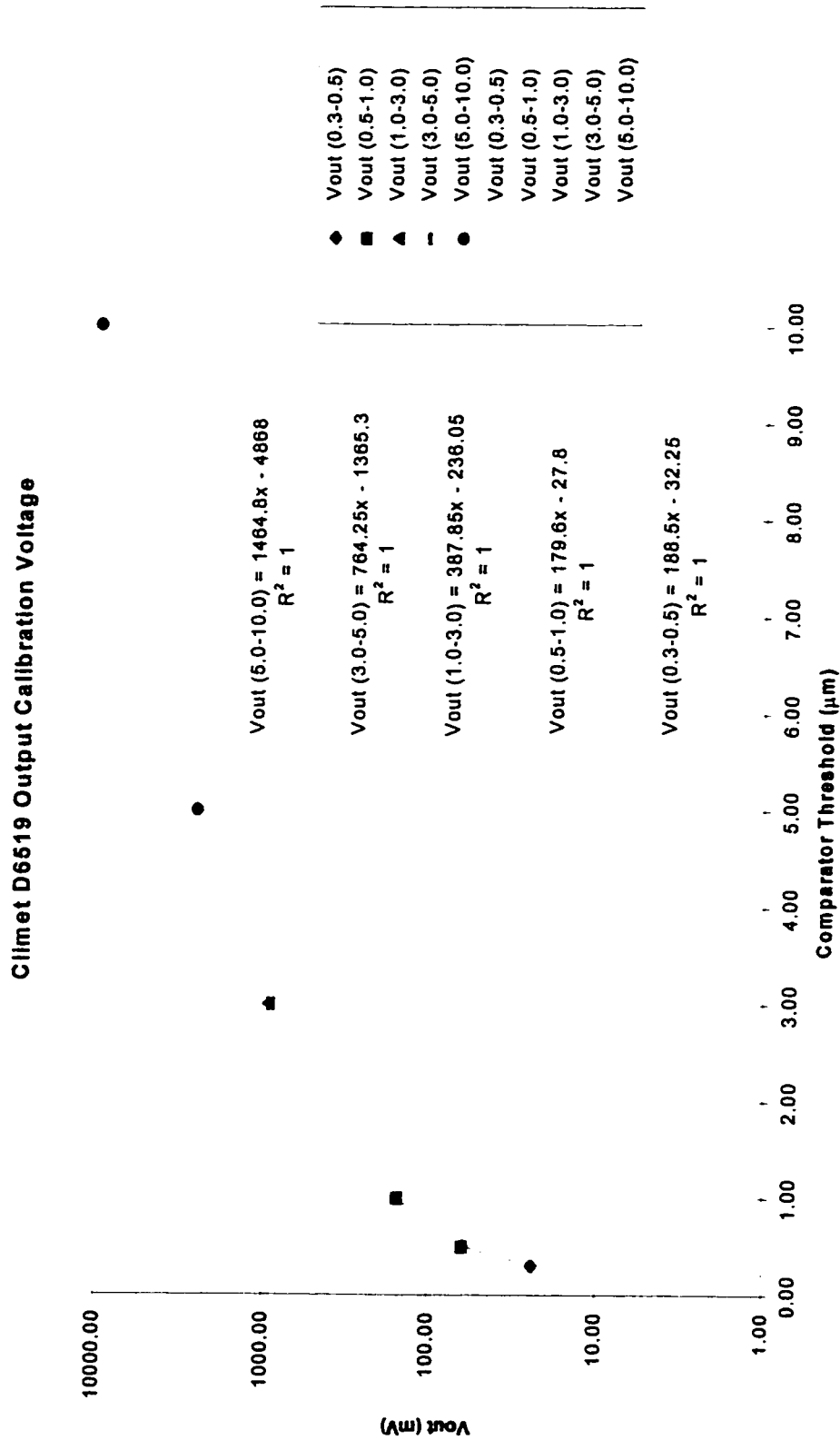
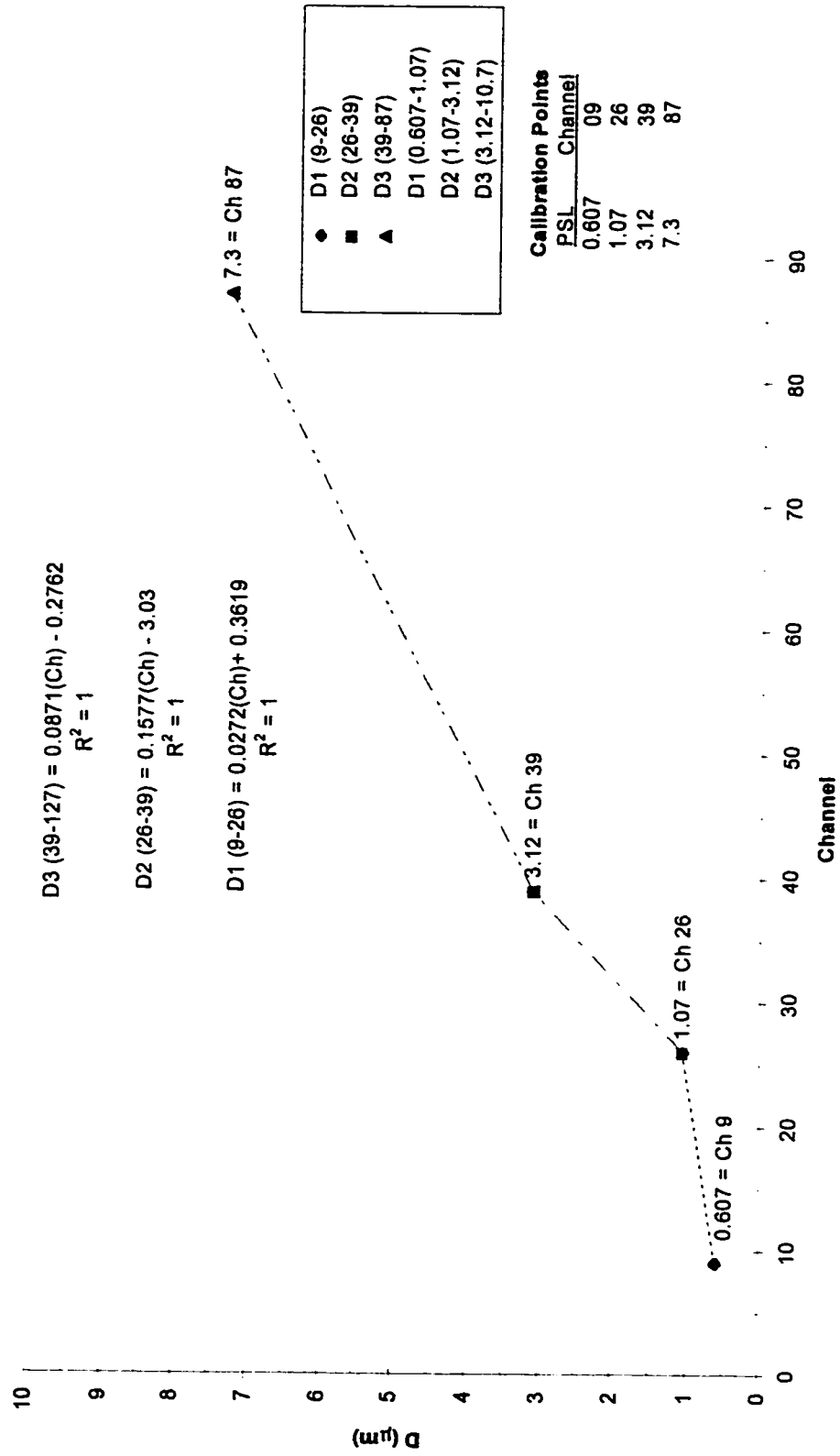


Figure II-7: CI-208 Calibration Curves

Climet Field Calibration: Taranaki March 1997



APPENDIX II-B

APSD DISTRIBUTIONS LOT 18C AND LOT 19

Figure II-8: APSD Lot 18C R-4

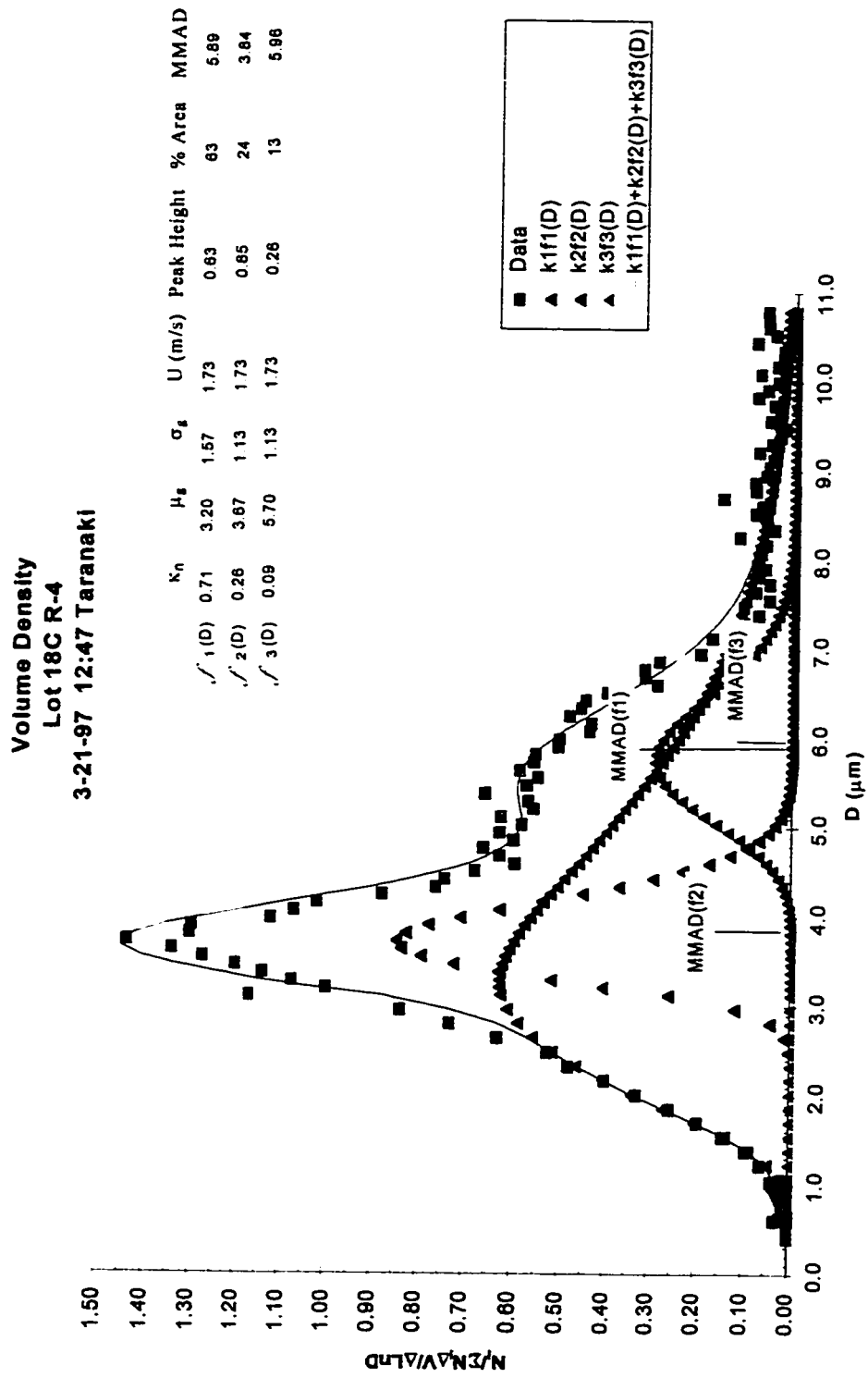


Figure II-9: APSD Lot 18C R-5

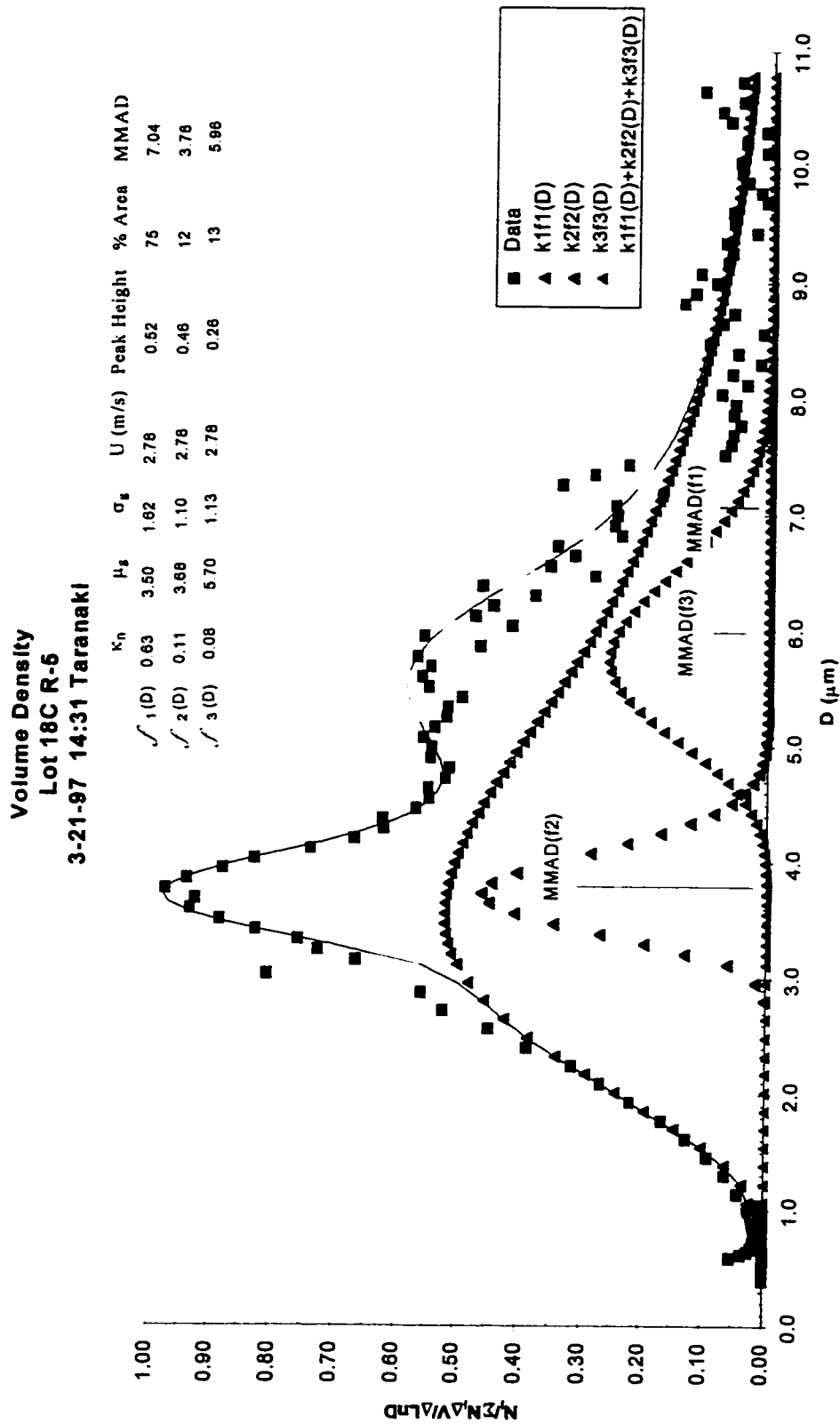


Figure II-10: APSD Lot 18C R-6

Volume Density
 Lot 18C R-6
 3-21-97 16:24 Taranaki

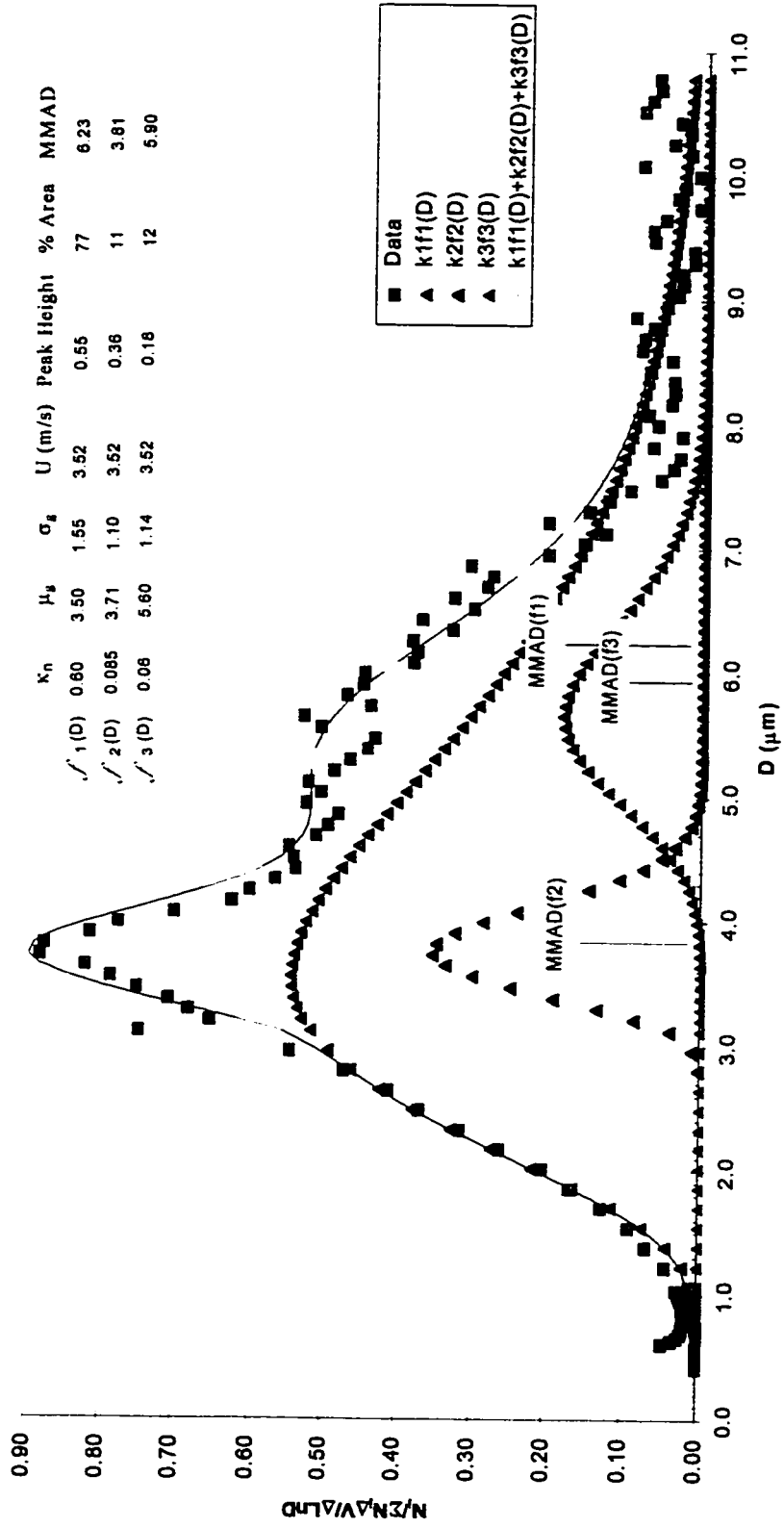


Figure II-11: APSD Lot 18C R-7

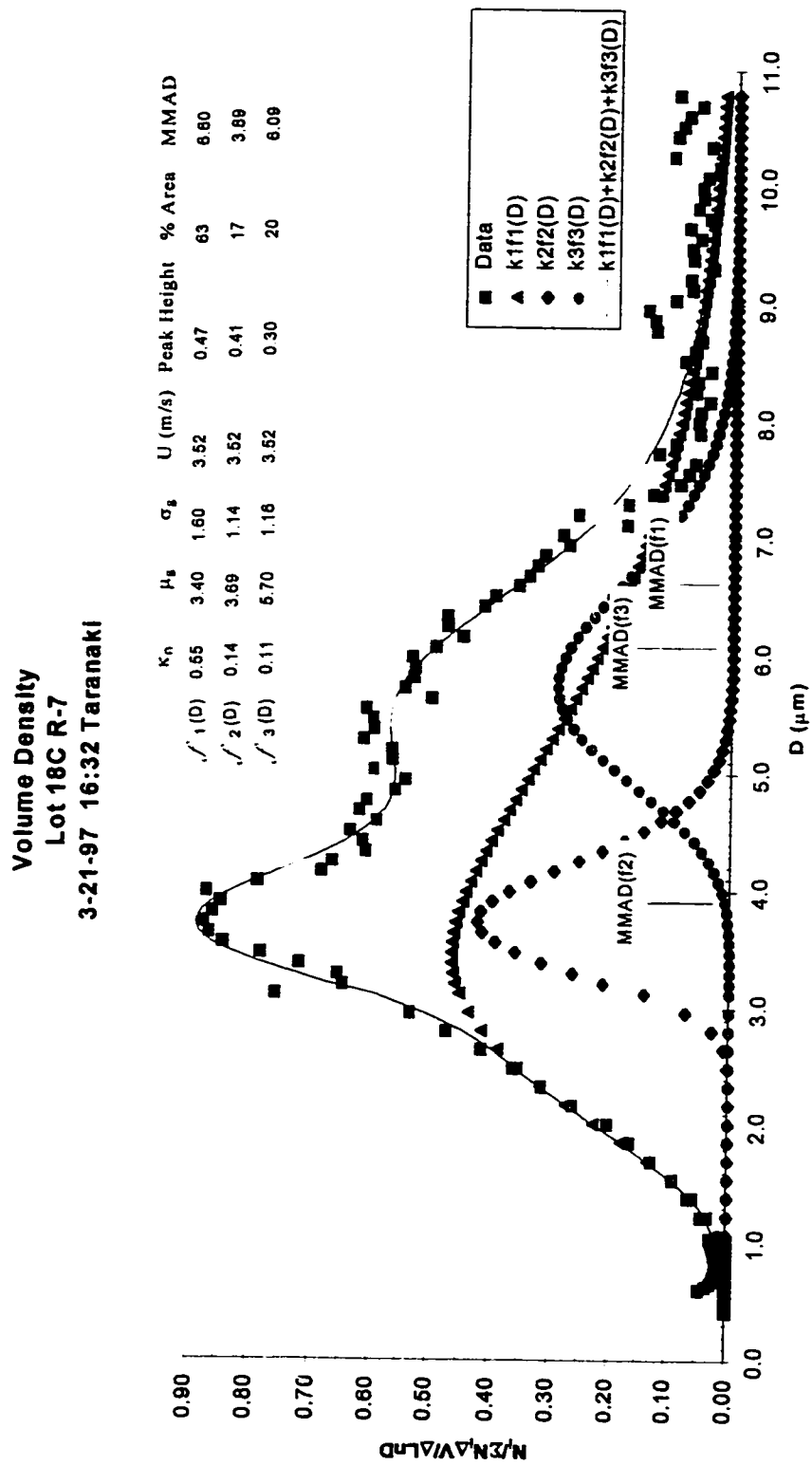


Figure II-12: APSD Lot 18C R-8:

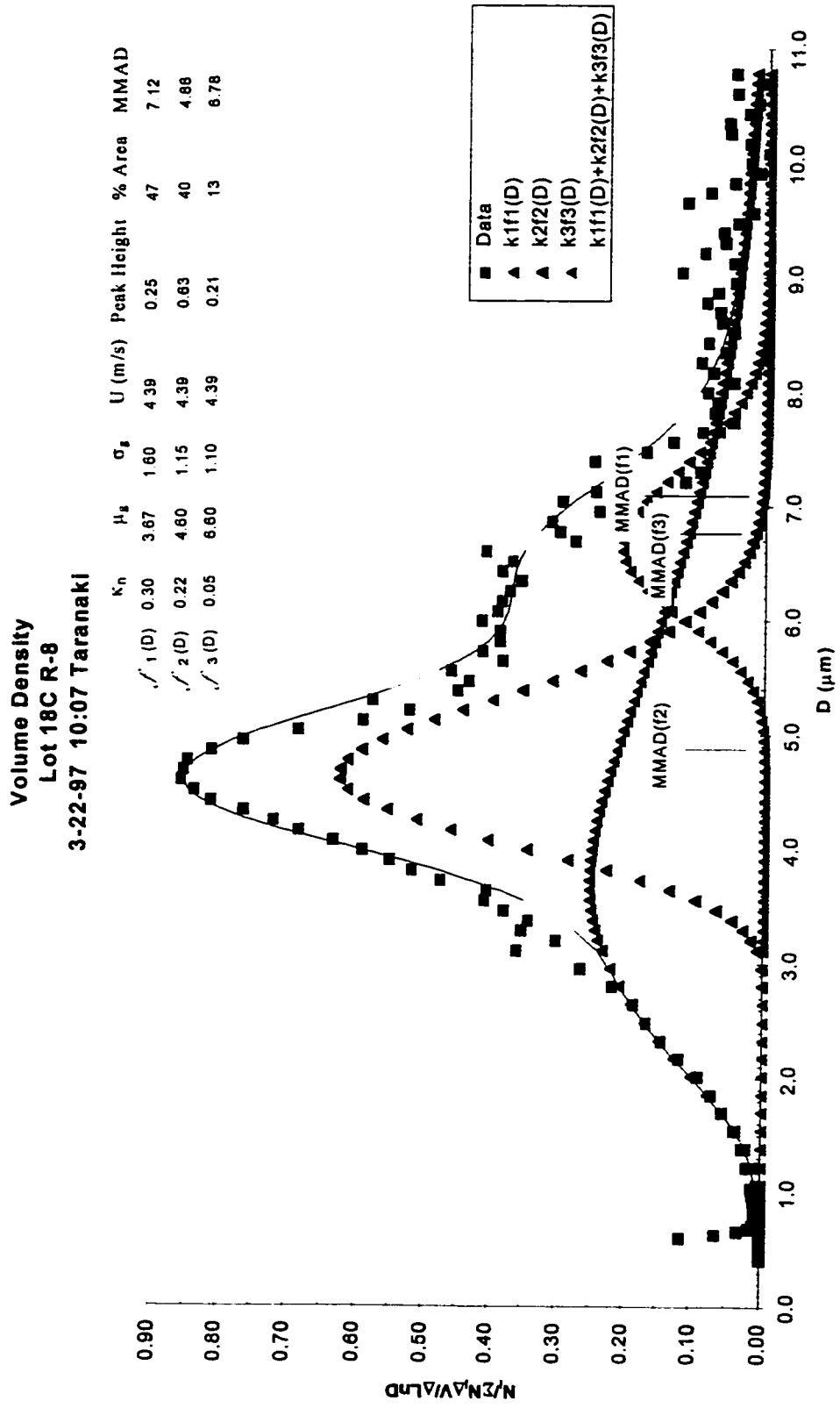


Figure II-13: APSD Lot 18C R-9

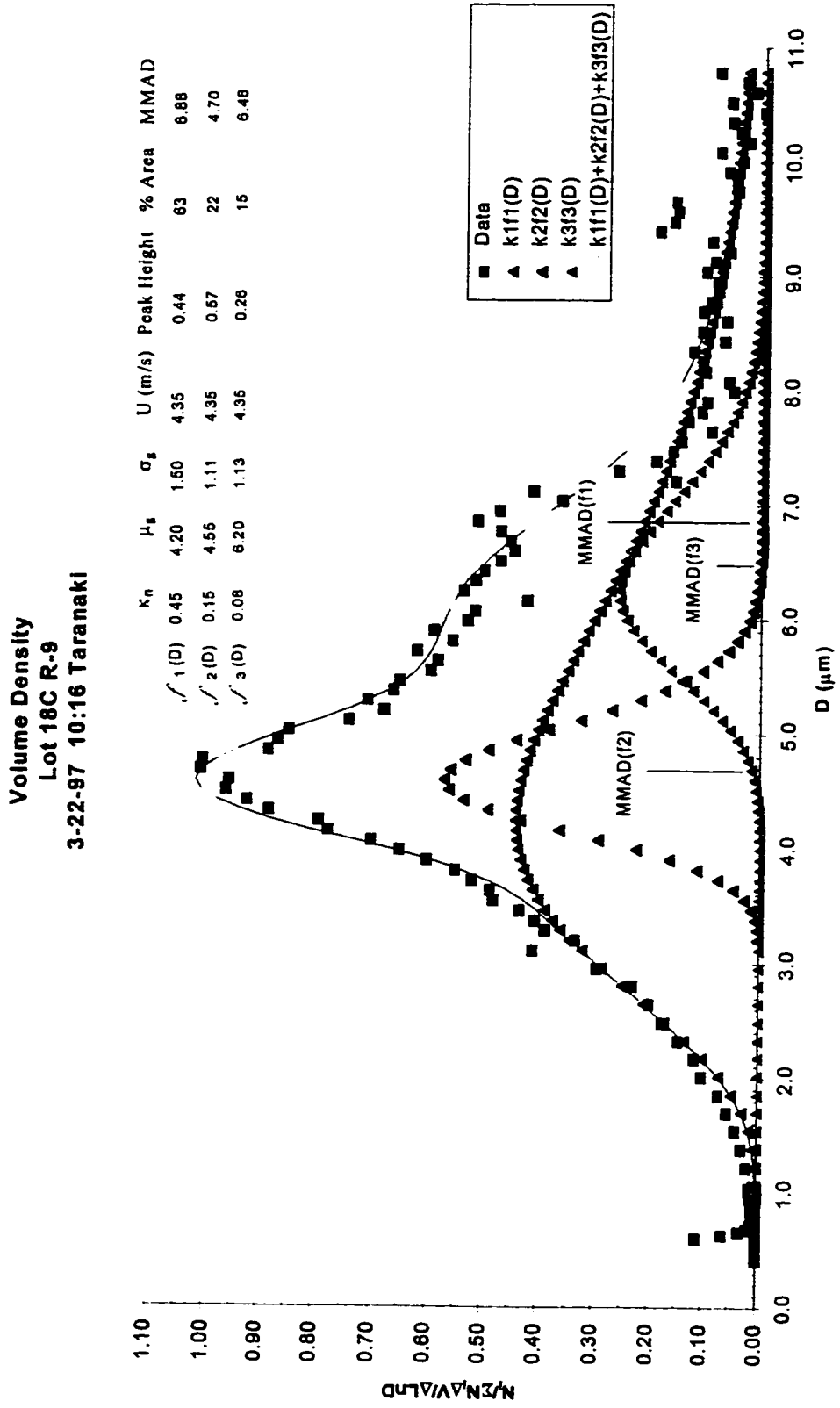


Figure II-14: APSD Lot 19 R-1

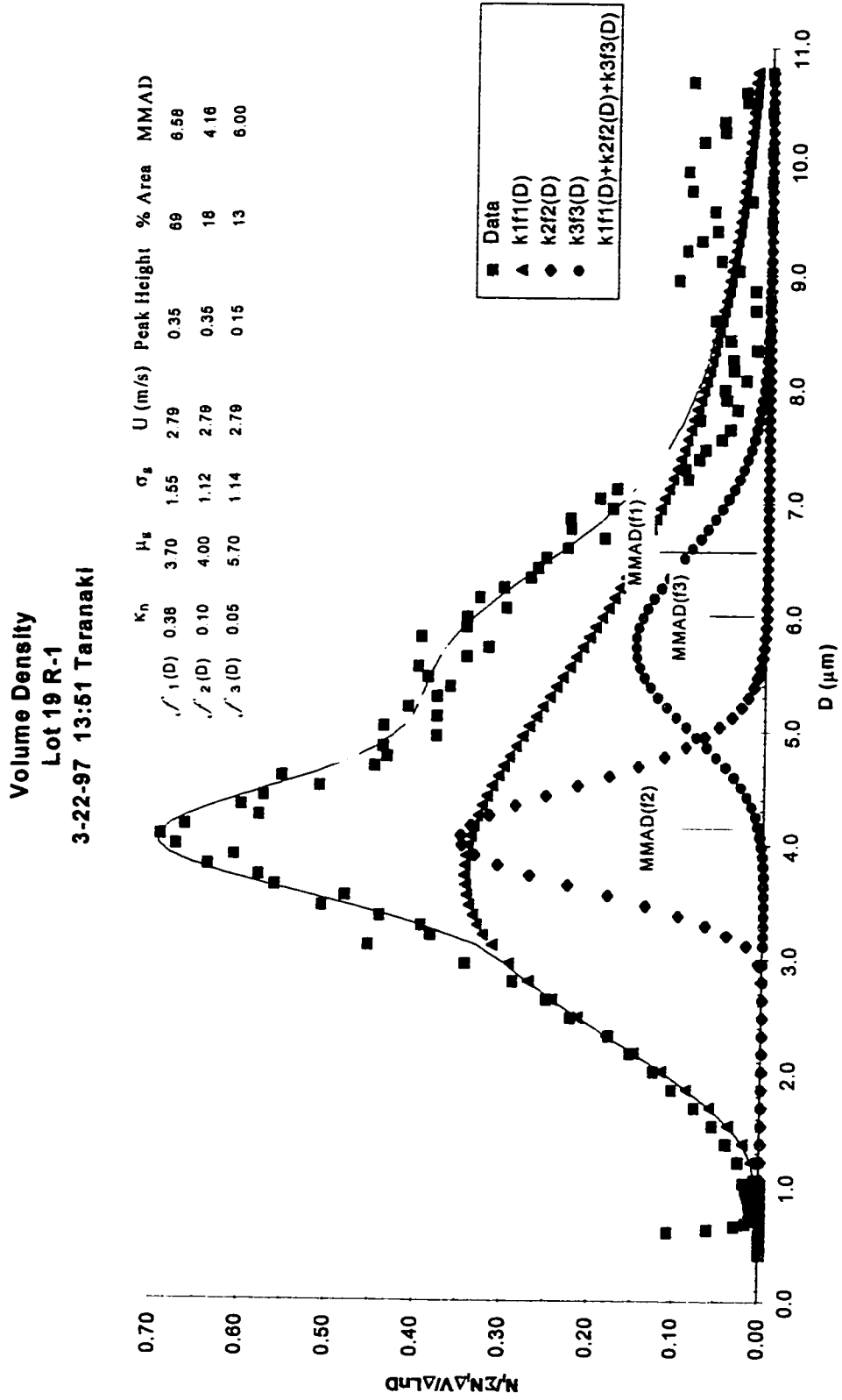


Figure II-15: APSD Lot 19 R-2

Volume Density
 Lot 19 R-2
 3-22-97 14:00 Taranaki

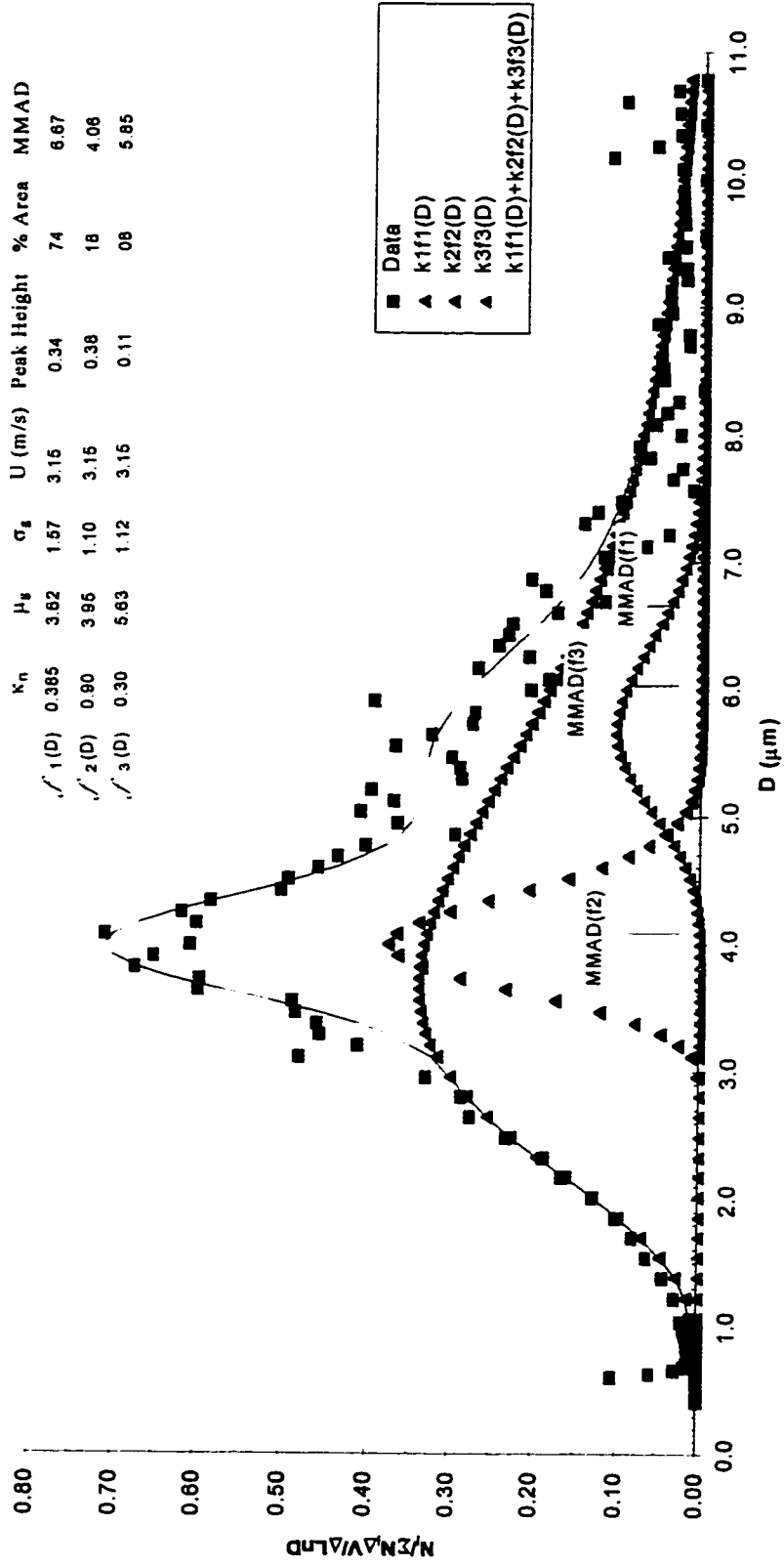


Figure II-16: APSD Lot 19 R-3

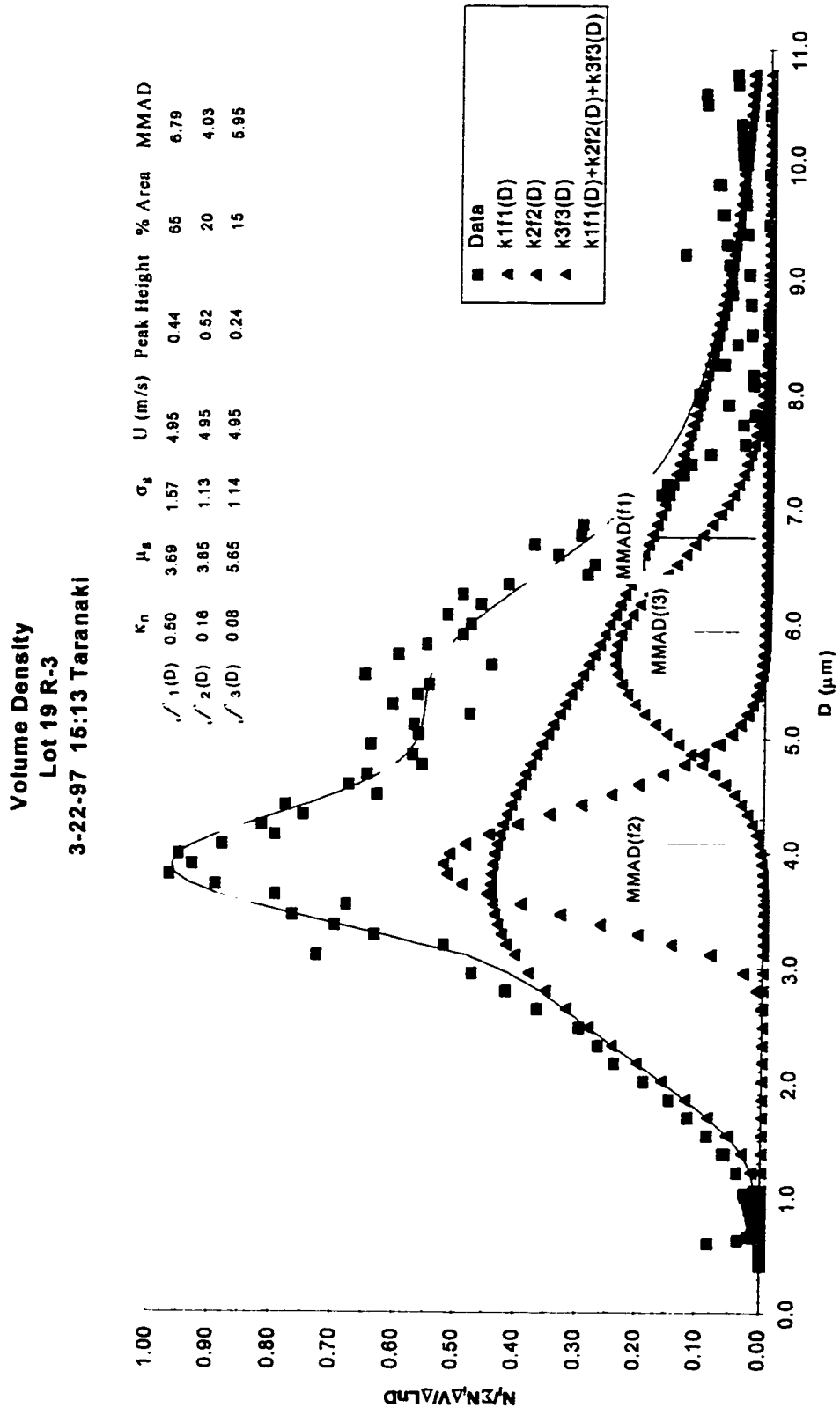


Figure II-17: APSD Lot 19 R-4

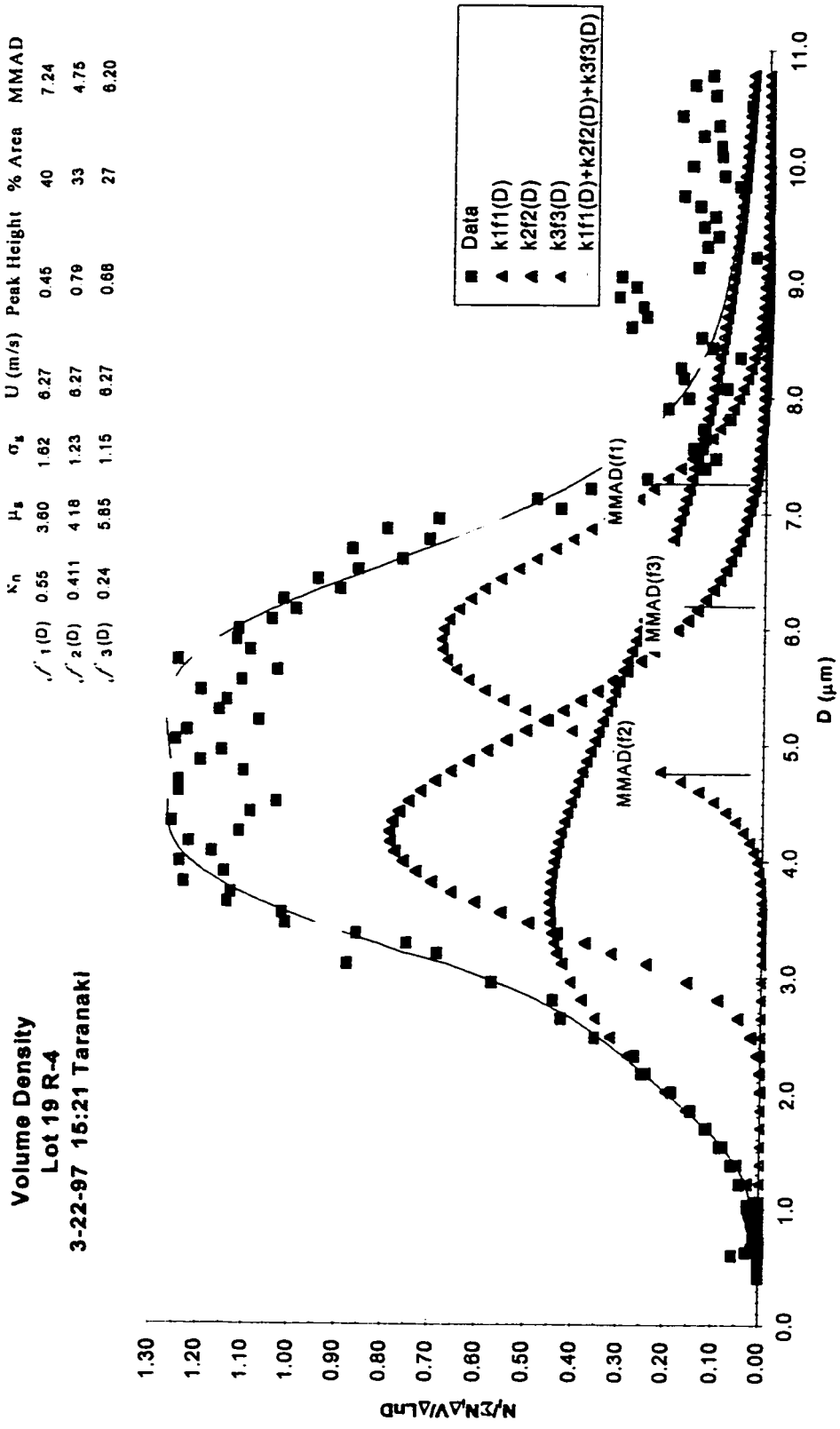


Figure II-18: APSD Lot 19 R-5

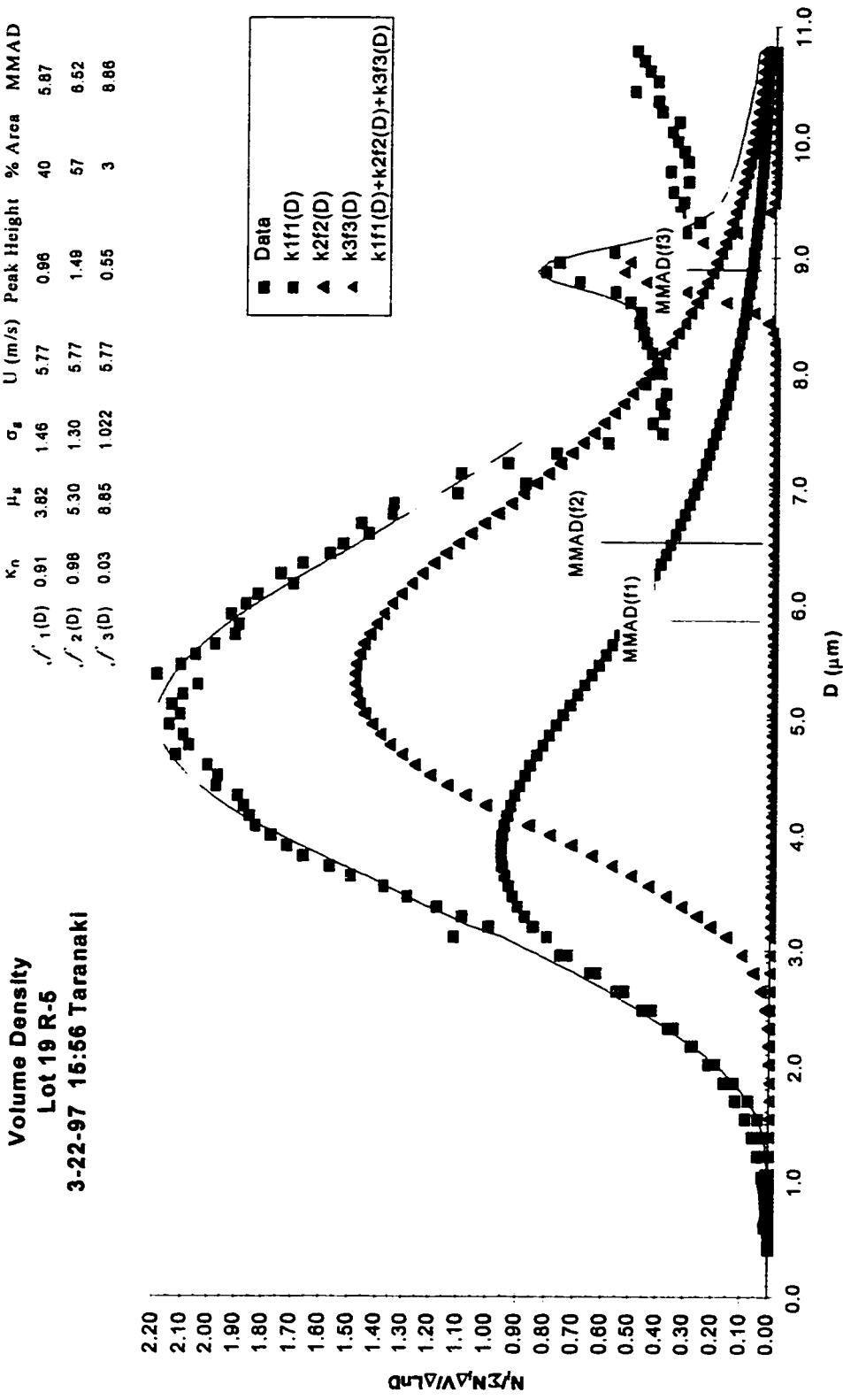


Figure II-19: APSD Lot 19 R-6

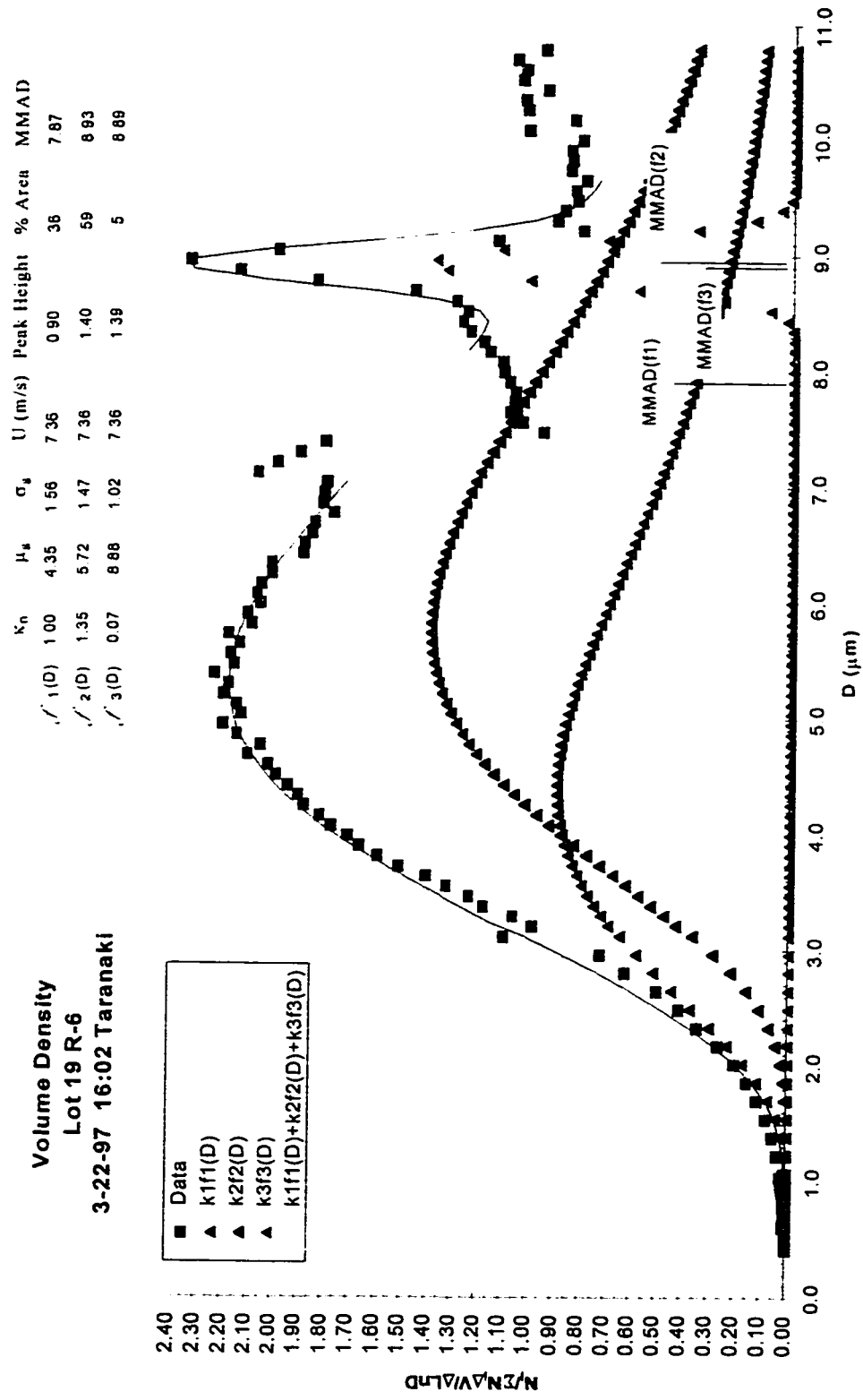


Figure II-20: APSD Lot 19 R-7

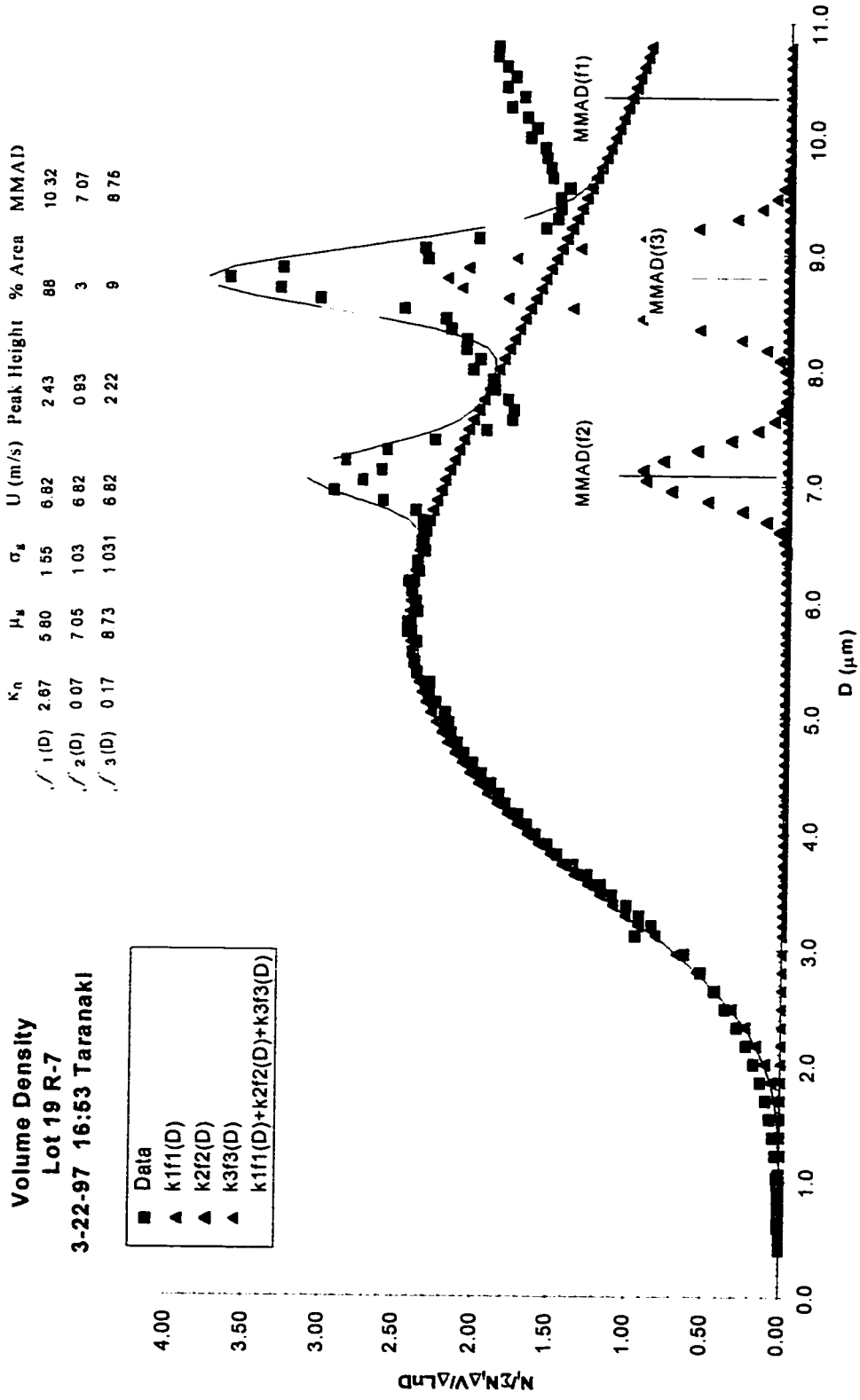


Figure II-21: APSD Lot 19 R-8

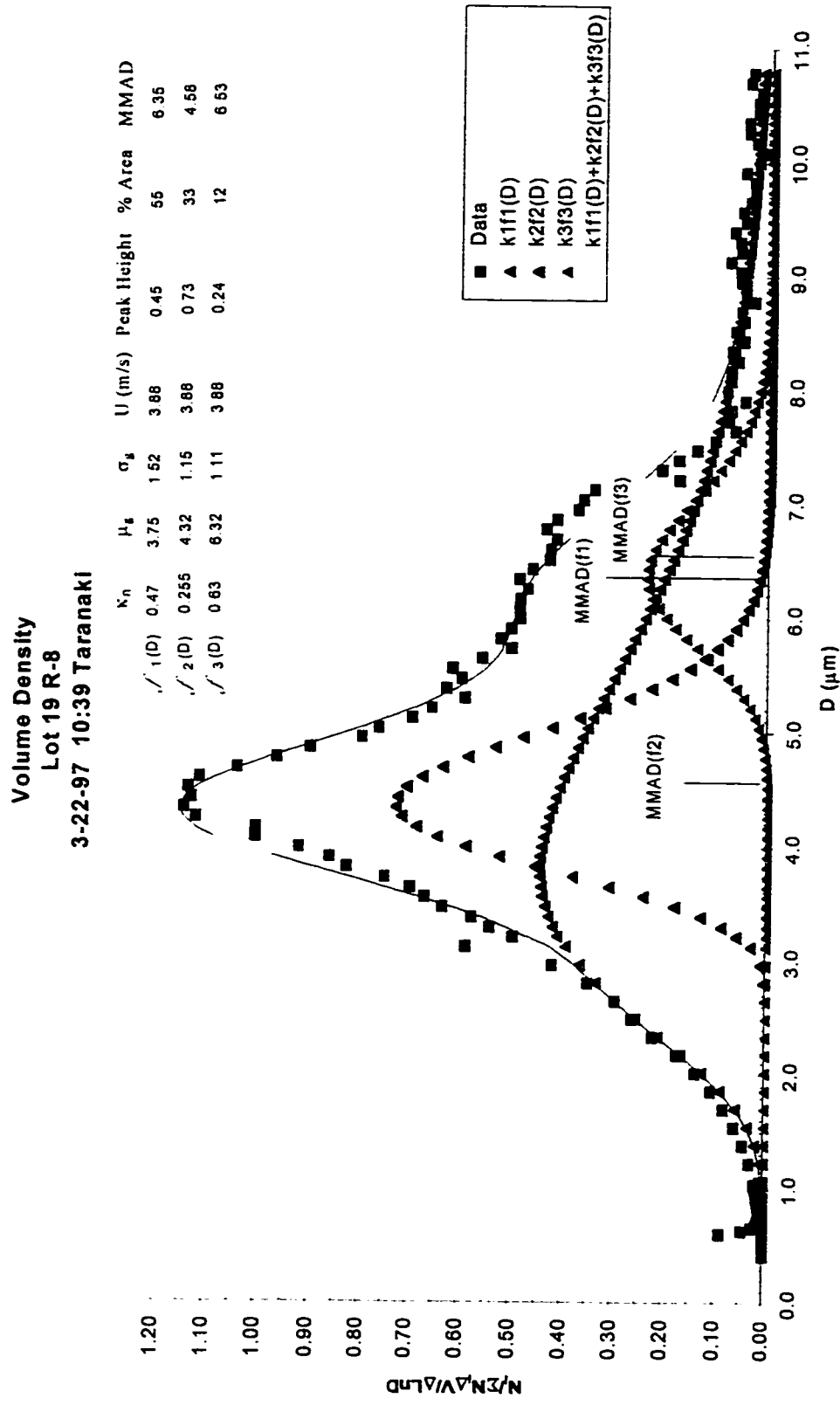
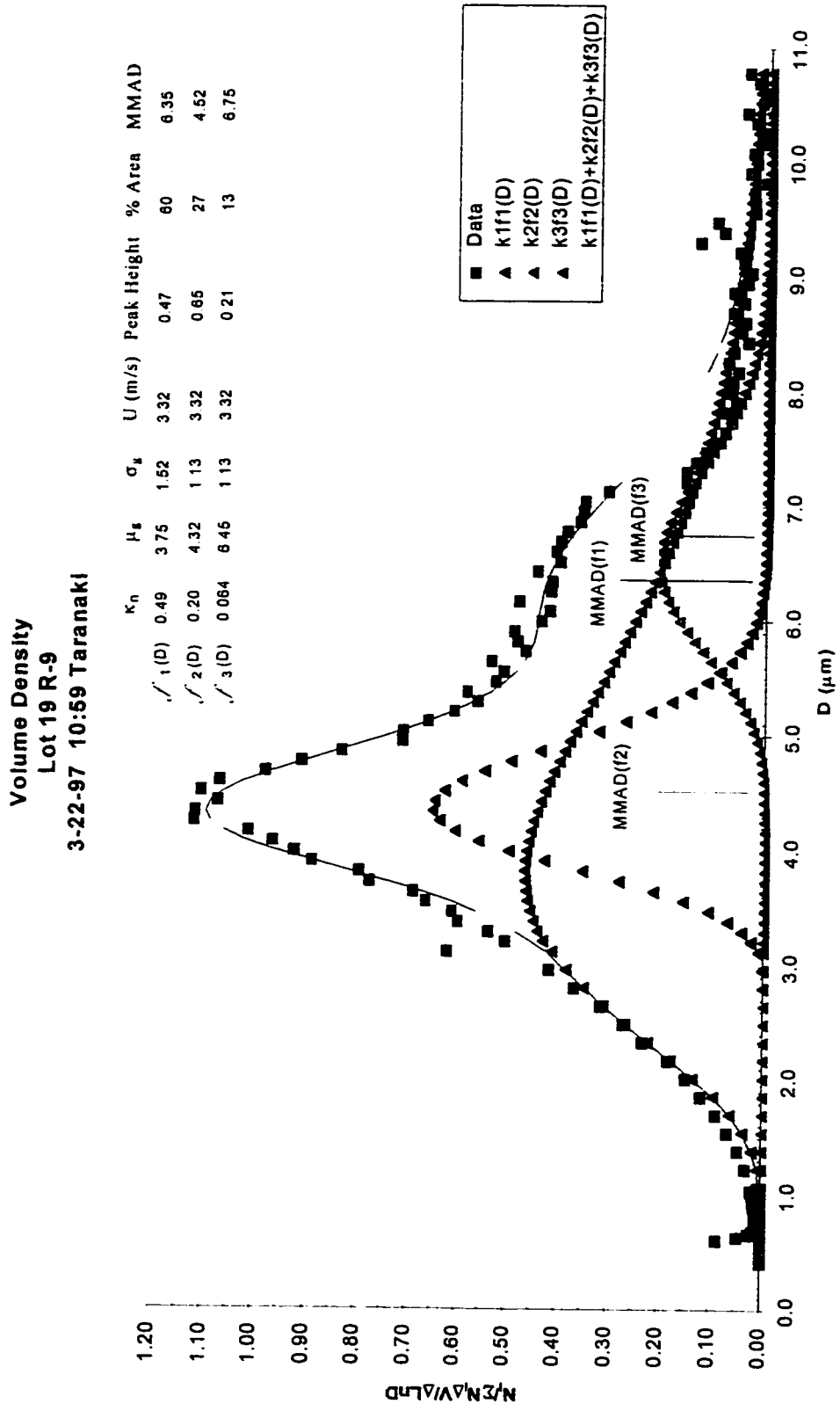


Figure II-22: APSD Lot 19 R-9



APPENDIX II-C
TARANAKI WINDS

Figure II-23: TARANAKI WINDS 3-19-97 at 2.18 m

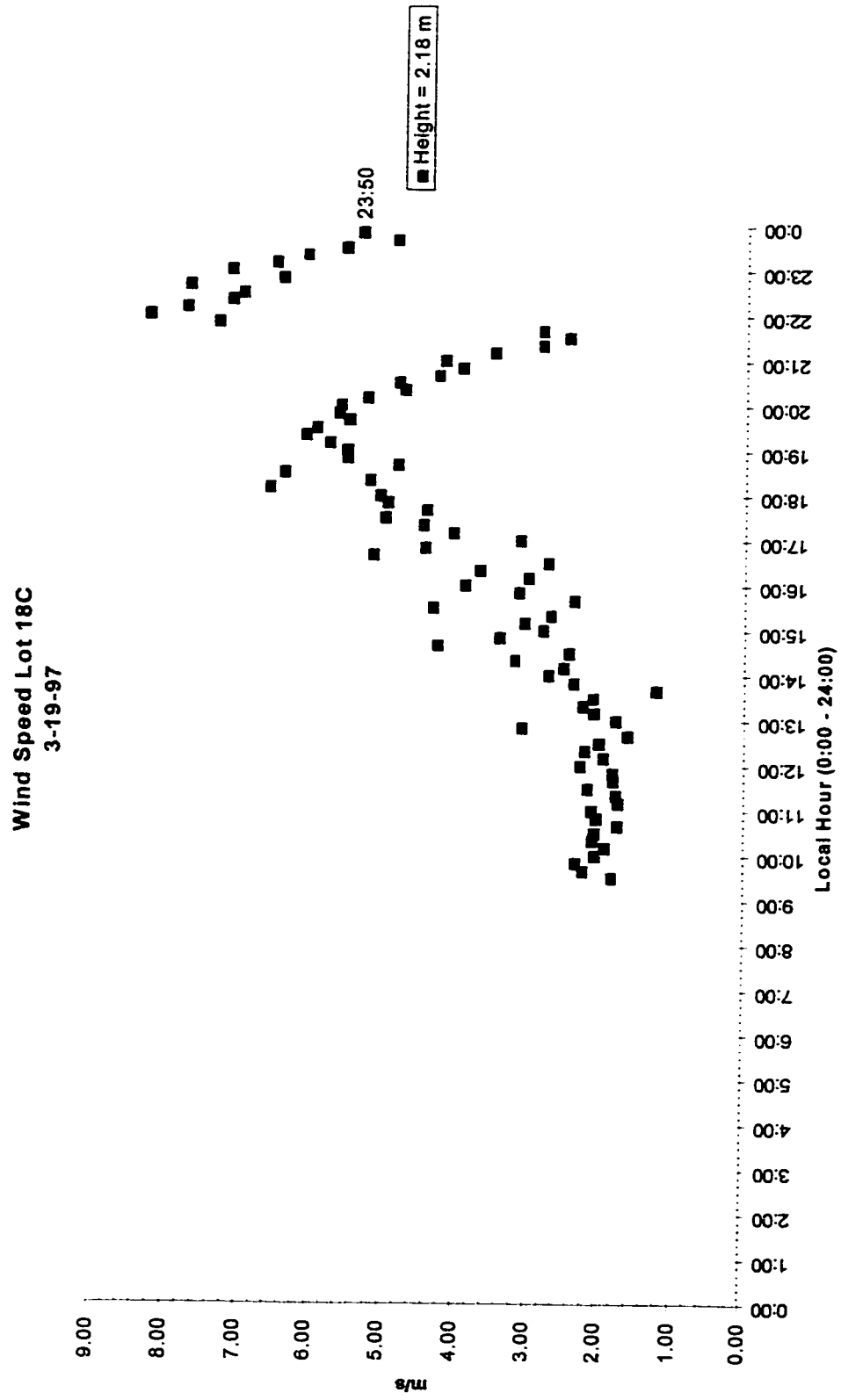


Figure II-24: TARANAKI WINDS 3-20-97 at 2.18 m

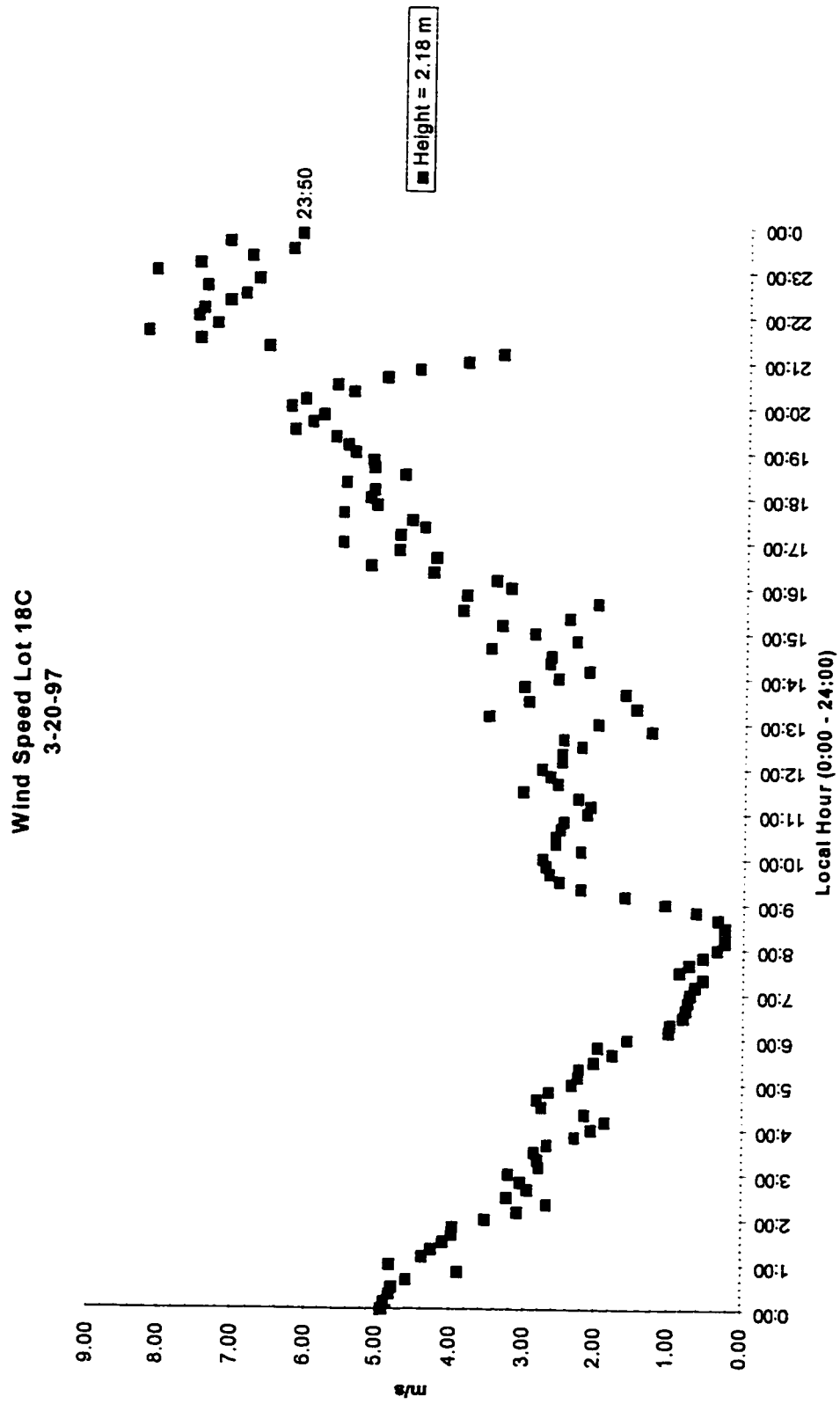


Figure II-25: TARANAKI WINDS 3-21-97 at 2.18 m

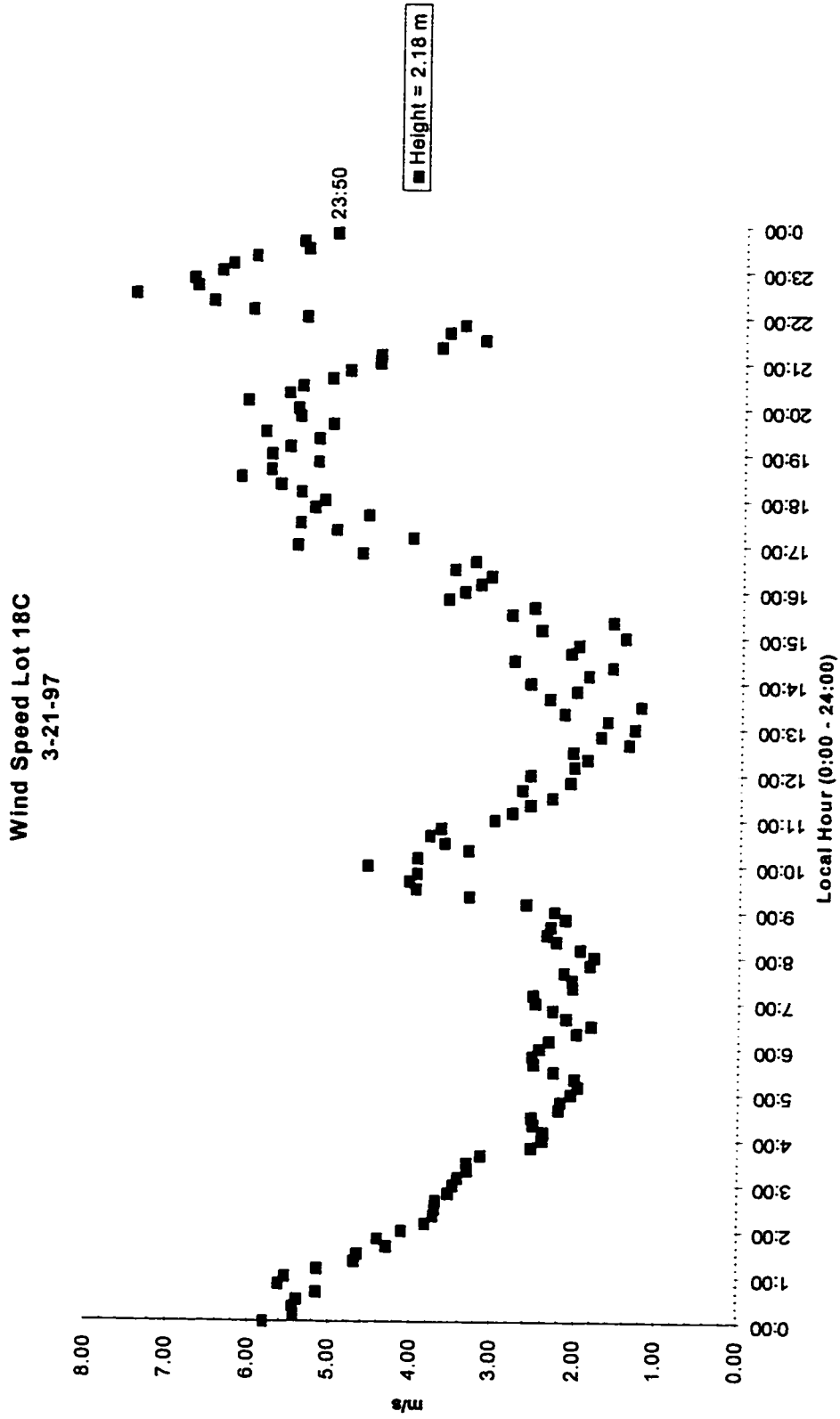


Figure II-26: TARANAKI WINDS 3-22-97 at 2.18 m

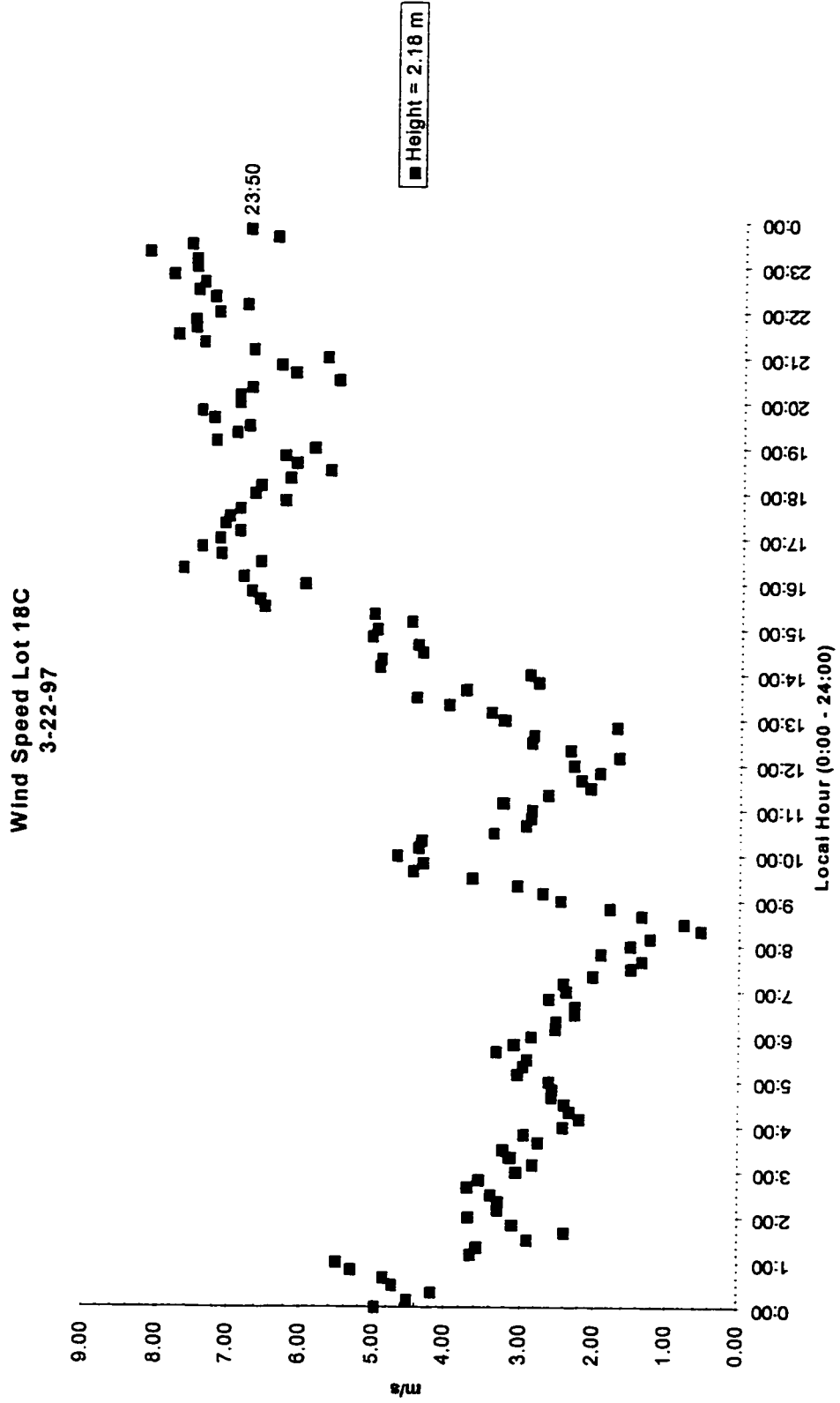


Figure II-27: TARANAKI WINDS 3-23-97 at 2.18 m

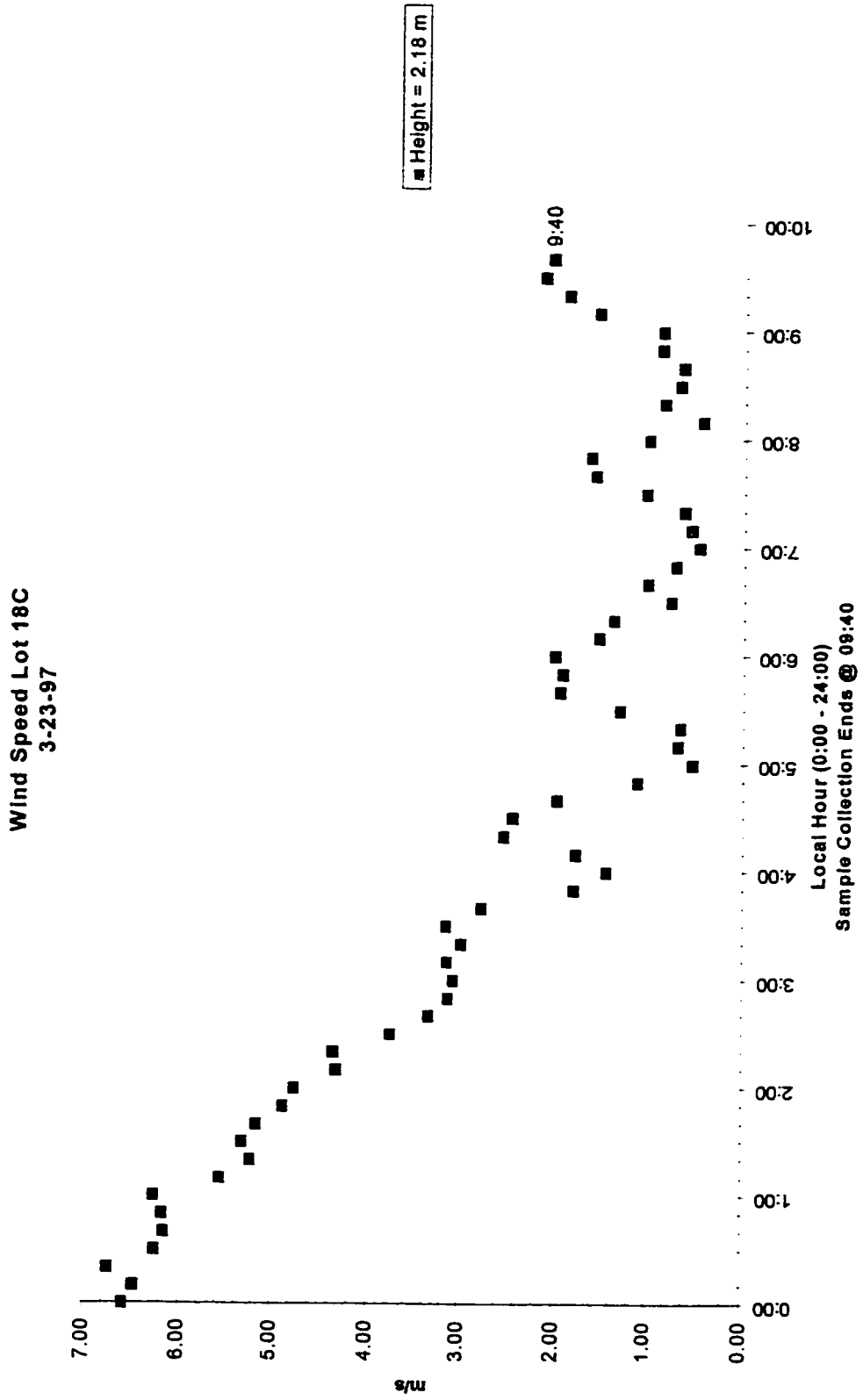


Figure II-28: TARANAKI WINDS 3-19-97 at 0.585 m and 2.18 m

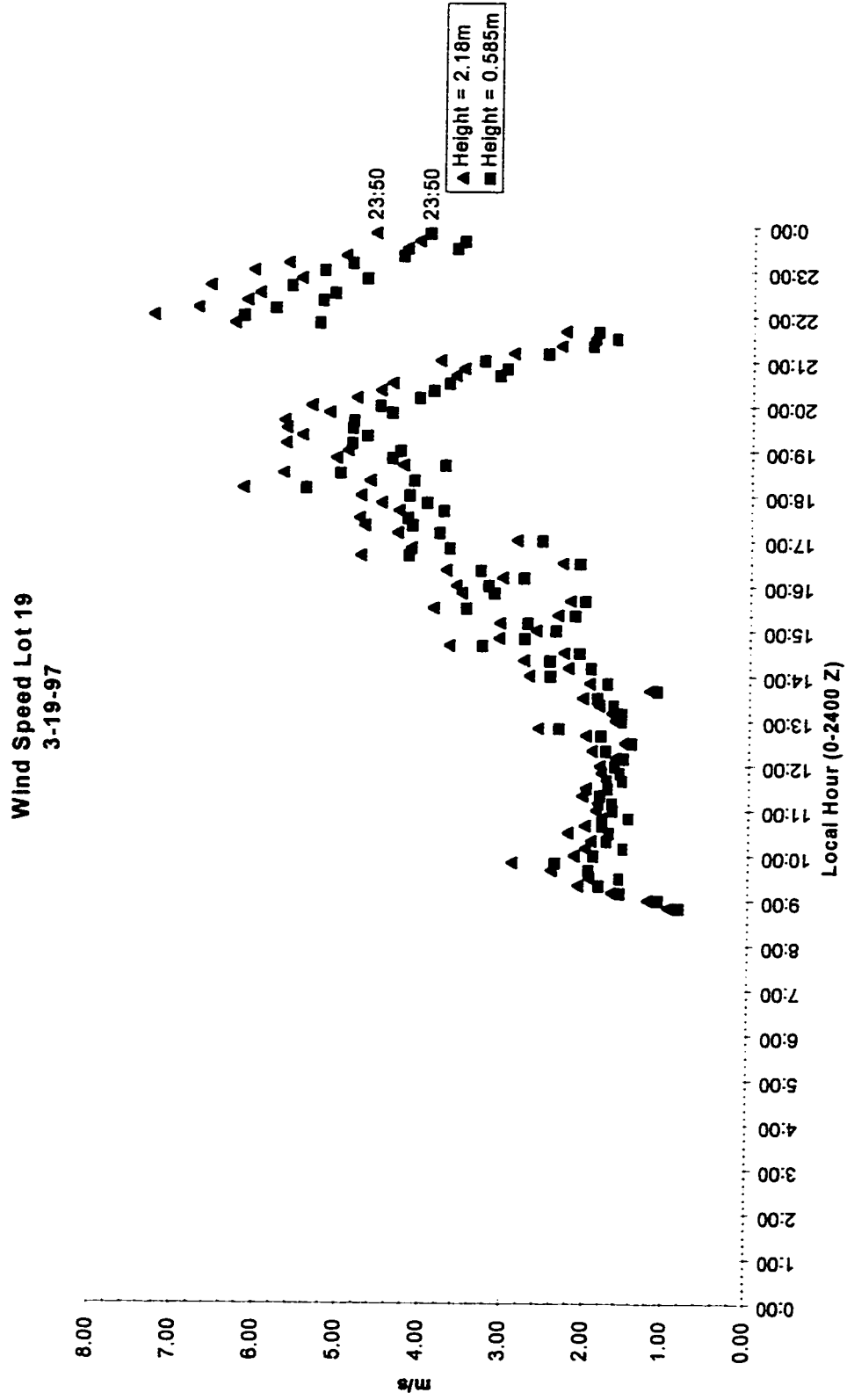


Figure II-29: TARANAKI WINDS 3-20-97 at 0.585 m and 2.18 m

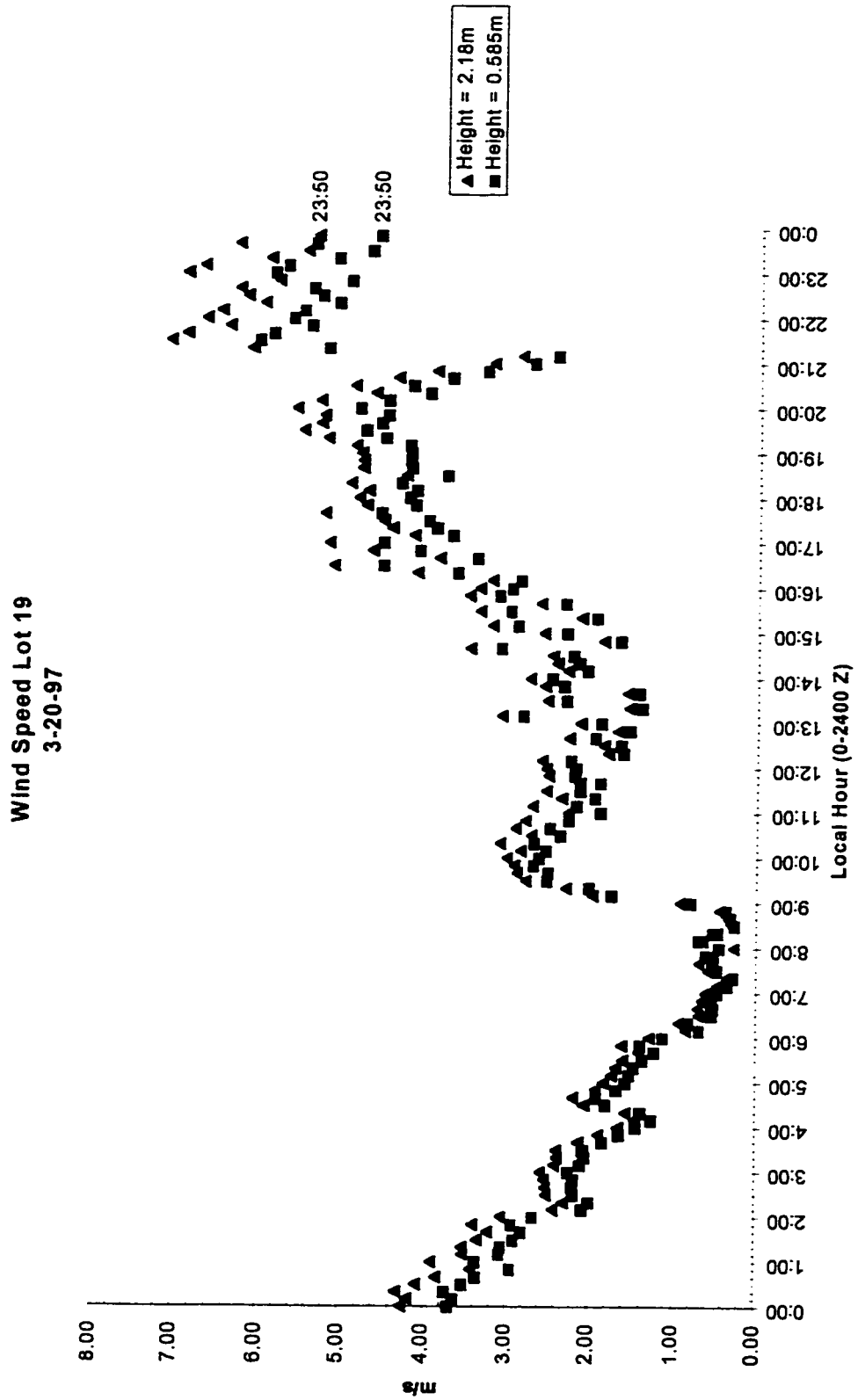


Figure II-30: TARANAKI WINDS 3-21-97 at 0.585 m and 2.18 m

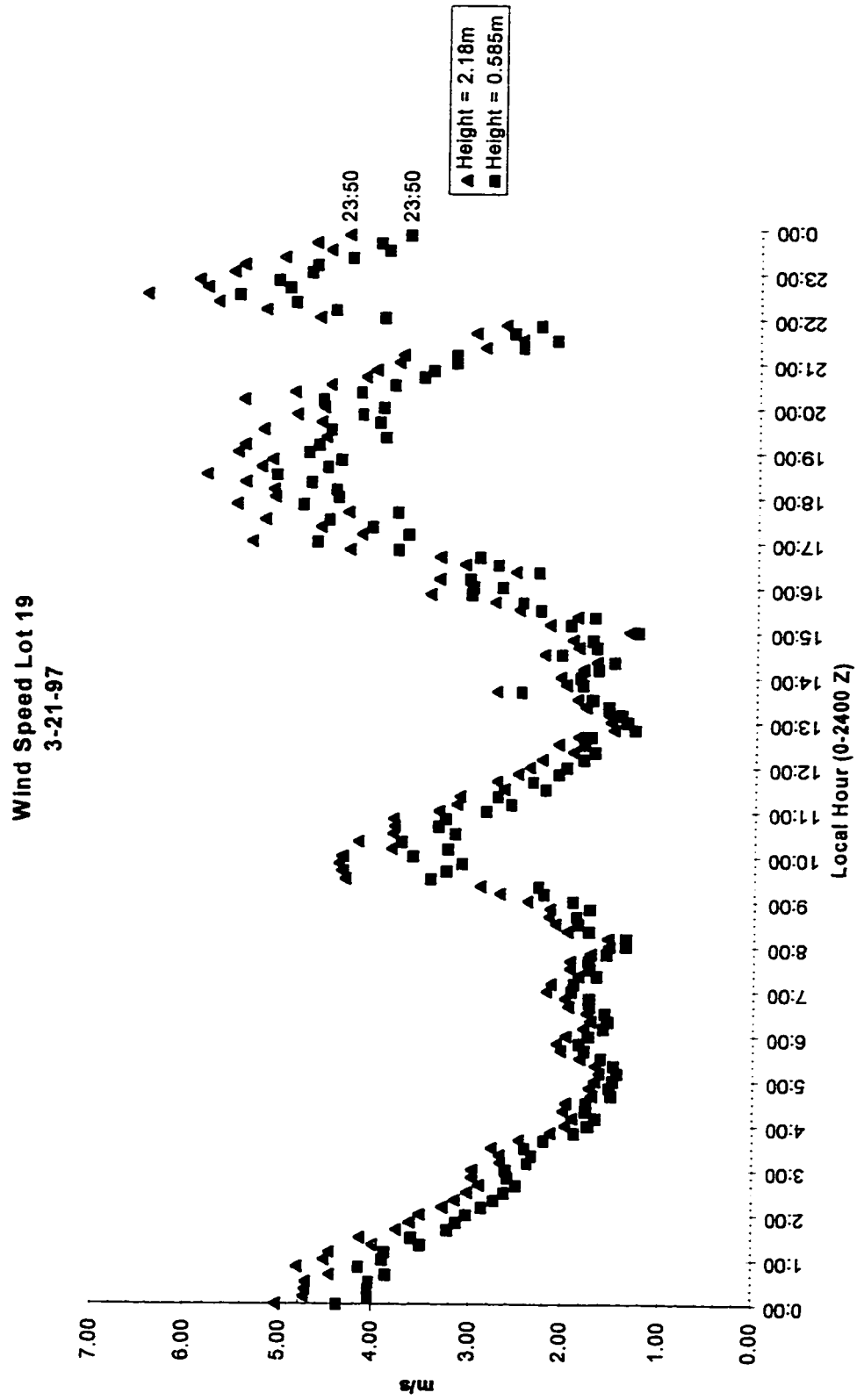


Figure II-31: TARANAKI WINDS 3-22-97 at 0.585 m and 2.18 m

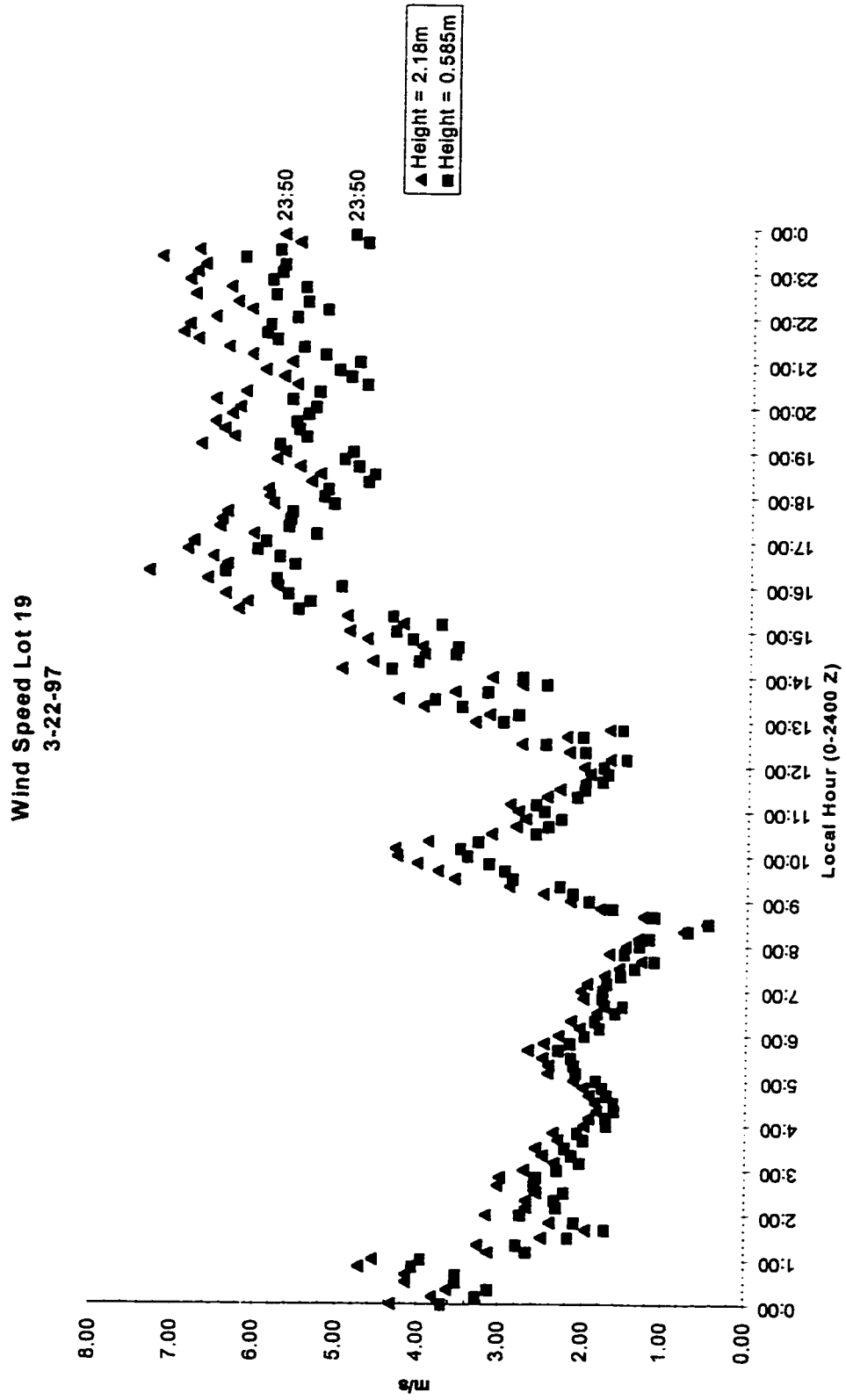
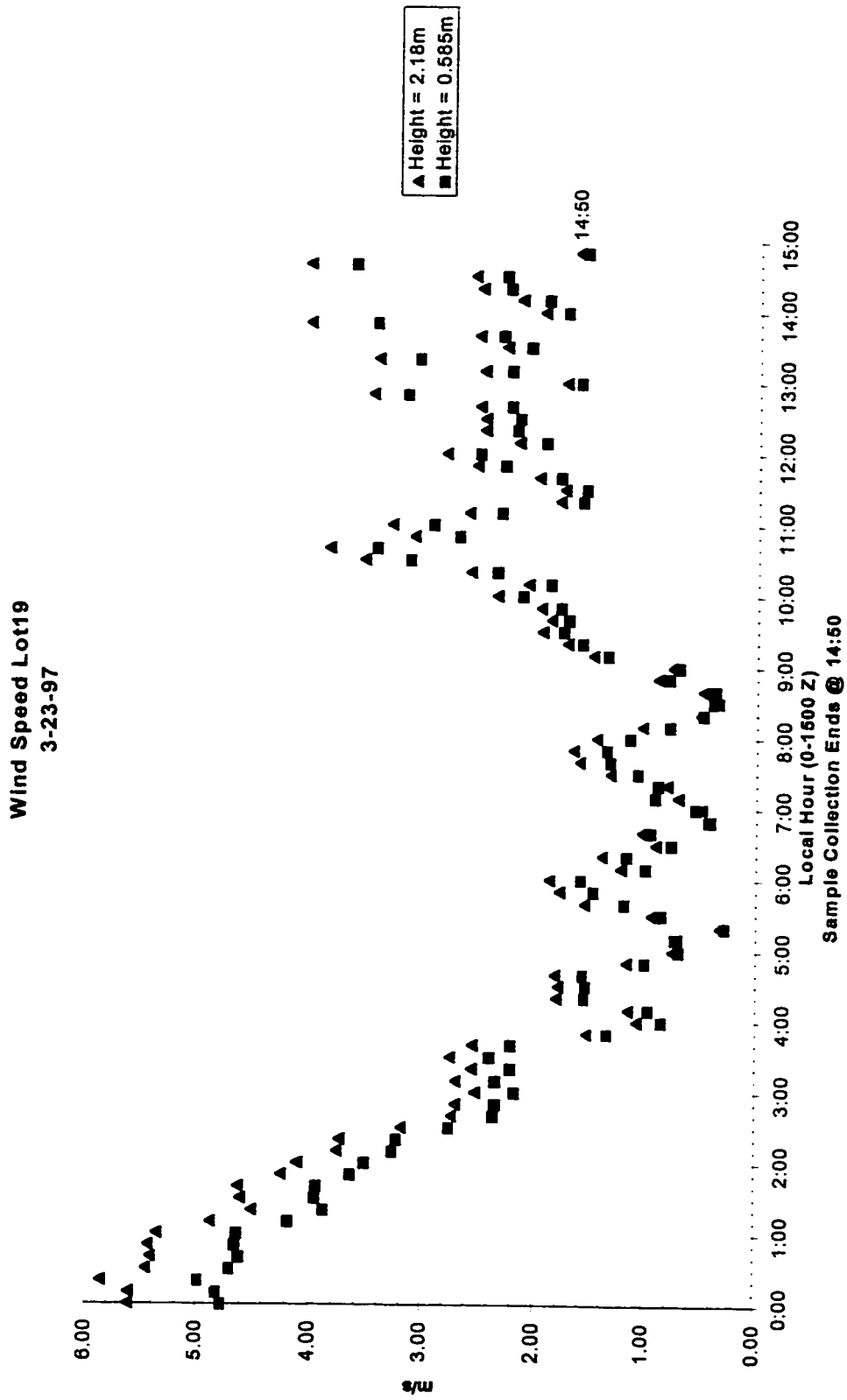


Figure II-32: TARANAKI WINDS Lot 19 3-23-97 at 0.585 m and 2.18 m



APPENDIX II-D

Table II-5 Serial I/O Cable Pin-Out for PHA 15 Pin to PC Nine Pin Connection

| |
|-------------------|
| PHA - 15 Pin |
| to |
| PC Serial - 9 Pin |

| |
|-------------|
| 5 PHA |
| to |
| 2 PC Serial |
| 6 PHA |
| to |
| 3 PC Serial |
| 15 PHA |
| to |
| 5 PC Serial |

Software Download Program: Modified from Davidson Company
Language: Basic

'Software for the Davidson 1056C PHA

'Type "M3" Board:

'Board Dip Switch Settings:

'SW: 1 on; 2 off; 3 off; 4 off

'Start of Program

CHAN = 126

DIM D(1024)

OPEN "COM1: 9600, e,7,,cs,ds,cd" FOR RANDOM AS #1

GOSUB TRANSFER

PRINT "TRANSFER COMPLETE"

GOSUB SAVED

PRINT "TRANSFER SAVED"

'PROGRAM

END

TRANSFER: 'Transfers the data from the PHA to the IBM PC

CLS

PRINT "READY TO TRANSFER DATA"

DO WHILE (INPUT\$(1,#1) <> "!")

LOOP

PRINT "PHA in I/O Mode"

PRINT #1,"&";

FOR S = 0 TO 7

IF T + S = 127 THEN RETURN

INPUT #1, D(T + S)

PRINT T + S + 1, D(T + S)

NEXT S

NEXT T

RETURN

SAVED:

OPEN "PHA.OUT" FOR APPEND AS #2

PRINT #2, DATE\$; " "; TIME\$; " "; " *****"

PRINT #2, "CHANNEL: "; AS

FOR T = 0 TO CHAN

WRITE #2, T + 1, D(T)

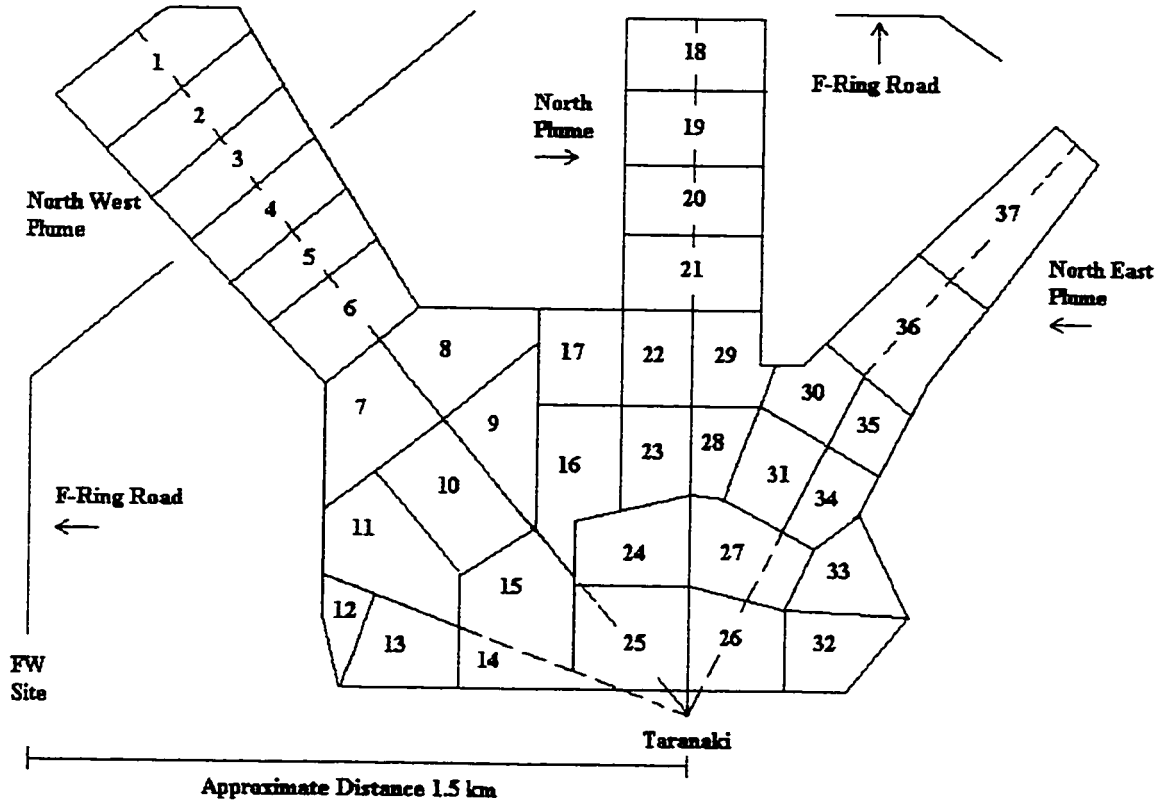
NEXT T

CLOSE #2

RETURN

APPENDIX II-E

Figure II-36: Lot Map of Taranaki Cleanup Site



APPENDIX II-F

Table II-9A: APSD Volume Density Function Parameter Summary for Lot 18C

| APSD Run | Date | Time | Sample Time (Sec) | U _{2.18} (m/s) | μ _g Overall | σ _g Overall | κ ₁ | κ ₂ | κ ₃ | μ _{g1} | μ _{g2} | μ _{g3} | σ _{g1} | σ _{g2} | σ _{g3} |
|----------|---------|-------|-------------------|-------------------------|------------------------|------------------------|----------------|----------------|----------------|-----------------|-----------------|-----------------|-----------------|-----------------|-----------------|
| | | | | | | | | | | | | | | | |
| 18C R-4 | 3/21/97 | 12:47 | 400 | 1.73 | 4.19 | 1.29 | 0.710 | 0.260 | 0.090 | 3.20 | 3.67 | 5.70 | 1.57 | 1.13 | 1.13 |
| 18C R-5 | 3/21/97 | 14:31 | 400 | 2.78 | 4.29 | 1.31 | 0.630 | 0.110 | 0.080 | 3.50 | 3.68 | 5.70 | 1.62 | 1.10 | 1.13 |
| 18C R-6 | 3/21/97 | 16:24 | 400 | 3.52 | 4.27 | 1.28 | 0.600 | 0.085 | 0.060 | 3.50 | 3.71 | 5.60 | 1.55 | 1.10 | 1.14 |
| 18C R-7 | 3/21/97 | 16:32 | 400 | 3.27 | 4.26 | 1.32 | 0.550 | 0.140 | 0.110 | 3.40 | 3.69 | 5.70 | 1.60 | 1.14 | 1.16 |
| 18C R-8 | 3/22/97 | 10:07 | 400 | 4.39 | 4.96 | 1.30 | 0.300 | 0.220 | 0.050 | 3.67 | 4.60 | 6.60 | 1.60 | 1.15 | 1.10 |
| 18C R-9 | 3/22/97 | 10:16 | 400 | 4.35 | 4.98 | 1.26 | 0.450 | 0.150 | 0.080 | 4.20 | 4.55 | 6.20 | 1.50 | 1.11 | 1.13 |

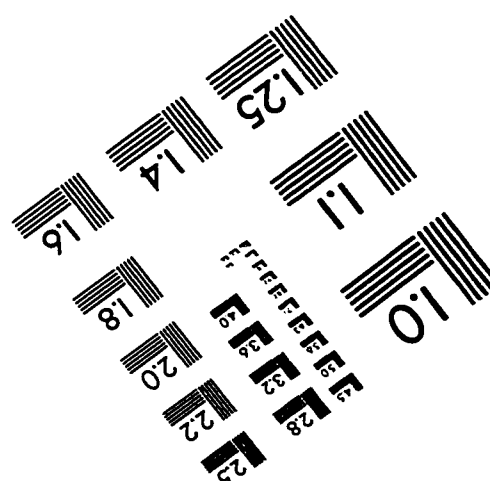
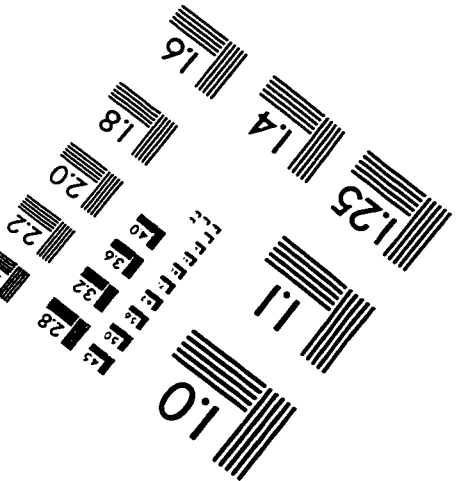
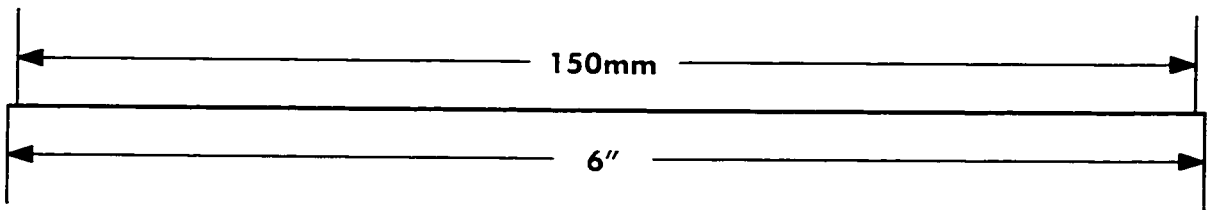
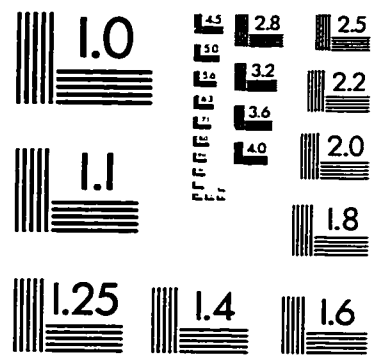
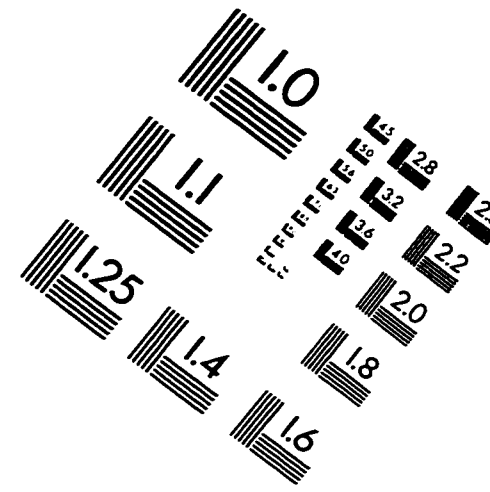
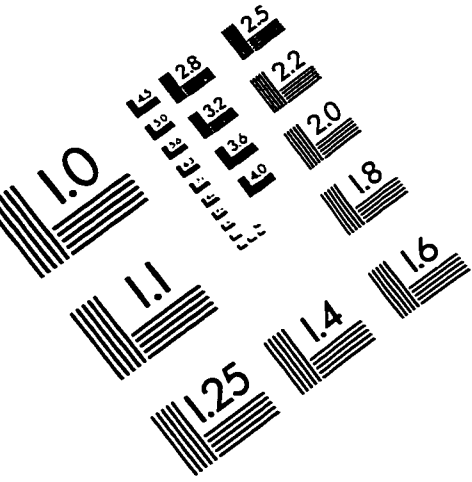
| APSD Run | Date | Time | Sample Time (Sec) | U _{2.18} (m/s) | μ _g Overall | σ _g Overall | ∫ ¹ (D) | | | ∫ ² (D) | | | ∫ ³ (D) | | |
|----------|------|------|-------------------|-------------------------|------------------------|------------------------|--------------------|--------|------|--------------------|--------|------|--------------------|--------|------|
| | | | | | | | Peak | Area 1 | % | Peak | Area 2 | % | Peak | Area 3 | % |
| 18C R-4 | * | * | * | * | * | * | 0.630 | 63.0 | 63.0 | 0.850 | 24.0 | 13.0 | 5.89 | 3.84 | 5.96 |
| 18C R-5 | * | * | * | * | * | * | 0.520 | 75.0 | 75.0 | 0.460 | 12.0 | 13.0 | 7.04 | 3.78 | 5.96 |
| 18C R-6 | * | * | * | * | * | * | 0.550 | 77.0 | 77.0 | 0.360 | 11.0 | 12.0 | 6.23 | 3.81 | 5.90 |
| 18C R-7 | * | * | * | * | * | * | 0.470 | 63.0 | 63.0 | 0.410 | 17.0 | 20.0 | 6.60 | 3.89 | 6.09 |
| 18C R-8 | * | * | * | * | * | * | 0.250 | 47.0 | 47.0 | 0.630 | 40.0 | 13.0 | 7.12 | 4.88 | 6.78 |
| 18C R-9 | * | * | * | * | * | * | 0.440 | 63.0 | 63.0 | 0.570 | 22.0 | 15.0 | 6.88 | 4.70 | 6.48 |

Table II-9B: APSD Volume Density Function Parameter Summary for Lot 19

| APSD Run | Date | Time | Sample Time (Sec) | U _{2,18} (m/s) | μ _g Overall | σ _g Overall | K ₁ | K ₂ | K ₃ | μ _{g1} | μ _{g2} | μ _{g3} | σ _{g1} | σ _{g2} | σ _{g3} |
|----------|---------|-------|-------------------|-------------------------|------------------------|------------------------|----------------|----------------|----------------|-----------------|-----------------|-----------------|-----------------|-----------------|-----------------|
| | | | | | | | | | | | | | | | |
| 19 R-1 | 3/22/97 | 13:51 | 400 | 2.79 | 4.47 | 1.29 | 0.380 | 0.100 | 0.050 | 3.70 | 4.00 | 5.70 | 1.550 | 1.120 | 1.140 |
| 19 R-2 | 3/22/97 | 14:00 | 400 | 3.15 | 4.40 | 1.28 | 0.385 | 0.090 | 0.030 | 3.62 | 3.95 | 5.63 | 1.570 | 1.100 | 1.120 |
| 19 R-3 | 3/22/97 | 15:13 | 400 | 4.95 | 4.40 | 1.30 | 0.500 | 0.160 | 0.080 | 3.69 | 3.85 | 5.65 | 1.570 | 1.130 | 1.140 |
| 19 R-4 | 3/22/97 | 15:21 | 400 | 6.27 | 4.53 | 1.35 | 0.550 | 0.411 | 0.240 | 3.60 | 4.18 | 5.85 | 1.620 | 1.230 | 1.150 |
| 19 R-5 | 3/22/97 | 15:56 | 1000 | 5.77 | 5.99 | 1.27 | 0.910 | 0.980 | 0.030 | 3.82 | 5.30 | 8.85 | 1.460 | 1.300 | 1.022 |
| 19 R-6 | 3/22/97 | 16:02 | 1000 | 7.36 | 6.32 | 1.37 | 1.000 | 1.350 | 0.070 | 4.35 | 5.72 | 8.88 | 1.560 | 1.470 | 1.020 |
| 19 R-7 | 3/22/97 | 16:53 | 1000 | 6.82 | 7.19 | 1.23 | 2.670 | 0.070 | 0.170 | 5.80 | 7.05 | 8.73 | 1.550 | 1.030 | 1.031 |
| 19 R-8 | 3/23/97 | 10:39 | 1000 | 3.88 | 4.80 | 1.27 | 0.470 | 0.255 | 0.630 | 3.75 | 4.32 | 6.32 | 1.520 | 1.150 | 1.110 |
| 19 R-9 | 3/23/97 | 10:59 | 1000 | 3.32 | 4.84 | 1.27 | 0.490 | 0.200 | 0.064 | 3.75 | 4.32 | 6.45 | 1.520 | 1.130 | 1.130 |

| APSD Run | Date | Time | Sample Time (Sec) | U _{2,18} (m/s) | μ _g Overall | σ _g Overall | K ₁ | K ₂ | K ₃ | μ _{g1} | μ _{g2} | μ _{g3} | σ _{g1} | σ _{g2} | σ _{g3} |
|----------|------|------|-------------------|-------------------------|------------------------|------------------------|----------------|----------------|----------------|-----------------|-----------------|-----------------|-----------------|-----------------|-----------------|
| | | | | | | | | | | | | | | | |
| 19 R-1 | * | * | * | * | * | * | 0.350 | 0.350 | 0.150 | 69.0 | 18.0 | 13.0 | 6.58 | 4.16 | 6.00 |
| 19 R-2 | * | * | * | * | * | * | 0.340 | 0.380 | 0.110 | 74.0 | 18.0 | 8.0 | 6.67 | 4.06 | 5.85 |
| 19 R-3 | * | * | * | * | * | * | 0.440 | 0.520 | 0.240 | 65.0 | 20.0 | 15.0 | 6.79 | 4.03 | 5.95 |
| 19 R-4 | * | * | * | * | * | * | 0.450 | 0.790 | 0.680 | 40.0 | 33.0 | 27.0 | 7.24 | 4.75 | 6.20 |
| 19 R-5 | * | * | * | * | * | * | 0.960 | 1.490 | 0.550 | 40.0 | 57.0 | 3.0 | 5.87 | 6.52 | 8.86 |
| 19 R-6 | * | * | * | * | * | * | 0.900 | 1.400 | 1.390 | 36.0 | 59.0 | 5.0 | 7.87 | 8.93 | 8.89 |
| 19 R-7 | * | * | * | * | * | * | 2.430 | 0.930 | 2.220 | 88.0 | 3.0 | 9.0 | 10.32 | 7.07 | 8.75 |
| 19 R-8 | * | * | * | * | * | * | 0.450 | 0.730 | 0.240 | 55.0 | 33.0 | 12.0 | 6.35 | 4.58 | 6.53 |
| 19 R-9 | * | * | * | * | * | * | 0.470 | 0.650 | 0.210 | 60.0 | 27.0 | 13.0 | 6.35 | 4.52 | 6.75 |

IMAGE EVALUATION TEST TARGET (QA-3)



APPLIED IMAGE, Inc
1653 East Main Street
Rochester, NY 14609 USA
Phone: 716/482-0300
Fax: 716/288-5989

© 1993, Applied Image, Inc., All Rights Reserved